



# Processing organic semiconductors

A thesis submitted for the degree  
of Doctor of Philosophy

by

**Mohammed Adnan Baklar**

School of Engineering and Materials Science  
Queen Mary, University of London  
Mile End Road  
London  
E1 4NS

June 2010



## Abstract

In recent years, there has been a considerable interest in organic semiconducting materials due to their potential to enable, amongst other things, low-cost flexible opto-electronic applications, such as large-area integrated circuitry boards, light-emitting diodes (OLEDs) and organic photovoltaics (OPVs). Promisingly, improved electronic performance and device structures have been realized with e.g. OLEDs entering the market and organic field-effect transistors (OFETs) reaching the performance of amorphous silicon devices; however, it would be too early to state that the field of organic semiconductors has witnessed the sought-after technological revolution.

Initial progress in the field was mostly due to synthetic efforts in the form of enhanced regularity and purity of currently used materials, the creation of new molecular species, etc. In this thesis we show that the advancement of physico-chemical aspects – notably materials processing – and the realisation of increased order and control of the solid state structure is critical to realize the full intrinsic potential that organic semiconductors possess. We first investigated how the bulk charge-transport properties of the liquid-crystalline semiconductor poly(2,5-bis(3-dodecylthiophen-2-yl)thieno[3,2-*b*]thiophenes) (pBTTT-C<sub>12</sub>) can be enhanced by annealing in the mesophase. To this end, temperature treatment of a period of hours was necessary to realize good bulk charge transport in the out-of-plane directions. This behaviour is in strong contrast to in-plane charge transport as measured in thin-film field-effect structures, for which it was shown that annealing times of 10 min and less are often sufficient to enhance device performance. Our observation

may aid in future to optimize the use of pBTTT polymers in electronic devices, in which good bulk charge transport is required, such as OPVs.

In the second part of thesis, we explored ink-jet printing of pBTTT-C<sub>12</sub>, in order to realize precise deposition of this material into pre-defined structures. In organic electronic applications this can, amongst other things, enable deposition of different semiconductors or reduction of the unwanted conduction pathways that often result in undesirable parasitic ‘cross-talk’, for instance, between pixels in display products. We demonstrate the integration of ink-jet printed transistors into unipolar digital logic gates that display the highest signal gain reported for unipolar-based logic gates.

Finally, recognizing that a broad range of conjugated organic species fall in the category of “plastic crystals”, we explored the option to process this class of materials in the *solid* state. We find that solid-state compression moulding indeed can effectively be applied to a wide spectrum of organic small molecular and polymeric semiconductors without affecting adversely the intrinsic favourable electronic characteristics of these materials. To the contrary, we often observe significantly enhanced [bulk] charge transport and essentially identical field-effect transistor performance when compared with solution- or melt-processed equivalents. We thus illustrate that fabrication of functional organic structures does not necessitate the use of solution processing methods, which often require removal of 99 wt% or more of solvent, or precursor side-products, nor application of cumbersome vapour deposition technologies.

Summarizing, the expanding variety of processing schemes that also allow organic semiconductors to be deposited into functional architectures offers new exciting opportunities in the area of plastic electronics device technologies. In this thesis we explored the potential of ink-jet printing and annealing of liquid crystalline polymers to produce high mobility structures both in the in-plane and out-plane directions. In addition, this thesis illustrates the potential of solid-state processing methods. A multitude of scientific and technical applications readily can be envisioned for all the processing schemes described in this thesis. The final chapter of the present work (chapter 5) focuses on three particular possible applications of them in the field of (organic) opto-electronic device technology.



## Content

Chapter 1	Introduction	11
Chapter 2	Structure control of liquid-crystalline poly(2,5- bis(3-dodecyl-thiophen-2-yl)thieno[3,2- <i>b</i> ]thiophene) (pBTTT-C <sub>12</sub> )	41
Chapter 3	Ink-jet printing of pBTTT	57
Chapter 4	Solid-state processing of organic semiconductors	75
Chapter 5	Outlook	105
Appendix I	$\alpha$ -Quaterthiophene-polyethylene blend: phase behaviour and electronic properties	121
Appendix II	Efficient, stable <i>bulk</i> charge transport in crystalline / crystalline semiconductor-insulator blends	141
	Acknowledgments	159
	Curriculum Vitae	163





*Truth is sought for its own sake ... Finding the truth is difficult, and the road to it is rough. For the truths are plunged in obscurity. ... God, however, has not preserved the scientist from error and has not safeguarded science from shortcomings and faults. If this had been the case, scientists would not have disagreed upon any point of science.\**

Al-Hasan ibn Al-Haytham (**Alhazen**) (born 965 in Iraq - died 1039 in Egypt)

\*Shmuel Sambursky, *Physical Thought from the Presocratics to the Quantum Physicists*, Pica Press, page 139, (1974).

*This work is dedicated to **Asmaa, Amaar and Yasser***



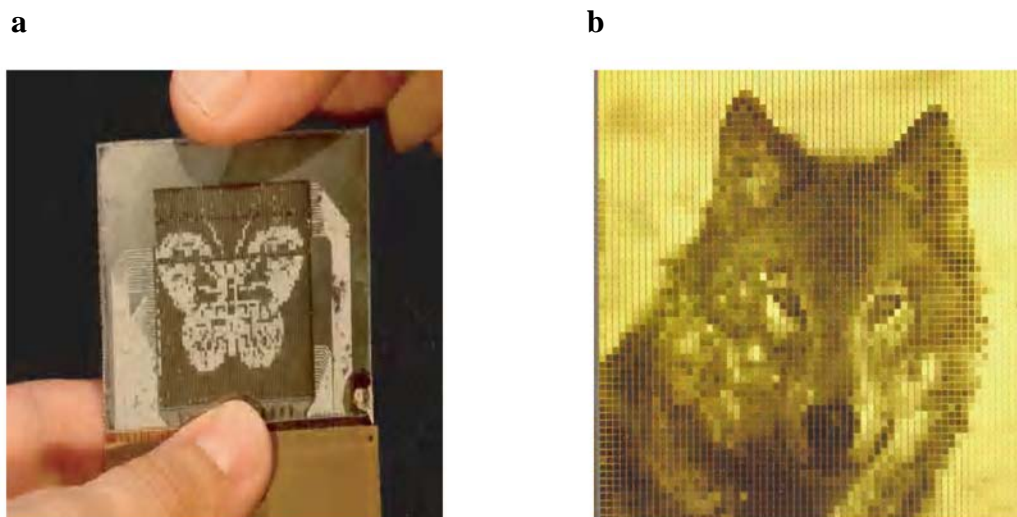
# Chapter 1

## Introduction

### 1.1. Plastic electronics

During the last few decades, the field of organic electronics has attracted significant attention from researchers working in academia as well as industry because certain organic materials have emerged as potential candidates to replace existing inorganic semiconductors, particularly in low-end electronic products, for example, organic displays<sup>1-3</sup> and radio-frequency identification tags (RFIDs).<sup>4-7</sup> Indeed, Polymer Vision, a spin-out company from Philips (Eindhoven, The Netherlands), presented rollable display proto-types with individual pixels driven by organic field-effect transistors (OFETs) based on solution-processed small organic molecules (Figure 1a,b).<sup>8,9</sup> The main advantages of organic materials are that they are potentially inexpensive, mechanical flexible, and can be deposited at low temperatures thus promising straight-forward up-scalability to roll-to-roll manufacturing. In contrast, inorganic materials are relatively expensive to process, difficult to functionalize and normally allow low through-put methodologies.

The majority of the organic materials used in these applications– small molecules and conjugated polymers are in general solution processable, although, they can rapidly degrade if exposed to air and light. However, there are

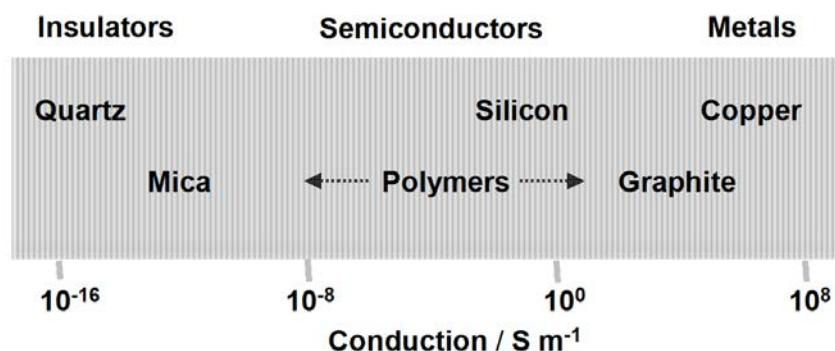


**Figure 1.** (a) Active-matrix display driven by solution-processed pentacene transistors. (b) Multipixel display driven by 4,096 thin-film transistors based on solution-processed poly(thienylene vinylene) (adopted from Ref. <sup>8</sup> and <sup>9</sup>).

possibilities to realise more efficient optical and electronic devices with better performance and greater stability in ambient conditions, for instance, by tailoring the molecular structure of these organic semiconductors to adjust the ionisation potential and improve molecular packing. Therefore, if the existing advancement within the field of organic electronics continues to evolve at current pace, it may indeed revolutionize the future of electronic products leading to truly flexible and large-area devices, and possibly replace the inorganic-based industry in some areas due to the significantly lower cost associated with organic products.

### 1.1.1. Background

The field of plastic electronics started in 1970's with the discovery by Shirakawa *et al.*,<sup>10</sup> where they demonstrated the first ever results showing polymers can have conducting-like properties (Figure 2).<sup>10-15</sup> This work was followed by detailed fundamental studies of various charge transport phenomena in a range of



**Figure 2.** Comparative electrical properties of conjugated polymers and other materials (reproduced from Ref. <sup>11</sup>).

organic semiconductors. However, the first organic light-emitting diode (OLED) device comprised of organic material was realised only in 1987 when Tang and van Slyke made a breakthrough by demonstrating an OLED based on two molecules, tris-(8-hydroxyquinoline) aluminum (Alq<sub>3</sub>) and an aromatic diamine.<sup>16</sup>

During the same period, Koezuka *et al.* for the first time demonstrated an organic field-effect transistor device,<sup>17</sup> where the organic layer (polythiophene) was deposited by electrochemical polymerization. Another group led by Friend *et al.*, on the other hand, presented their findings on polyacetylene-based Schottky diodes and organic field-effect transistors where the active layer was processed and deposited from solution using Durham *et al.* precursor route.<sup>18</sup>

In 1995 a research group from Philips published the world's first results on organic integrated circuits, which were already of a reasonable electronic performance.<sup>19</sup> The organic field-effect mobility  $\mu_{\text{FET}}$  was in the range of 10<sup>-2</sup> cm<sup>2</sup> V<sup>-1</sup> s<sup>-1</sup> facilitating the fabrication of logic gates with sufficient voltage amplification. These findings further supported the concept of using organic

semiconductors as an alternative to existing inorganic materials, especially when aimed at low-end electronic applications.

## **1.2. Organic semiconductors**

Organic semiconductors can be divided into two main categories; small molecular species (small molecules and oligomers) and macromolecular species (polymers). This classification is solely based on the molecular size of the material which can have influence, amongst other things, its crystal packing and molecular ordering.

### **1.2.1. Small molecules**

The term “small molecule” is generally referred to compounds of well-defined low molecular weight. Examples are organic semiconductors such as polycycles based on acene homologues, i.e. pentacene, tetracene and perylene derivatives. In addition to small molecules and conjugated polymers which were employed in the early studies mentioned above, oligomers such as oligothiophenes have also shown the potential to be used as active components in practical electronic devices. Oligothiophene oligomers have for instance been reported to show promising FET characteristics.<sup>20,21</sup>

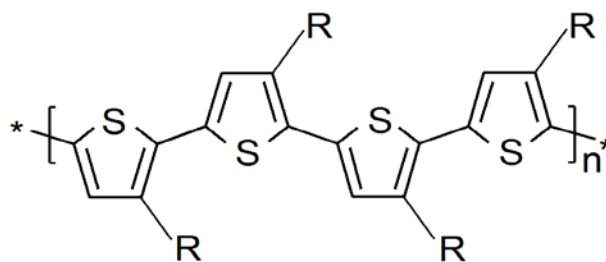
Initially many unsubstituted small molecules were poorly soluble in organic solvents and thus were deposited via thermal evaporation involving high-vacuum and high-temperature steps. However, as mentioned earlier, alterations in the molecular design have led to the synthesis of organic small molecules

displaying excellent room temperature solubility, such as the pentacene derivative 6,13-bis(tri-isopropylsilylethynyl) (TIPS) pentacene.<sup>22-24</sup>

### 1.2.2. Polymers

Polymers are comprised of repeating monomer units that are covalently bound to form long-chain structures (macromolecules). They differentiate themselves from their small molecular equivalents discussed above only by their length, thus providing interesting characteristics, such as mechanical flexibility and toughness, as well as desirable processing properties, for instance, higher melt- and solution- viscosities depending on the molecular weight of the macromolecule. Initially, unsubstituted conjugated polymers were usually insoluble,<sup>25</sup> therefore precursor routes were advanced<sup>26-28</sup> or side-chains introduced,<sup>29,30</sup> which resulted in soluble macromolecular compounds. Nowadays, the latter pathway is the most preferred method to impart good solubility to conjugated polymers.

The most common polymer semiconductors are based on conjugated macromolecular structures, such as poly(3-hexylthiophene) (P3HT) (see Figure 3), poly(thienylene vinylene) (PTV), poly(*p*-phenylene vinylene) (PPV) and polyfluorenes, such as poly(9,9-dioctylfluorene) (F8), poly(9,9'-di-octyl-fluorene-co-benzothiadiazole) (F8BT) and (9,9'-di-octyl-fluorene-co-N-(4-butyl-phenyl)-diphenylamine) (TFB).<sup>31,32</sup> More recently, liquid-crystalline polymers, such as poly(2,5-bis(3-alkylthiophen-2-yl)thieno[3,2-b]thiophene) (pBTTT) derivatives (Figure 4) have been introduced which display field-effect mobilities of up to  $1.0 \text{ cm}^2 \text{ V}^{-1} \text{ s}^{-1}$ .<sup>33-35</sup>



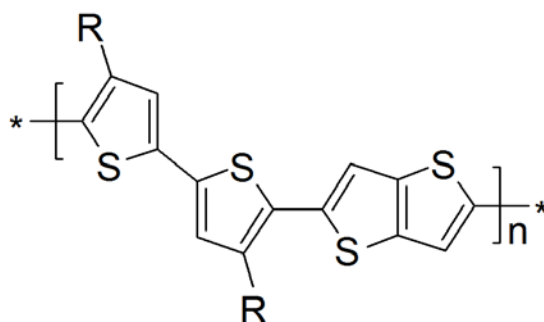
**Figure 3.** Chemical structure of regioregular poly(3-alkylthiophenes) P3ATs. An example of the head-to-tail regio-chemical isomer (R = alkyl group) is shown.

### 1.2.2.1. Poly(3-alkylthiophene)

Two routes were first reported for the synthesis of unsubstituted polythiophenes (PT); namely the Yamamoto<sup>25</sup> and the Lin and Dudek<sup>36</sup> route. This encouraged other groups to further examine such polymers, leading to solution-processable polythiophenes. In 1985 Elsenbaumer *et al.* reported, for instance, the synthesis of solution processable polythiophene derivatives via the incorporation of sufficiently long alkyl chains into the polythiophene moieties.<sup>29,37</sup> Subsequently, regioregular head-to-tail poly(3-alkylthiophenes) (rr-P3ATs) were reported by McCullough and Lowe.<sup>30</sup>

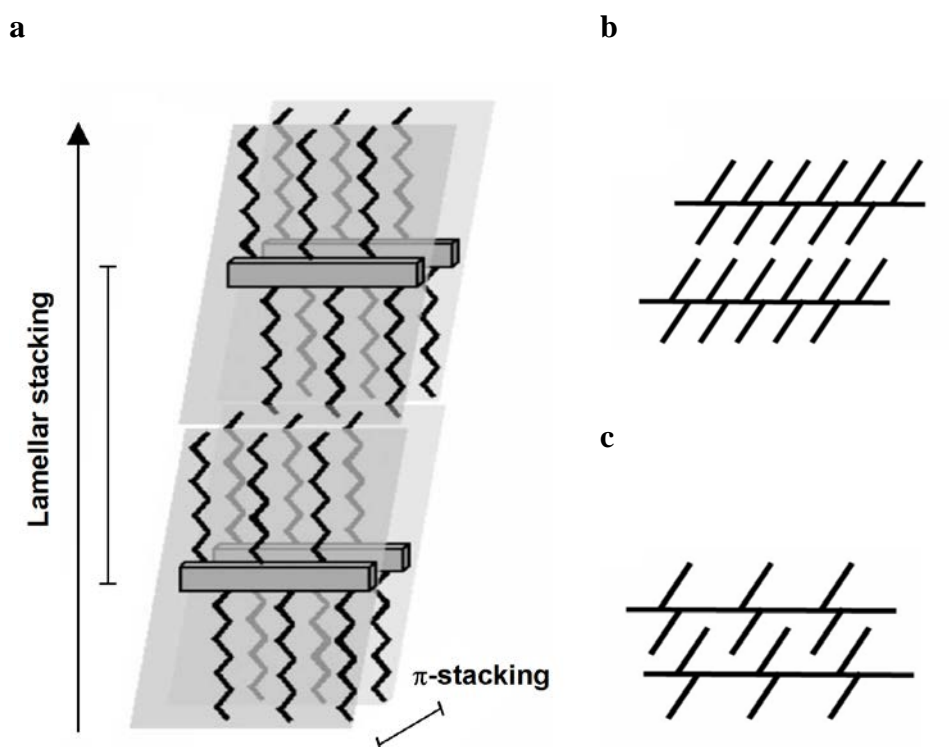
The polymerisation of the 3-alkylthiophene monomer can afford three regio-isomers depending on the arrangement of the alkyl side chains, head-to-head, tail-to-tail or head-to-tail. Regioregularity is defined as the % of HT coupling in the polymer backbone. Control of the degree of regio-regularity in P3HT significantly influences the solid-state microstructure and hence affects the electronic properties of such polymer structures. Sirringhaus *et al.* have demonstrated, for example, that higher percentages of regio-regularity in P3HT





**Figure 4.** Chemical structure of poly(2,5-bis(3-alkylthiophen-2-yl)thieno[3,2-b]thiophene) pBTTT (R = alkyl group).

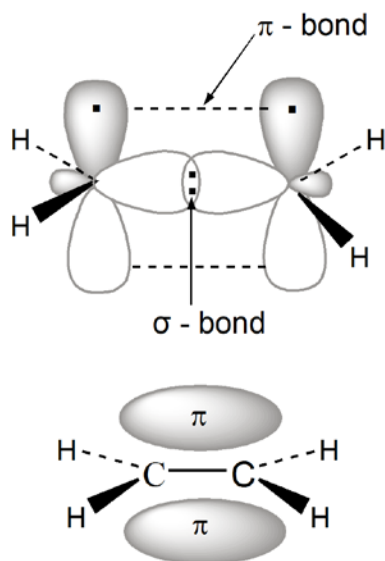
resulted in an enhanced semiconducting performance with field-effect mobilities increasing by two orders of magnitude.<sup>38</sup> This was mainly due to the improved structural arrangement of the rr-macromolecules upon deposition from solution, forming lamellae-like sheets with their side chains orientated parallel to the substrate plane. Later results by Salleo *et al.* showed faster charge transport can be achieved when there is small misorientation between neighbouring grains with respect to the polymer chain axis.<sup>39</sup> Furthermore, depending on the molecular weight, P3HT may also possess other advantageous properties, such as high viscosity and good mechanical properties, and thus has often been employed as a reference material for bench-marking other compounds. However, just like many other organic semiconductors, P3HT experiences degradation in ambient conditions due to the relatively low ionization potential (IP), where IP refers to the energy required to remove or free an electron from the ground state, also known as highest occupied molecular orbital (HOMO), to the outermost level of the molecule i.e. the vacuum level ( $E_{vac}$ ).



**Figure 5.** (a) Schematic of the packing structure of layered alkylated polymers where the side chains cause lamellar stacking whilst the planar backbones  $\pi$ -stack. The side chains might be layered end-to-end (b) or interdigitated (c) depending on their attachment density along the backbone and whether they are linear or branched (reproduced from Ref. 41).

#### 1.2.2.2. Poly(2,5-bis(3-alkylthiophen-2-yl) thieno[3,2-b]thiophene)s

The relatively poor stability of P3HT under ambient conditions reduces the overall reliability and hence long-term performance of devices fabricated with this material. Therefore, chemists have developed polymers with much higher ionization potentials (IP). For instance, McCulloch *et al.* have advanced new liquid-crystalline thienothiophene derivatives (Figure 4) that have higher ionization potentials in comparison to P3HT.<sup>33,40,41</sup> In addition, liquid-crystalline materials can simultaneously exhibit properties of a liquid (flow) as well as a solid crystal, thus annealing these polymers in the “mesophase” allows to manipulate their molecular ordering. For instance, a lamellae-like arrangement has been observed

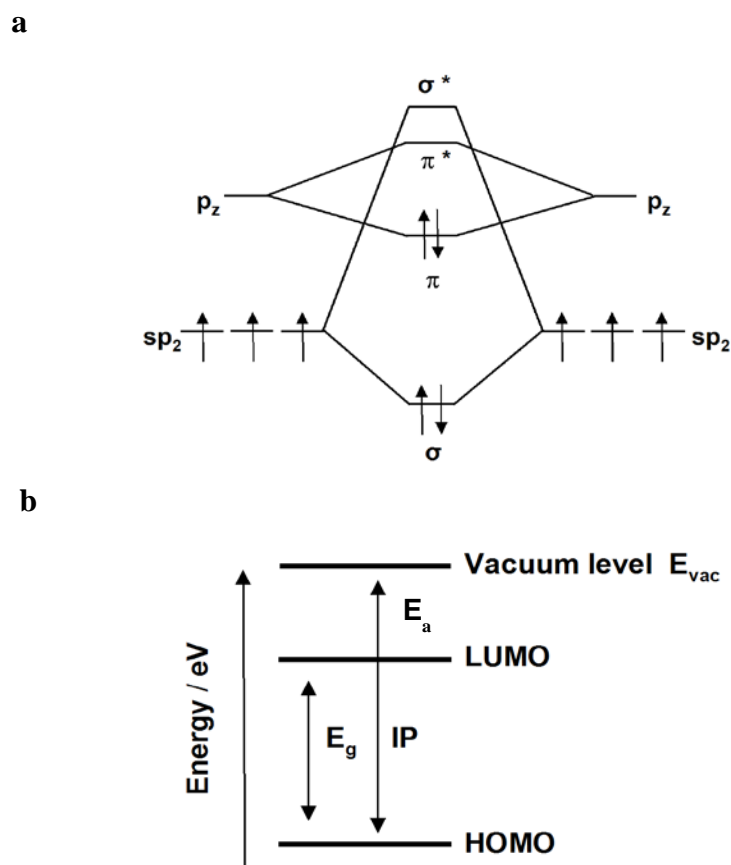


**Figure 6.**  $\sigma$ - and  $\pi$ -bonds in ethene  $C_2H_4$ , as an example for the simplest conjugated  $\pi$ -electron system (reproduced from Ref. 45).

for pBTTT polymers (Figure 5a,b) after annealing,<sup>42-44</sup> with their side chains interdigitating<sup>45</sup> (see Figure 5c).<sup>42</sup> The side chains thereby do not only contribute to the solubility of the pBTTT polymer but also promote larger size crystalline domains to form.<sup>33,46</sup>

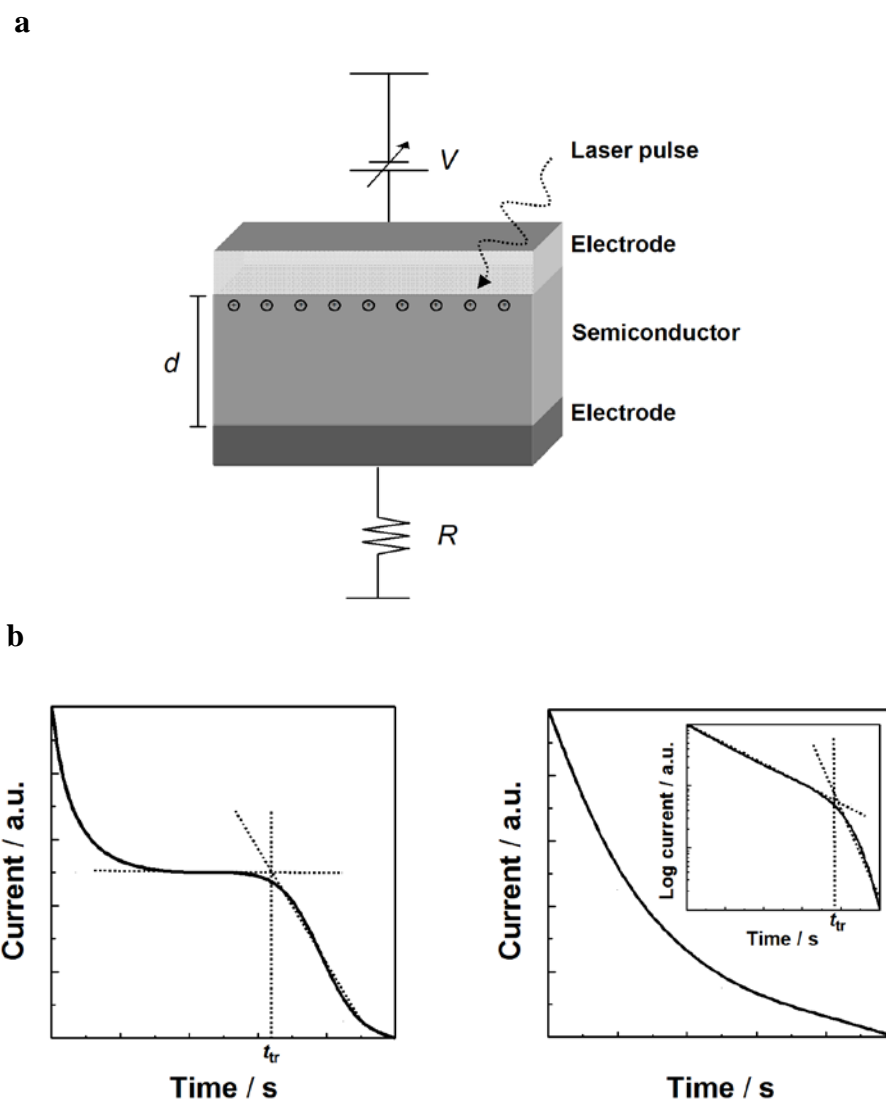
### 1.3. Charge transport in organic semiconductors

Organic semiconducting molecules are comprised of  $sp^2$  hybridized carbon atoms. The hybridization of  $2s$ ,  $2p_x$  and  $2p_y$  orbitals results in the formation of three hybrid orbitals that adopt a trigonal planar geometry and will be involved in  $\sigma$ -bonds, while the  $2p_z$  orbitals, which are perpendicular to the plane of the hybrid orbitals, will form  $\pi$ -bonds (see Figure 6).<sup>47</sup> Therefore two neighbouring  $sp^2$  hybridized carbon atoms will develop a double bond: a  $\sigma$ -bond through the head-to-head overlap of the hybrid orbital and the  $\pi$ -bond from the overlap of the unhybridized  $2p_z$  orbitals. The alternation in a molecule of single and double bonds is known as conjugation.



**Figure 7.** (a) The energy scheme of ethene  $C_2H_4$  (reproduced from Ref. <sup>48</sup>). (b) General description of energy levels of  $\pi$ -conjugated semiconducting materials.

The semiconducting properties of conjugated small molecules and polymers result therefore from the  $\pi$ -orbital delocalization along their backbone. The molecular overlap of  $\pi$ -orbitals gives rise to energy bands known as  $\pi$ -bonding and  $\pi^*$ -antibonding (Figure 7a),<sup>48</sup> which are known as the highest occupied molecular orbital (HOMO) and the lowest unoccupied molecular orbital (LUMO), respectively (Figure 7b). The band gap energy  $E_g$  between HOMO and LUMO, the activation energy  $E_a$  and the ionization potential IP influence the optical and electronic properties of organic semiconductors. Thus, molecular tailoring of the HOMO and LUMO with respect to the vacuum level is critical when considering the synthesis of new materials of high performance and good ambient stability.



**Figure 8.** (a) General time-of-flight set up. (b) Typical transient photocurrent, *left panel*: non-dispersive, and *right panel*: dispersive (reproduced from Ref. <sup>49</sup>).

Finally it is important to note that, the fundamental mechanism of charge transport in organic semiconductors is dominated by intermolecular transport where the charge carriers “hop” between the neighbouring molecules. Therefore inducing structural order and chain packing is often essential for enhancing their electronic performance. Intermolecular charge transport can in addition be improved by maintaining the planarity of the polymer backbone ( $\pi$ -stacking) such that lamella-like sheets are formed as observed in P3HT and pBTTTs.

### 1.3.1. Assessment of electronic properties in organic structures

Organic semiconductors are frequently employed as active materials in a variety of electronic devices including organic field-effect transistors, organic light-emitting diodes and organic photovoltaic cells. It is therefore important to characterize the electronic properties of these materials for instance, by time-of-flight (TOF) photoconductivity measurements<sup>49</sup> or using a field-effect transistor configuration.<sup>50</sup>

#### 1.3.1.1. Time-of-flight photoconductivity

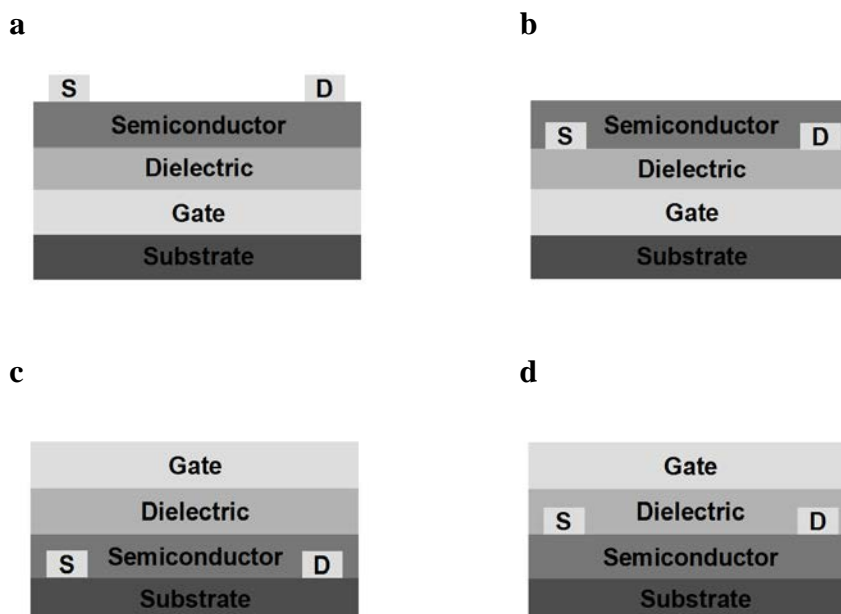
The TOF technique (see Figure 8a)<sup>51</sup> is applied to probe charge transport of organic semiconductors in the bulk. With a pulsed laser, charge carriers are excited at the electrode/semiconductor interface which then drift across the semiconductor layer from one electrode to the other when an electric field is applied. The time that it takes these charge carriers to arrive at the counter-electrode is defined as the arrival time (transient time  $t_{tr}$ ). This transient time can be identified in dispersive systems by drawing two lines as shown in Figure 8b.<sup>49</sup> Consequently the time-of-flight mobility of charge carriers  $\mu_{TOF}$  can be calculated from  $t_{tr}$  as follows:

$$\mu_{TOF} = d^2/V \cdot t_{tr} \quad (1.1)$$

Where  $d$  is the sample thickness and  $V$  the applied voltage.

#### 1.3.1.2. Organic field-effect transistors

In 1947 Bardeen, Brattain and Shockley at Bell Laboratories demonstrated the first point-contact bipolar transistor that showed amplification.<sup>52-54</sup> As a result of



**Figure 9.** Different geometries of organic field-effect transistors. Source and drain electrodes (S,D), organic semiconductor, dielectric and gate electrode are indicated. The transport takes place at the interface between semiconductor layer and gate insulator layer. Bottom-gate geometry; (a) top-contact, (b) bottom-contact. Top-gate geometry; (c) bottom-contact, (d) top-contact.

this discovery they were awarded the Nobel Prize in Physics in 1956. The first metal-oxide semiconductor field-effect transistor (MOS-FET) was introduced by Khang and Attala in 1960 using silicon dioxide ( $\text{SiO}_2$ ) as gate insulator and silicon (Si) as semiconductor.<sup>55</sup> Organic transistors are also based on a field-effect configuration. They are comprised of an insulating layer, semiconducting layer as well as three electrodes: the source (S), the drain (D) and the gate electrode, the latter of which is isolated by the insulator (dielectric) from the two other electrodes (see Figure 9a,d). The gate dielectric acts as a capacitor, as a consequence of which the charge carrier density is dependent on the applied  $V_G$  at the gate electrode. Indeed, when applying a negative gate voltage, the gate dielectric is polarized, inducing positive charges at the interface between the semiconducting and insulating layer (more charge carriers are accumulated at higher  $V_G$ ). The

accumulated charges can then be driven and collected by applying a drain voltage ( $V_D$ ) across the source/drain channel. Organic semiconductors that have positive charges (holes) as the dominant charge carriers are known as p-type materials. On the other hand, when applying a positive gate voltage, negative charges are induced at the semiconductor/dielectric interface. If negative charges represent the dominant charge carriers in a material, it is referred to as n-type semiconductor.

The initial theory developed for characterization of MOSFET has been widely used in the measurements and modelling of OFETs.<sup>47,56-61</sup> For instance, in OFETs there are two distinct driving regions. In the linear regime, where  $V_D < V_G - V_T$  (gate voltage – threshold voltage), the current between the source and drain depends linearly on the applied gate voltage:

$$I_D = (W/L) \mu \cdot C_i (V_G - V_T) \cdot V_D \quad (1.2)$$

When the  $V_D > V_G - V_T$  the current is no longer linearly dependent. This so-called saturation regime is represented by equation 1.3:

$$I_D = (W/2L) \mu \cdot C_i (V_G - V_T)^2 \quad (1.3)$$

Equations 1.2 and 1.3 can be used to estimate the field-effect mobilities of organic semiconductors. The determination of such device mobilities is important not only to compare various materials with each other, but also to estimate the switching speed in more integrated electronic structures. In addition to the mobility, other important device parameters are the on/off ratio and the sub-



threshold slope. The former is associated with the differences in current between the off-state (non-conducting) and the on-state (conducting) of the electronic devices, while the latter dictates how fast the device can switch from the off-state to the on-state.

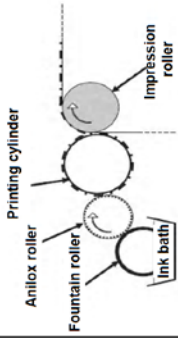
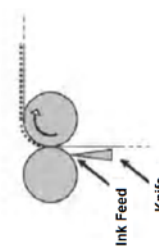
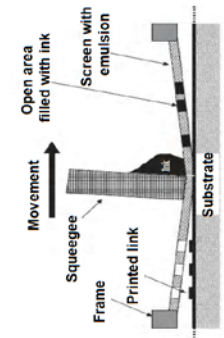
#### **1.4. Device fabrication**

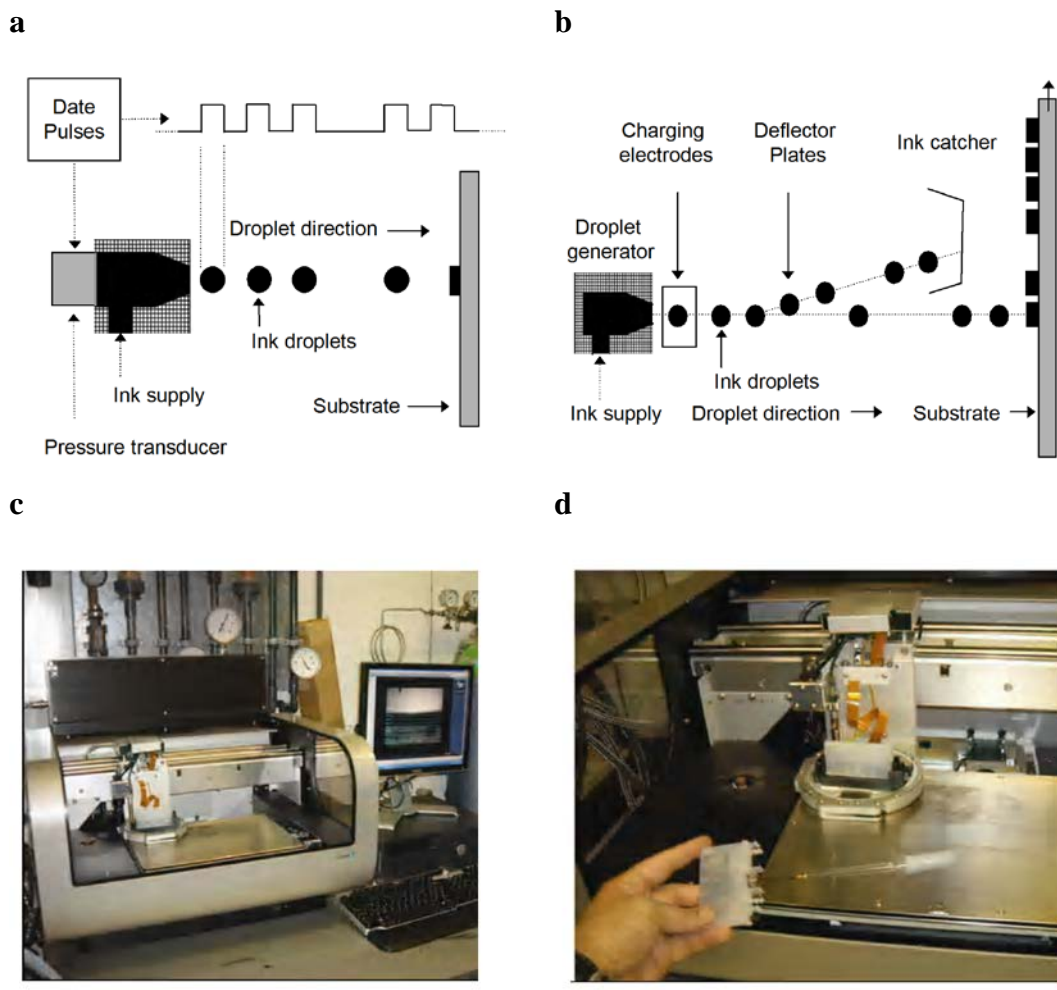
As earlier mentioned, organic semiconductors have a major advantage over their inorganic counterparts due to the variety of processing methods that can be used to fabricate active devices. Most interesting so far have been solution-based processing methods which promise to be easily up-scalable to fast and inexpensive roll-to-roll manufacturing. Indeed, in addition to the common batch scale processing such as solution-casting and spin-coating, recently, there has been significant progress in the development and use of fast and up-scalable printing and coating methods, such as gravure, flexography, screen, slot-die, offset, lamination and doctor blading methodologies.<sup>62-64</sup> Table 1 lists selected methods and describes them in terms of their characteristics, main features and applications.

##### **1.4.1. Inkjet printing**

Inkjet printing of organic semiconductors has gained considerable attention due to its associated advantages in comparison to other existing printing methods described in Table 1.<sup>62-68</sup> This is due to the fact that ink-jetting is defined as a non-contact patterning process where only small size droplets (pico-liters) are deposited onto a given substrate. The substrate can be rigid such as silicon or glass but also flexible like plastic films. Patterning is enabled by descending the organic

Table 1. Comparison of various coating and printing methods used in the organic electronic area (partly reproduced from the cited References).

Printing techniques	Layer thickness ( $\mu\text{m}$ )	Feature size ( $\mu\text{m}$ )	Viscosity (mPas)	Registration ( $\mu\text{m}$ )	Applications	Schematics	References
Flexography	0.8-2.5	80	50-500	<200	Packaging; newspaper & labels		61-64
Gravure	0.8-8	75	50-200	>10	Magazines; plastic film & metal foils; banknotes		61-64
Screen printing	30-100	20-100	500-50000	>25	Textiles; CDs; large posters		61-64
Inkjet-printing	<0.5	20-50	1-30	5-20	Desktops; variable data	(See figure 10)	



**Figures 10.** Schematic of the ink-jet printing process using a data pulse train to generate droplets on demand via a pressure transducer (a), or employing a system where droplets are generated continuously and the pattern is created by deflecting the unwanted droplets away from the substrate (b) (reproduced from Ref. <sup>63</sup>). Photographs of the laboratory ink-jet printer (c) and printing cartridges (d) used in this thesis.

solution drop by drop onto substrate(s) as preferred. Indeed, this printing method is very similar to that employed in commercially available printers used in offices and households today, where digital data is transferred onto paper or other flexible substrates.

There are two main types of inkjet printing; continuous and drop-on-demand (impulse) jetting. In continuous jetting, the ink (i.e. a solution containing the

organic semiconductor and potentially other additives such as wetting agents, high-molecular weight polymers to adjust the viscosity and the like) is ejected through a nozzle by means of pressure (thermal) within the reservoir, which then generates a continuous stream of ink (see Figure 10a). The excess drops are deflected into a tray for re-circulation. In drop-on-demand or impulse jetting, ink drops are created only when it is required, which can minimise material usage. The release of the droplets is thereby achieved via a piezoelectric transducer that regulates a pressure in the ink reservoir as shown in Figure 10b,d.

One key driving force behind the use of inkjet printing for the manufacturing of organic electronic devices was the work by Sirringhaus *et al.*, who demonstrated the inkjet printing of the source/drain electrodes of all-polymer field-effect transistor (FET) circuits,<sup>69</sup> which illustrated that inkjet printing can be used as an alternative method to other expensive deposition techniques. Inkjet printing of the organic semiconductor as active layer in OFETs was later demonstrated by Paul *et al.*, who realised a device performance with a mobility of up to  $0.1 \text{ cm}^2 \text{ V}^{-1} \text{ s}^{-1}$  using poly(3,3-dialkylquaterthiophene) (PQT). More interestingly, the device-to-device cross-talk was significantly reduced because of the patterning of the active layer.<sup>70</sup> Since then, inkjet printing has found use in numerous organic electronics applications ranging from active-matrix displays, organic light-emitting diodes and more recently organic photovoltaics.<sup>71-75</sup> Nonetheless, despite its various advantages over other printing and coating techniques, inkjet-printing faces other complexities; for instance, this process permits working only in a relatively small solution-viscosity window, it also

requires tedious control of droplet size and a careful adjustment of the surface energy of the substrate.

### **1.5. Objective and scope of thesis**

In this thesis, we illustrate that optimizing the structural order and molecular arrangement is critical to realise good electronic performance in organic semiconductors. To this end, we focus first on the liquid-crystalline thienothiophene polymer pBTTT as a model material. The bulk charge-transport properties of this semiconductor are investigated and the influence of thermal annealing in the mesophase on the electronic characteristics is studied. The effects of temperature as well as annealing times are assessed to obtain relevant structure/property intercorrelations.

We also investigate the solubility of pBTTT polymers in various organic solvents using differential scanning calorimetry and visual analysis to select suitable formulations for the use in inkjet printing methods. The latter have the advantage to allow patterning of the active material into desired geometries and size, thus permitting realization of structured discrete devices e.g. for use in unipolar inverter structures. These represent the backbone of complementary circuits, indeed a much sought-after electronic component for the manufacturing of large-scale integrated circuits.

In Chapter 4, this thesis explores the option to process organic semiconductors in the solid state. This fabrication method does not necessitate the use of solution processing methods, which often require removal of 99 wt% or

more of solvent, or precursor side-products, nor application of cumbersome vapor deposition technologies. We investigate how solid-state compression molding can be applied to organic small molecular and polymeric semiconductors, and study the influence of processing conditions on the intrinsic electronic characteristics of these materials. To this end, we probe the [bulk] charge transport of such structures and compare these results with their solution- or melt-processed equivalents. Furthermore, field-effect transistors are fabricated and characterized in order to demonstrate the wide-applicability of this approach.

The outlook chapter of the present work (Chapter 5) focuses on three particular potential applications of such processing schemes in the field of (organic) opto-electronic device technology.

Finally, in the appendix part I, we demonstrate that blending of  $\alpha$ -quaterthiophene 4T with high-density polyethylene HDPE under judicious chosen processing conditions. We investigate the influence of the insulator content on the electronic properties of the semiconducting species. In part II of the Appendix, we explore charge transport in the bulk of crystalline / crystalline, P3HT / HDPE systems by time-of-flight (TOF) photoconductivity measurements. We study different blend compositions and compare it to the bulk charge-transport property of neat P3HT.

## **1.6. Author declaration**

It will become apparent to the reader that this thesis was a result of a multidisciplinary effort. The author's contribution comprise of all issues related to

the material science aspects of this work presented here. In chapters 2, 3 and 4 major contributions were made by collaborators to whom the author is deeply indebted: Time-of-flight measurements (chapter 2 and 4) carried out by Dr. Theo Kreouzis, Dr. Seema Barrard and Avinesh Kumar (Queen Mary University of London); in chapter 3 inverters were characterized by Dr. Thomas Anthopoulos and Dr. Paul Wöbkenberg (Imperial College London); in chapter 4 wide-angle X-ray diffraction patterns, polymers density and mechanical toughness measurements were performed by Pascal Wolfer, Felix Koch and Jan Giesbrecht (ETH Zurich) and the reflectivity measurements were conducted by Dr. Mariano Campoy-Quiles (ICMAB, Barcelona). Furthermore, the author is indebted to the following people for guide and support with the use of the characterization methods described in this thesis: Dr. Monisha Philips and Dr. Rory Wilson (Queen Mary University of London) for help with differential scanning calorimetry (DSC), particle sizer, viscometer and wide-angle X-ray diffractometer; Magda Gonçalves, Phil May, David Sparrowe and Dr. Katie Patterson (Merck Chemicals, Southampton) for help with the Dimatix ink-jet printer.

## 1.7. References

1. J. A. Rogers, Z. Bao, Printed plastic electronics and paperlike displays, *J. Polym. Sci., Part A: Polym. Chem.* **2002**, *40*, 3327.
2. H. Sirringhaus, materials and applications for solution-processed organic field-effect transistors, *Proc. IEEE* **2009**, *97*, 1570.
3. J. K. Borchardt, Developments in organic displays, *Mater. Today* **2004**, *7*, 42.

4. E. Cantatore, T. C. T. Geuns, G. H. Gelinck, E. van Veenendaal, A. F. A. Gruijthuijsen, L. Schrijnemakers, S. Drews, D. M. de Leeuw, A 13.56-MHz RFID system based on organic transponders, *IEEE J. Solid-State Circuits* **2007**, *42*, 84.
5. R. Rotzoll, S. Mohapatra, V. Olariu, R. Wenz, M. Grigas, K. Dimmler, O. Shchekin, A. Dodabalapur, Radio frequency rectifiers based on organic thin-film transistors, *Appl. Phys. Lett.* **2006**, *88*, 123502.
6. S. Steudel, K. Myny, V. Arkhipov, C. Deibel, S. De Vusser, J. Genoe, P. Heremans, 50MHz rectifier based on an organic diode, *Nat. Mater.* **2005**, *4*, 597.
7. M. Berggren, D. Nilsson, N. D. Robinson, Organic materials for printed electronics, *Nat. Mater.* **2007**, *6*, 3.
8. G. H. Gelinck, H. E. A. Huitema, E. Van Veenendaal, E. Cantatore, L. Schrijnemakers, J. Van der Putten, T. C. T. Geuns, M. Beenhakkers, J. B. Giesbers, B. H. Huisman, E. J. Meijer, E. M. Benito, F. J. Touwslager, A. W. Marsman, B. J. E. Van Rens, D. M. De Leeuw, Flexible active-matrix displays and shift registers based on solution-processed organic transistors, *Nat. Mater.* **2004**, *3*, 106.
9. H. E. A. Huitema, G. H. Gelinck, J. van der Putten, K. E. Kuijk, C. M. Hart, E. Cantatore, P. T. Herwig, A. van Breemen, D. M. de Leeuw, Plastic transistors in active-matrix displays - The handling of grey levels by these large displays paves the way for electronic paper, *Nature* **2001**, *414*, 599.



10. H. Shirakawa, E. J. Louis, A. G. MacDiarmid, C. K. Chiang, A. J. Heeger, Synthesis of electrically conducting organic polymers: halogen derivatives of polyacetylene,  $(\text{CH})_x$ , *J. Chem. Soc., Chem. Commun.* **1977**, 474, 578.
11. D. Fichou, G. Horowitz, Molecular and polymer semiconductors, conductors, and superconductors: overview, *Encyclopedia of Materials: Science and Technology*, **2001**, 1<sup>st</sup> Edition, 5748.
12. A. Pron, P. Rannou, Processible conjugated polymers: from organic semiconductors to organic metals and superconductors, *Prog. Polym. Sci.* **2002**, 27, 135.
13. R. McNeil, R. Siudak, J. H. Wardlaw, D. E. Weiss, Electron conduction in polymers: 1. The chemical structure of polypyrrole, *Aust. J. Chem.* **1963**, 16, 1056.
14. B. A. Bolto, D. E. Weiss, Electron conduction in polymers: 2. The electrochemical reduction of polypyrrole at controlled potential, *Aust. J. Chem.* **1963**, 16, 1076.
15. B. A. Bolto, R. McNeil, D. E. Weiss, Electronic conduction in polymers: 3. Electronic properties of polypyrrole, *Aust. J. Chem.* **1963**, 16, 1090.
16. C. W. Tang, S. A. Vanslyke, Organic electroluminescent diodes, *Appl. Phys. Lett.* **1987**, 51, 913.
17. H. Koezuka, A. Tsumura, T. Ando, Field-effect transistor with polythiophene thin-film, *Syn. Met.* **1987**, 18, 699.
18. J. H. Burroughes, C. A. Jones, R. H. Friend, New semiconductors device physics in polymer diodes and transistors, *Nature* **1988**, 335, 137.

19. A. R. Brown, A. Pomp, C. M. Hart, D. M. de Leeuw, Logic gates made from polymer transistors and their use in ring oscillators, *Science* **1995**, *270*, 972.
20. F. Garnier, G. Horowitz, D. Fichou, Conjugated polymers and oligomers as active material for electronic devices, *Synth. Met.* **1989**, *28*, C705.
21. D. Fichou, G. Horowitz, Y. Nishikitani, F. Garnier, Semiconducting conjugated oligomers for molecular electronics, *Synth. Met.* **1989**, *28*, C723.
22. J. E. Anthony, D. L. Eaton, S. R. Parkin, A road map to stable, soluble, easily crystallized pentacene derivatives, *Org. Lett.* **2002**, *4*, 15.
23. J. E. Anthony, M. Heeney, B. S. Ong, Synthetic aspects of organic semiconductors, *MRS Bull.* **2008**, *33*, 698.
24. J. E. Anthony, J. S. Brooks, D. L. Eaton, S. R. Parkin, Functionalized pentacene: improved electronic properties from control of solid-state order, *J. Am. Chem. Soc.* **2001**, *123*, 9482.
25. T. Yamamoto, K. Sanechika, A. Yamamoto, Preparation of thermostable and electric-conducting poly(2,5-thienylene), *J. Polym. Sci., Part C: Polym. Lett.* **1980**, *18*, 9.
26. J. H. Edwards, W. J. Feast, A new synthesis of poly(acetylene), *Polymer* **1980**, *21*, 595.
27. A. Afzali, C. D. Dimitrakopoulos, T. O. Graham, Photosensitive pentacene precursor: Synthesis, photothermal patterning, and application in thin-film transistors, *Adv. Mater.* **2003**, *15*, 2066.

28. P. T. Herwig, K. Mullen, A soluble pentacene precursor: synthesis, solid-state conversion into pentacene and application in a field-effect transistor, *Adv. Mater.* **1999**, *11*, 480.
29. R. L. Elsenbaumer, K. Y. Jen, R. Oboodi, Processible and environmentally stable conducting polymers, *Synth. Met.* **1986**, *15*, 169.
30. R. D. McCullough, R. D. Lowe, Enhanced electrical-conductivity in regioselectively synthesized poly(3-alkylthiophenes), *J. Chem. Soc., Chem. Commun.* **1992**, *1*, 70.
31. A. Facchetti, Semiconductors for organic transistors, *Mater. Today* **2007**, *10*, 28.
32. A. Salleo, Charge transport in polymeric transistors, *Mater. Today* **2007**, *10*, 38.
33. I. McCulloch, M. Heeney, C. Bailey, K. Genevicius, I. Macdonald, M. Shkunov, D. Sparrowe, S. Tierney, R. Wagner, W. M. Zhang, M. L. Chabinyc, R. J. Kline, M. D. McGehee, M. F. Toney, Liquid-crystalline semiconducting polymers with high charge-carrier mobility, *Nat. Mater.* **2006**, *5*, 328.
34. B. H. Hamadani, D. J. Gundlach, I. McCulloch, M. Heeney, Undoped polythiophene field-effect transistors with mobility of  $1 \text{ cm}^2 \text{ V}^{-1} \text{ s}^{-1}$ , *Appl. Phys. Lett.* **2007**, *91*, 243512.
35. T. Umeda, D. Kumaki, S. Tokito, Surface-energy-dependent field-effect mobilities up to  $1 \text{ cm}^2 \text{ V}^{-1} \text{ s}^{-1}$  for polymer thin-film transistor, *J. Appl. Phys.* **2009**, *105*, 024516.
36. J. W. P. Lin, L. P. Dudek, Synthesis and properties of poly(2,5-thienylene), *J. Polym. Sci., Part A: Polym. Chem.* **1980**, *18*, 2869.

37. K. Y. Jen, M. R. Oboodi, R. L. Elsenbaumer, Processible and environmentally stable conducting polymers, *Abstr. Papers Am. Chem. Soc.* **1985**, *190*, 17.
38. H. Sirringhaus, P. J. Brown, R. H. Friend, M. M. Nielsen, K. Bechgaard, B. M. W. Langeveld-Voss, A. J. H. Spiering, R. A. J. Janssen, E. W. Meijer, P. Herwig, D. M. de Leeuw, Two-dimensional charge transport in self-organized, high-mobility conjugated polymers, *Nature* **1999**, *401*, 685.
39. H. L. Jimison, M. F. Toney, I. McCulloch, M. Heeney, A. Salleo, Charge-transport anisotropy due to grain boundaries in directionally crystallised thin films of regioregular poly(3-hexylthiophene), *Adv. Mater.* **2009**, *21*, 1.
40. M. Heeney, C. Bailey, K. Genevicius, M. Shkunov, D. Sparrowe, S. Tierney, I. McCulloch, Stable polythiophene semiconductors incorporating thieno[2,3-b]thiophene, *J. Am. Chem. Soc.* **2005**, *127*, 1078.
41. I. McCulloch, M. Heeney, M. L. Chabinyc, D. DeLongchamp, R. J. Kline, M. Coelle, W. Duffy, D. Fischer, D. Gundlach, B. Hamadani, R. Hamilton, L. Richter, A. Salleo, M. Shkunov, D. Sparrowe, S. Tierney, W. Zhong, Semiconducting thienothiophene copolymers: design, synthesis, morphology, and performance in thin-film organic transistors, *Adv. Mater.* **2009**, *21*, 1091.
42. M. L. Chabinyc, Characterization of semiconducting polymers for thin film transistors, *J. Vac. Sci. Technol., B* **2008**, *26*, 445.
43. P. Brocorens, A. Van Vooren, M. L. Chabinyc, M. F. Toney, M. Shkunov, M. Heeney, I. McCulloch, J. Cornil, R. Lazzoroni, Solid-state

- supramolecular organization of polythiophene chains containing thienothiophene units, *Adv. Mater.* **2009**, *21*, 1193.
44. T. Umeda, S. Tokito, D. Kumaki, High-mobility and air-stable organic thin-film transistors with highly ordered semiconducting polymer films, *J. Appl. Phys.* **2007**, *101*, 054517.
45. D. M. DeLongchamp, R. J. Kline, Y. Jung, E. K. Lin, D. A. Fischer, D. J. Gundlach, S. K. Cotts, A. J. Moad, L. J. Richter, M. F. Toney, M. Heeney, I. McCulloch, Molecular basis of mesophase ordering in a thiophene-based copolymer, *Macromolecules* **2008**, *41*, 5709.
46. I. W. Hwang, J. Y. Kim, S. Cho, J. Yuen, N. Coates, K. Lee, M. Heeney, I. McCulloch, D. Moses, A. J. Heeger, Bulk heterojunction materials composed of poly(2,5-bis(3-tetradecylthiophen-2-yl)thieno[3,2-b] thiophene): ultrafast electron transfer and carrier recombination, *J. Phys. Chem. C* **2008**, *112*, 7853.
47. W. Brütting, *Physics of Organic Semiconductors*, Wiley-VCH, Weinheim, **2005**.
48. Z. Bao, J. Locklin, *Organic Field-Effect Transistors*, CRC Press, Boca Raton, **2007**.
49. Y. Shirota, H. Kageyama, Charge carrier transporting molecular materials and their applications in devices, *Chem. Rev.* **2007**, *107*, 953.
50. G. Horowitz, Organic field-effect transistors, *Adv. Mater.* **1998**, *10*, 365.
51. A. M. Ballantyne, J. S. Wilson, J. Nelson, D. D. C. Bradley, J. R. Durrant, M. Heeney, W. Duffy, I. McCulloch, TOF mobility measurements in pristine films of P3HT: control of hole injection and influence of film thickness, *Organic Photovoltaics VII* **2006**, 6334, U21.

52. J. Bardeen, Surface states and rectification at a metal semi-conductor contact, *Phys. Rev.* **1947**, *71*, 717.
53. W. H. Brattain, W. Shockley, Density of surface states on silicon deduced from contact potential measurements, *Phys. Rev.* **1947**, *72*, 345.
54. J. Bardeen, Semiconductor research leading to the point contact transistor, *Nobel Lecture December 11*, **1956**.
55. D. Khang, M. M. Atalla, in *IRE Solid-State Devices Res. Conf*, Carnegie Institute of Technology, Pittsburg, **1960**.
56. A. R. Brown, C. P. Jarrett, D. M. de Leeuw, M. Matters, Field-effect transistors made from solution-processed organic semiconductors, *Synth. Met.* **1997**, *88*, 37.
57. G. Horowitz, Organic thin film transistors: From theory to real devices, *J. Mater. Res.* **2004**, *19*, 1946.
58. G. Horowitz, R. Hajlaoui, R. Bourguiga, M. Hajlaoui, Theory of the organic field-effect transistor, *Syn. Met.* **1999**, *101*, 401.
59. H. Sirringhaus, Device physics of solution-processed organic field-effect transistors, *Adv. Mater.* **2005**, *17*, 2411.
60. M. C. Hamilton, S. Martin, J. Kanicki, Field-effect mobility of organic polymer thin-film transistors, *Chem. Mater.* **2004**, *16*, 4699.
61. Y. M. Sun, Y. Q. Liu, D. B. Zhu, Advances in organic field-effect transistors, *J. Mater. Chem.* **2005**, *15*, 53.
62. T. A. Skotheim, J. R. Reynolds, *Handbook of Conducting Polymers, (Processing and Applications)*, CRC Press, Boca Raton, **2007**.

63. F. C. Krebs, Fabrication and processing of polymer solar cells: A review of printing and coating techniques, *Sol. Energy Mater. Sol. Cells* **2009**, *93*, 394.
64. H. Klauk, *Organic Electronics*, WILEY-VCH, Weinheim, **2006**.
65. A. A. Tracton, *Coatings Technology (Fundamentals, Testing and Processing Techniques)*, CRC Press, Boca Raton **2007**.
66. W. Clemens, I. Fix, J. Ficker, A. Knobloch, A. Ullmann, From polymer transistors toward printed electronics, *J. Mater. Res.* **2004**, *19*, 1963.
67. P. Calvert, Inkjet printing for materials and devices, *Chem. Mater.* **2001**, *13*, 3299.
68. R. A. Street, W. S. Wong, S. E. Ready, I. L. Chabinyk, A. C. Arias, S. Limb, A. Salleo, R. Lujan, Jet printing flexible displays, *Mater. Today* **2006**, *9*, 32.
69. H. Sirringhaus, T. Kawase, R. H. Friend, T. Shimoda, M. Inbasekaran, W. Wu, E. P. Woo, High-resolution inkjet printing of all-polymer transistor circuits, *Science* **2000**, *290*, 2123.
70. K. E. Paul, W. S. Wong, S. E. Ready, R. A. Street, Additive jet printing of polymer thin-film transistors, *Appl. Phys. Lett.* **2003**, *83*, 2070.
71. A. C. Arias, S. E. Ready, R. Lujan, W. S. Wong, K. E. Paul, A. Salleo, M. L. Chabinyk, R. Apte, R. A. Street, Y. Wu, P. Liu, B. Ong, All jet-printed polymer thin-film transistor active-matrix backplanes, *Appl. Phys. Lett.* **2004**, *85*, 3304.
72. S. E. Burns, P. Cain, J. Mills, J. Z. Wang, H. Sirringhaus, Inkjet printing of polymer thin-film transistor circuits, *MRS Bull.* **2003**, *28*, 829.

73. T. Kawase, T. Shimoda, C. Newsome, H. Sirringhaus, R. H. Friend, Inkjet printing of polymer thin film transistors, *Thin Solid Films* **2003**, 438, 279.
74. C. N. Hoth, S. A. Choulis, P. Schilinsky, C. J. Brabec, High photovoltaic performance of inkjet printed polymer: Fullerene blends, *Adv. Mater.* **2007**, 19, 3973.
75. C. N. Hoth, P. Schilinsky, S. A. Choulis, C. J. Brabec, Printing highly efficient organic solar cells, *Nano Lett.* **2008**, 8, 2806.



## Chapter 2

### Structure control of liquid-crystalline polymer semiconductors based on poly(2,5-bis(3-dodecylthiophen-2-yl)thieno[3,2-*b*]thiophene) (pBTTT-C<sub>12</sub>)

#### 2.1. Introduction

Polymeric semiconductors have been extensively studied due to their promising electronic and optical properties.<sup>1, 2</sup> Liquid-crystalline polymers are a particularly interesting sub-class of semiconducting polymers, because of their ability to influence macro- and microscopic order by processing within the mesophase.<sup>1, 3-5</sup> A recent class of liquid-crystalline polymers that has attracted widespread interest are poly(2,5-bis(3-alkylthiophen-2-yl)thieno[3,2-*b*] thiophene)s, pBTTTs (Figure 1a, inset).<sup>6, 7</sup> Charge-carrier mobilities exceeding  $1 \text{ cm}^2 \text{ V}^{-1} \text{ s}^{-1}$  have been demonstrated for these polymers in field-effect transistor devices,<sup>8, 9</sup> and blends of pBTTTs with [6,6]-phenyl C<sub>61</sub>-butyric acid methyl ester PCBM have shown promising organic photovoltaic (OPV) performance.<sup>10, 11</sup>

We demonstrate in this chapter how the bulk charge-transport properties of the organic semiconductor poly(2,5-bis(dodecylthiophen-2-yl)thieno[3,2-*b*] thiophene), pBTTT-C<sub>12</sub>, can be influenced by annealing in the mesophase, over a period of hours realising good bulk charge transport in the out-of-plane directions. This is contrary to in-plane charge transport measured in thin-film field-effect structures, for which it was shown that annealing times of 10 minutes and less are often

sufficient to enhance device performance.<sup>6</sup> This improved bulk, out-of-plane charge transport can be attributed to increased order, as deduced from wide-angle X-ray diffraction, UV-vis absorption spectroscopy and a Novikov analysis of the time-of-flight (TOF) photoconductivity measurements data (correlated disorder model).

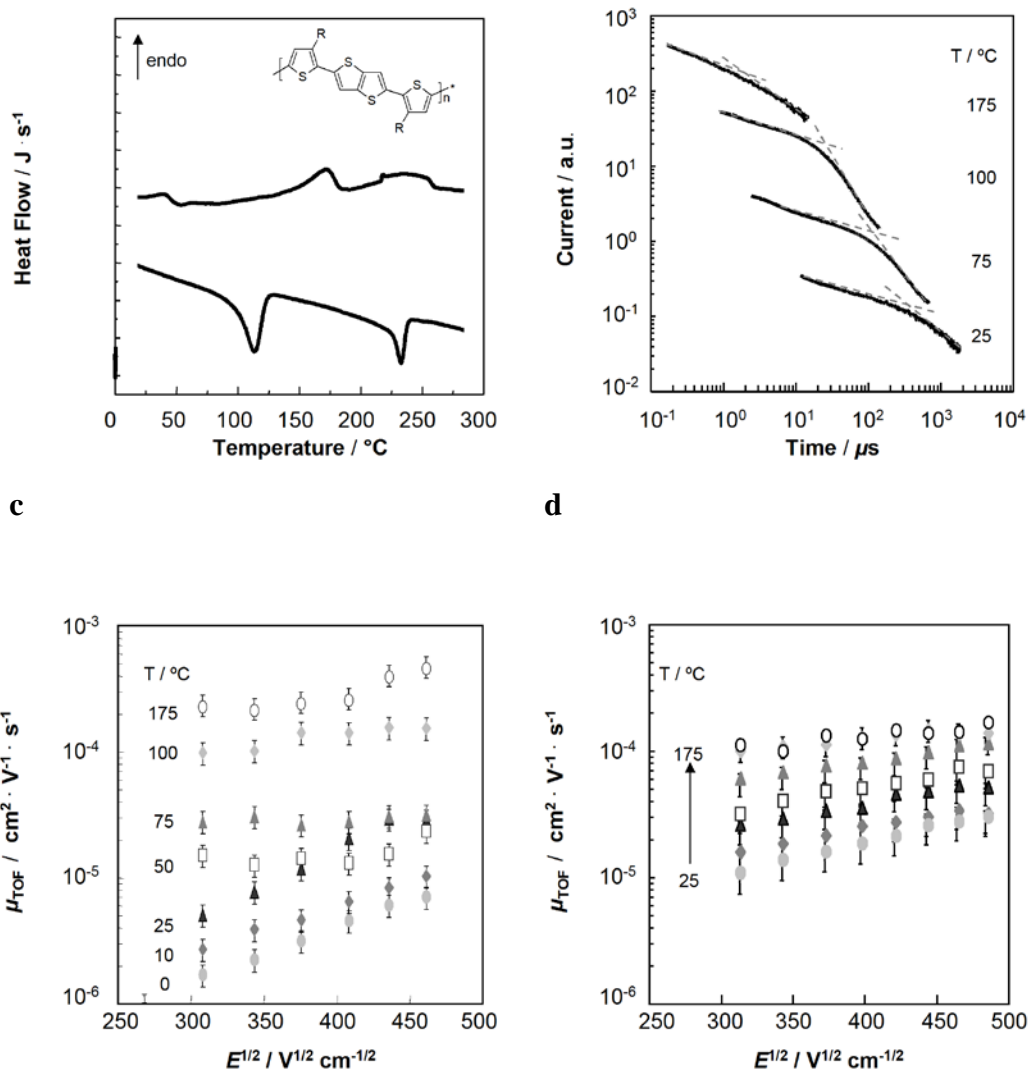
## **2.2. Results and Discussions**

### **2.2.1. Thermal properties**

The thermal behaviour of as-cast films of pBTTT-C<sub>12</sub>, as determined by differential scanning calorimetry (DSC), is shown in Figure 1a. The first endotherm around 50 °C is only observed on the first heating cycle; and as previously reported by DeLongchamp and co-workers, we ascribe this to a metastable phase.<sup>12</sup> Upon further heating, a second endotherm occurs around 150 °C. Previous studies have demonstrated that this transition can be attributed to melting of the side chains to enter a smectic-like phase,<sup>12</sup> and it has been shown that brief annealing within this smectic-like phase gives rise to well-ordered domains upon cooling that exhibit high levels of order as evident from specular and grazing incidence X-ray diffraction, and excellent field-effect mobilities<sup>13, 14</sup> (the transition at 230 °C has been ascribed to backbone melting<sup>15</sup>). It should be noted, though, that these previous studies have focused upon thin films of pBTTTs, on the order of 20-50 nm, which are representative of thin-film field-effect transistor (FET) devices. In this study we are interested in investigating the annealing effects on the bulk out-of-plane transport properties of

**a**

**b**



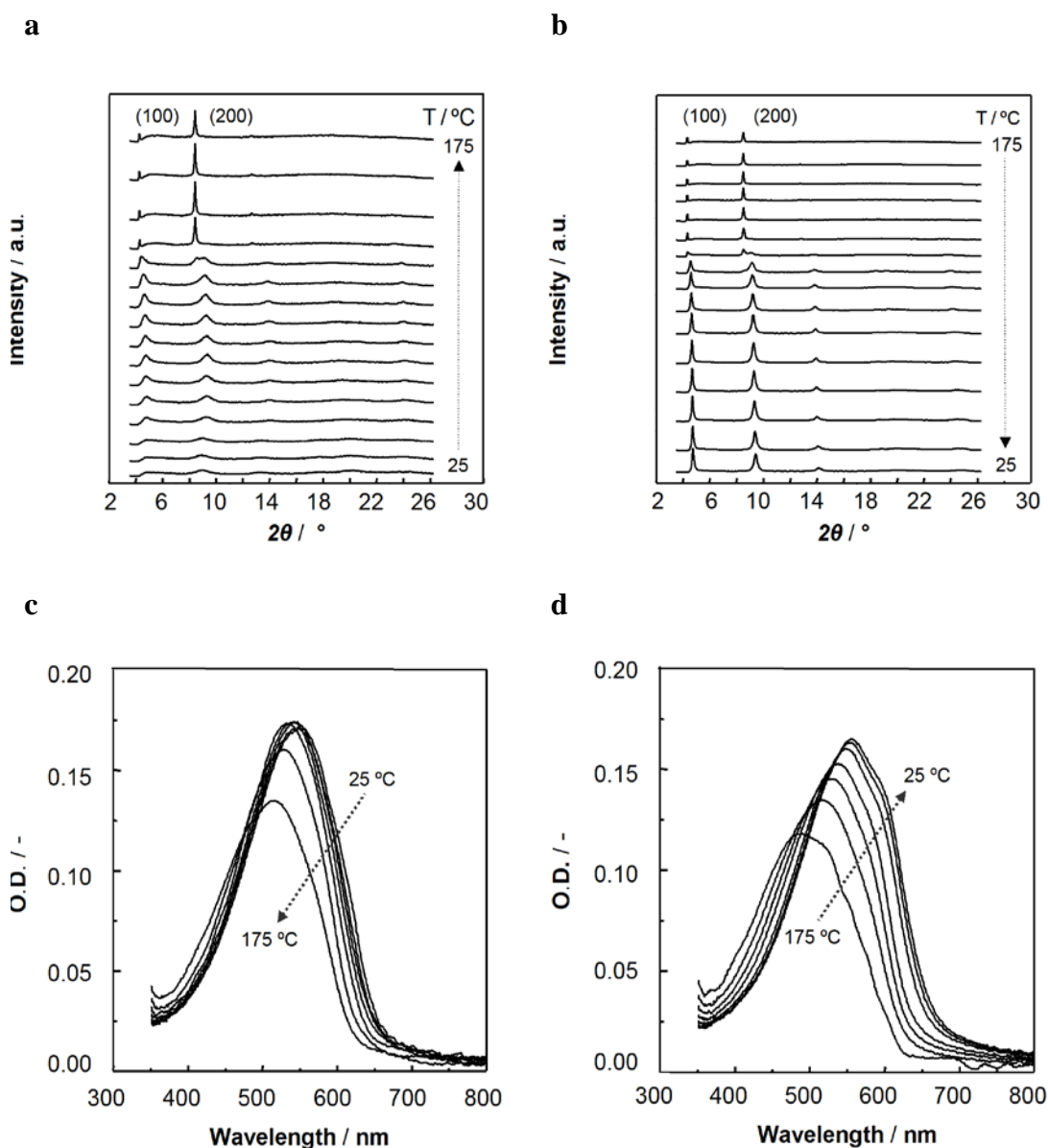
**Figure 1.** (a) Differential scanning calorimetry (DSC) first heating and cooling thermograms of as-cast poly(2,5-bis(3-dodecylthiophen-2-yl)thieno[3,2-*b*]thiophene (pBTTT-C<sub>12</sub>) film. The inset shows the chemical structure of the pBTTT-C<sub>12</sub> derivative utilized in this study. (b) Hole photocurrent transients across as-cast,  $3.9 \pm 0.7 \mu\text{m}$  thick films of pBTTT-C<sub>12</sub> at 46 V bias, measured at the temperatures indicated (*i.e.*, parametric in temperature). Poole-Frenkel plots of hole mobility, measured at the temperatures indicated, of (c) as-cast pBTTT-C<sub>12</sub> (film thickness of  $3.9 \mu\text{m} \pm 0.4 \mu\text{m}$ ), and (d) annealed architectures for (7 hrs/175 °C, film thickness of  $4.7 \pm 0.4 \mu\text{m}$ ). The data for annealed pBTTT-C<sub>12</sub> was recorded in temperature steps of 25 °C. The negligible difference between mobility data obtained for annealed pBTTT-C<sub>12</sub>, measured at 100 °C and 175 °C (light grey diamond symbols and white circles, respectively) is reminiscent of the temperature independent mobilities displayed by liquid-crystalline systems within a given phase (see Ref. 16) and is consistent with the liquid-crystalline like behaviour expected at high temperatures.

pBTTT-C<sub>12</sub>, which are important in diode type devices such as solar cells. To this end, we focused on annealing pBTTT-C<sub>12</sub> in the mesophase (*i.e.* at 175 °C), in order to be able to compare with the previous FET studies.<sup>14,15</sup>

### 2.2.2. Bulk-charge transport

Time-of-flight measurements are an excellent tool to gain understanding of bulk charge-transport phenomena. Figure 1b shows the photoconduction measurements of a few micrometer-thick pBTTT-C<sub>12</sub> films as a function of temperature, from as-cast to 175 °C. We find that upon heating, as-cast pBTTT-C<sub>12</sub> display the expected increase in carrier mobility with temperature (Figure 1b), previously reported also for other liquid-crystalline polymer semiconductor systems.<sup>17</sup> We note that the relatively high dispersion evident in the photocurrents could be exacerbated by the thickness non-uniformity of our pBTTT-C<sub>12</sub> films. The inflection point arrival time, however, is clearly distinguishable and allows us to generate mobility parameters with respect to electric field and temperature (Figure 1c).

A comparison of as-cast and annealed (7 hrs / 175 °C) pBTTT-C<sub>12</sub> films based on Poole-Frenkel plots is shown in Figure 1c,d. Interestingly, and in strong contrast to FET architectures,<sup>14,15</sup> no significant increase in the room temperature bulk mobility is observed in the annealed pBTTT-C<sub>12</sub> structures at high fields ( $E^{1/2} > 400 \text{ (V cm}^{-1}\text{)}^{1/2}$ ; Figure 1c,d). However, annealing in the mesophase had a significant effect on other bulk charge transport properties of pBTTT-C<sub>12</sub>, as deduced from the distinctly different field and temperature behaviour (Figure 1c,d). In fact, as-cast pBTTT-C<sub>12</sub> displayed a significantly stronger temperature dependent

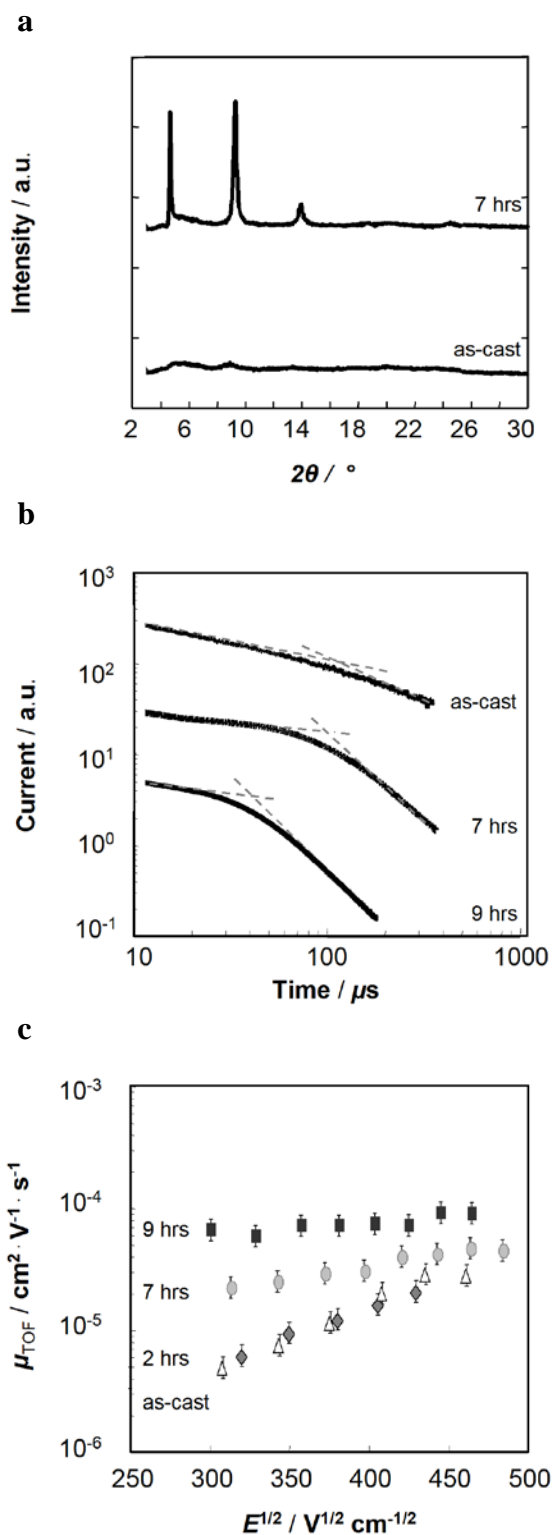


**Figure 2.** Wide-angle X-ray (WAXS) diffractograms of poly(2,5-bis(3-dodecylthiophen-2-yl)thieno[3,2-*b*]thiophene (pBTTT-C<sub>12</sub>) films, recorded for as-cast films, then heated from 25 °C to 175 °C in temperature steps of 10 °C (WAXS) (a) and cooled (b). (c) and (d) Ultraviolet-visible (UV-vis) absorption spectra during heating and subsequent cooling to room temperature (25 °C steps).

mobility than annealed architectures. A more pronounced field-dependence in mobility was also found in as-cast pBTTT-C<sub>12</sub>, which was more distinct at lower temperatures ( $T < 25$  °C).

### 2.2.3. Microstructure

The observations made in TOF may partly be explained by a microstructural analysis based on wide-angle X-ray diffraction and UV-vis absorption spectroscopy (Figure 2a,d). For instance, whilst as-cast pBTTT-C<sub>12</sub> structures were found to be of very low molecular order giving rise to only very weak X-ray diffractions (Figure 2a), WAXS data recorded during heating and cooling cycles (Figure 2a,b respectively) which took in total 6.5 hours each, reveal that upon heating, the wide-angle X-ray diffractions (WAXS) at  $2\theta \approx 8^\circ$  significantly intensified above 140 °C, in agreement with the observed DSC transition. Concomitantly, the half-width of the maxima narrowed and a slight shift to lower diffraction angles is observed (Figure 2a; see also Ref. 12). Subsequent cooling from 175 °C to room temperature led to a more crystalline structure compared to the as-cast films, which is expected to result in a lower field- and temperature dependence of the bulk charge-carrier mobility as observed in TOF (Figure 2b). Similarly, in UV-vis absorption spectroscopy, we find more distinct structures developing after heating pBTTT-C<sub>12</sub> to 175 °C, indicating stronger molecular interactions in such heat-treated structures compared to as-cast architectures (Figure 2c,d).<sup>18</sup> Moreover, WAXS data on films that underwent an identical heat treatment as those used for TOF experiments described above (*i.e.* annealing at 175 °C for 7 hours) illustrate the significant improvement in molecular order that is obtained in such annealed structures compared to as-cast pBTTT-C<sub>12</sub> (Figure 3a).



**Figure 3.** (a) Wide-angle X-ray diffraction of poly(2,5-bis(3-dodecylthiophen-2-yl)thieno[3,2-*b*]thiophene (pBTTT-C<sub>12</sub>) films. (b) Room temperature time-of-flight photocurrent transients for pBTTT-C<sub>12</sub>, as-cast and subjected to a range of annealing times (2, 7 and 9 hrs; film thickness of 3.9 to 5.1  $\mu\text{m}$ ; electric field  $\sim 1.6 \times 10^5 \text{ V cm}^{-1}$ ). (c) Corresponding Poole-Frenkel plots of room temperature hole mobility of as-cast pBTTT-C<sub>12</sub> and thin-film structures that were subjected to different annealing times.

#### 2.2.4. Electronic disorder

Information on the electronic disorder was obtained by analysing the electric field and temperature dependence of the mobility using the correlated disorder model by Novikov and his co-workers.<sup>19</sup> The corresponding transport parameters (energetic disorder,  $\sigma$ , positional disorder,  $\sqrt{\Gamma}$ , prefactor mobility,  $\mu_0$ , and intersite distance,  $R$ ) were extracted for both pBTTT-C<sub>12</sub> films, as-cast and annealed (7 hrs/175 °C).<sup>20, 21</sup> The non-annealed pBTTT-C<sub>12</sub> was found to be considerably disordered, both energetically ( $\sigma = 148$  meV) and positionally ( $\sqrt{\Gamma} = 2.40$ ), having a large intersite distance ( $R = 2.8$  nm). In contrast, annealing resulted in significantly enhanced order ( $\sigma = 98$  meV;  $\sqrt{\Gamma} = 1.46$ ) with a smaller intersite distance ( $R = 1.2$  nm), which is consistent with the carriers being localised to a single monomer unit and with an efficient overlap between these units. This enhancement in positional order,  $\sqrt{\Gamma}$ , is as expected from the observed microscopic changes occurring upon annealing, which DeLongchamp *et al.* attributed to an increase in the backbone order and  $\pi - \pi^*$  stacking.<sup>12</sup> The improvement in energetic order,  $\sigma$ , on the other hand, can be explained as a result of the reduction in the distribution of carrier delocalisation lengths (conjugation lengths) within the sample.<sup>17</sup> We note, though, one internal inconsistency within the model, given the site distances obtained, namely, the larger prefactor mobility calculated for the unannealed sample ( $\mu_0 = 0.088$  cm<sup>2</sup> V<sup>-1</sup> s<sup>-1</sup>) compared to the annealed case ( $\mu_0 = 0.011$  cm<sup>2</sup> V<sup>-1</sup> s<sup>-1</sup>). This remains as yet unexplained.

Unexpectedly and in contrast to the relatively short annealing times required for the thin-film field-effect architectures that were previously reported<sup>6</sup> (ca. 10 mins), we find that extended annealing times are necessary for realizing



good overall bulk, out-of-plane charge transport (Figure 3). As discussed above, annealing times up to 7 hours resulted in a strong qualitative improvement of charge transport in the form of reduced dispersion, consistent with the higher order deduced from the above Novikov analysis as well as with the increased crystallinity evident in WAXS (Figure 3a). Annealing times over 7 hours at 175 °C resulted, in addition, in significantly shorter TOF arrival times compared to as-cast structures and, as a consequence, in higher room temperature hole mobilities (Figure 3b,c). Interestingly, the relative increase in mobility for bulk, out-of-plane charge transport upon annealing is comparable to that observed in FET devices – namely one order of magnitude.<sup>6</sup> Obviously, the absolute mobility values differ greatly ( $\sim 10^{-5}$  cm<sup>2</sup> V<sup>-1</sup> s<sup>-1</sup> in TOF, compared to 0.2–0.6 cm<sup>2</sup> V<sup>-1</sup> s<sup>-1</sup> in FETs), which is consistent with the highly ordered lamella structures reported for pBTTTs.<sup>6</sup>

### 2.3. Conclusions

Clearly, our results show that controlled heat treatment procedures can be exploited to enhance bulk charge transport in this interesting class of materials. This may aid, in future, to optimize the use of pBTTT polymers in electronic devices in which good bulk charge transport is required. Annealing times are longer compared to FETs, which may not be surprising given the need to induce order throughout few micron-thick pBTTT-C<sub>12</sub> structures. As a consequence, a good compromise must be found between optimization in charge transport, molecular order, manufacturing throughput and material degradation due to long-time exposure to elevated temperatures.

## 2.4. Experimental

### 2.4.1. Materials

Poly(2,5-bis(3-dodecylthiophen-2-yl)thieno[3,2-*b*]-thiophene), (pBTTT-C<sub>12</sub>) ( $M_n = 27.9 \text{ kg mol}^{-1}$ ;  $M_w = 51.4 \text{ kg mol}^{-1}$ ), was generously supplied by Merck Chemicals. 1,2,4-trichlorobenzene (TCB) was purchased from Aldrich and used as received.

### 2.4.2. Sample preparation

Homogeneous thin films for time-of-flight (TOF) photoconduction experiments were prepared by first dissolving pBTTT-C<sub>12</sub> (total polymer content: 0.5 wt%) in 1,2,4-trichlorobenzene (TCB) at ~ 80 °C. The hot solutions were then cast onto indium tin oxide (ITO) coated substrates (gold thickness = 50 nm) kept at 50 °C until the solvent had evaporated. This resulted in films of 5 – 6 μm thickness (measured with a Veeco Dektak<sup>3</sup> ST surface profile measuring system). 50 nm thin counter electrodes were then thermally evaporated. For wide-angle X-ray diffraction, thinner films of approximately 0.5 to 2 μm were prepared accordingly, using the same solution concentration. Finally, for temperature-dependent UV-vis absorption spectroscopy, films of thicknesses around ~100 nm were spin-coated from 0.5 wt% hot solution (~ 80 °C) at 500 rpm for 30 seconds followed by 2000 rpm for 30 seconds.

### **2.4.3. Thermal analysis**

Differential scanning calorimetry (DSC) was conducted under nitrogen at a scan rate of  $10\text{ }^{\circ}\text{C min}^{-1}$  with a Mettler Toledo DSC822 instrument. The sample weight was  $\sim 5\text{ mg}$ .

### **2.4.4. Wide-angle X-ray diffraction**

Standard transmission wide-angle X-ray diffraction was carried out with an X'Pert Pro - PAN analytical instrument using  $\text{CuK}_{\alpha}$ -radiation ( $\lambda = 1.5418\text{ \AA}$ ), equipped with an Anton Parr HTK16 furnace which was operated between  $25\text{ }^{\circ}\text{C}$  and  $175\text{ }^{\circ}\text{C}$  at a rate of  $60\text{ }^{\circ}\text{C per minute}$ . Platinum heating strips with Pt/10 % RhPt thermocouple welded to the underside of the strip were utilised to give accurate temperature measurements. To this end, an Anton Parr TCU 2000 temperature control unit to provide temperature control was used.

### **2.4.5. UV-vis absorption spectroscopy**

A Perkin Elmer Lambda 900 spectrophotometer was employed equipped with a temperature-controlled demountable liquid flow cell (TFC-S25). All experiments were conducted under  $\text{N}_2$  atmosphere.

### **2.4.6. Time-of-flight photoconductivity**

All measurements were carried out in a nitrogen atmosphere. The  $6\text{ ns}$ ,  $337\text{ nm}$  wavelength, pulsed output of an EG101 Lambda Physik gas laser provided the optical excitation to create electron-hole pairs within a penetration depth of  $\sim 100\text{ nm}$  of the top electrode in the case for neat pBTTT- $\text{C}_{12}$ , the  $6\text{ ns}$ ,  $532\text{ nm}$  wavelength output of a frequency doubled insert model Nd:YAG laser

provided the optical excitation, as the pBTTT-C<sub>12</sub> displays an absorption peak close to this wavelength. All measurements were carried out under a DC bias from a low noise power supply. The laser pulse intensity was kept sufficiently low. As a consequence, the photogenerated charge was less than 10 % of the charge stored across the sample ( $C \cdot V$ , where  $C$  is the sample capacitance and  $V$  the applied potential), avoiding space-charge effects that would result in a non-uniform electric field. The transient current was measured as a voltage drop across a range of load resistors (typically 47  $\Omega$  for fast signals and 2.31 k $\Omega$  for slow signals) at the input of a gain 11 amplifier whose output was connected to an Agilent Infinium digitizing oscilloscope. Signal averaging (typically over 128 pulses) and background subtraction were performed in order to minimize both random and coherent radio frequency noise. Charge carrier mobility  $\mu_{\text{TOF}}$  was calculated using the expression:

$$\mu_{\text{TOF}} = d^2/V \cdot t_{\text{tr}} \quad (2.1)$$

where  $d$  is the sample thickness and  $t_{\text{tr}}$  the arrival time obtained from a double logarithmic plot of the photocurrent transient, and  $V$  the applied voltage. The electronic response time of the circuit,  $\tau$ , was kept well below the time base of the measurement.

## 2.5. References

1. M. Grell, W. Knoll, D. Lupo, A. Meisel, T. Miteva, D. Neher, H. G. Nothofer, U. Scherf, A. Yasuda, Blue polarized electroluminescence from a liquid-crystalline polyfluorene, *Adv. Mater.* **1999**, *11*, 671.

2. R. J. Kline, M. D. McGehee, Morphology and charge transport in conjugated polymer, *Polymer Reviews* **2006**, *46*, 27.
3. H. Sirringhaus, R. J. Wilson, R. H. Friend, M. Inbasekaran, W. Wu, E. P. Woo, M. Grell, D. D. C. Bradley, Mobility enhancement in conjugated field-effect transistors through chain alignment in a liquid-crystalline phase, *Appl. Phys. Lett.* **2000**, *77*, 406.
4. Z. J. Zheng, K. H. Yim, M. S. M. Saifullah, M. E. Welland, R. H. Friend, J. S. Kim, W. T. S. Huck, Uniaxial alignment of liquid-crystalline conjugated polymers by nanoconfinement, *Nano Lett.* **2007**, *7*, 987.
5. M. Grell, M. Redecker, K. S. Whitehead, D. D. C. Bradley, M. Inbasekaran, E. P. Woo, W. Wu, Monodomain alignment of thermotropic fluorene copolymers, *Liq. Cryst.* **1999**, *26*, 1403.
6. I. McCulloch, M. Heeney, C. Bailey, K. Genevicius, I. MacDonald, M. Shkunov, D. Sparrowe, S. Tierney, R. Wagner, W. Zhang, M. L. Chabinyc, R. J. Kline, M. D. McGehee, M. F. Toney, Liquid-crystalline semiconducting polymers with high charge-carrier mobility, *Nat. Mater.* **2006**, *5*, 328.
7. I. McCulloch, M. Heeney, M. L. Chabinyc, D. M. Delongchamp, R. J. Kline, M. Colle, W. Duffy, D. Fischer, D. Gundlach, B. Hamadani, R. Hamilton, L. Richter, A. Salleo, M. Shkunov, D. Sparrowe, S. Tierney, W. Zhang, Semiconducting thienothiophene copolymers: design, synthesis, morphology and performance in thin-film organic transistors, *Adv. Mater.* **2009**, *21*, 1091.

8. B. H. Hamadani, D. J. Gundlach, I. McCulloch, M. Heeney, Undoped polythiophene field-effect transistor with mobility of  $1 \text{ cm}^2 \text{ V}^{-1} \text{ s}^{-1}$ , *Appl. Phys. Lett.* **2007**, *91*, 243512.
9. T. Umeda, D. Kumaki, S. Tokito, Surface-energy-dependent field effect mobilities up to  $1 \text{ cm}^2 \text{ V}^{-1} \text{ s}$  for polymer thin-film transistor, *J. Appl. Phys.* **2009**, *105*, 024516.
10. J. E. Parmer, A. C. Mayer, B. E. Hardin, S. R. Scully, M. D. McGehee, M. Heeney, I. McCulloch, Organic bulk heterojunction solar cells using poly(2,5-bis(3-tetradecylthiophen-2-yl)thieno[3,2-b]thiophene), *Appl. Phys. Lett.* **2008**, *92*, 113309.
11. I. W. Hwang, J. Y. Kim, S. Cho, J. Yuen, N. Coates, K. Lee, M. Heeney, I. McCulloch, D. Moses, A. J. Heeger, Bulk heterojunction materials composed of poly(2,5-bis(3-tetradecylthiophen-2-yl)thieno[3,2-b] thiophene): ultrafast electron transfer and carrier recombination, *J. Phys. Chem. C* **2008**, *112*, 7853.
12. D. M. DeLongchamp, R. J. Kline, Y. Jung, E. K. Lin, D. A. Fischer, D. J. Gundlach, S. K. Cotts, A. J. Moad, L. J. Richter, M. F. Toney, M. Heeney, I. McCulloch, Molecular basis of mesophase ordering in a thiophene-based copolymer, *Macromolecules* **2008**, *41*, 5709.
13. D. M. DeLongchamp, R. J. Kline, E. K. Lin, D. A. Fischer, L. J. Richter, L. A. Lucas, M. Heeney, I. McCulloch, J. E. Northrup, High carrier mobility polythiophene thin films: structure determination by experiment and theory, *Adv. Mater.* **2007**, *19*, 833.

14. M. L. Chabinyo, M. F. Toney, R. J. Kline, I. McCulloch, M. Heeney, X-ray scattering study of thin films of poly(2,5-bis(3-alkylthiophen-2-yl)thieno[3,2-b]thiophene), *J. Am. Chem. Soc.* **2007**, *129*, 3226.
15. D. M. DeLongchamp, R. J. Kline, Y. Jung, D. S. Germack, E. K. Lin, A. J. Moad, L. J. Richter, M. F. Toney, M. Heeney, I. McCulloch, Controlling the orientation of terraced nanoscale "ribbons" of a poly(thiophene) semiconductor, *ACS Nano* **2009**, *3*, 780.
16. R. J. Baldwin, T. Kreouzis, M. Shkunov, M. Heeney, W. Zhang, I. McCulloch, A comprehensive study of the effect of reactive end groups on the charge carrier transport within polymerized and nonpolymerized liquid-crystals, *J. Appl. Phys.* **2007**, *101*, 23713
17. T. Kreouzis, D. Poplavskyy, S. M. Tuladhar, M. Campoy-Quiles, J. Nelson, A. J. Campbell, D. D. C. Bradley, Temperature and field dependence of hole mobility in poly(9,9-dioctylfluorene), *Phys. Rev. B.* **2006**, *73*, 235201.
18. J. Clark, C. Silva, R. H. Friend, F. C. Spano, Role of intermolecular coupling in the photophysics of disordered organic semiconductors: aggregate emission in regioregular polythiophene, *Phys. Rev. Lett.* **2007**, *98*, 206406
19. S. V. Novikov, D. H. Dunlap, V. M. Kenkre, P. E. Parris, A. V. Vannikov, Essential role of correlations in governing charge transport in disordered organic materials, *Phys. Rev. Lett.* **1998**, *81*, 4472.
20. S. Barard, M. Heeney, L. Chen, M. Colle, M. Shkunov, I. McCulloch, N. Stingelin, M. Philips, T. Kreouzis, Separate charge transport pathways

determined by the time of flight method in bimodal polytriarylamine, *J. Appl. Phys.* **2009**, *105*, 13701.

21. R. U. A. Khan, D. Poplavskyy, T. Kreouzis, D. D. C. Bradley, Hole mobility within arylamine-containing polyfluorene copolymers: a time-of-flight transient-photocurrent study, *Phys. Rev. B.* **2007**, *75*, 35215.



## Chapter 3

### Ink-jet printing of pBTTT

#### 3.1. Introduction

The simplification in manufacturing of organic semiconductor devices is a critically required step towards the realization of flexible, portable electronic applications.<sup>1-6</sup> One prerequisite thereby is to gain the ability to fabricate fundamental microelectronic building blocks, such as thin-film transistors, at significantly lower cost than their prevalent silicon-based counterparts; which generally are produced via elaborate photolithographic and etching procedures, consisting of many sub-let processes, such as photo-resist coating, baking and alike.

Promisingly, first demonstrations of printed organic electronics illustrate the potential of solution-based technologies to realize straight-forward patterning of critical field-effect transistor components.<sup>7-16</sup> Thereby, the process of ink-jet printing allows precise deposition of relevant compounds into pre-defined structures and offers advantages when compared to other printing procedures as this methodology requires relatively undemanding waste fluid management strategies, and provides simple patterning options. Indeed, digital deposition

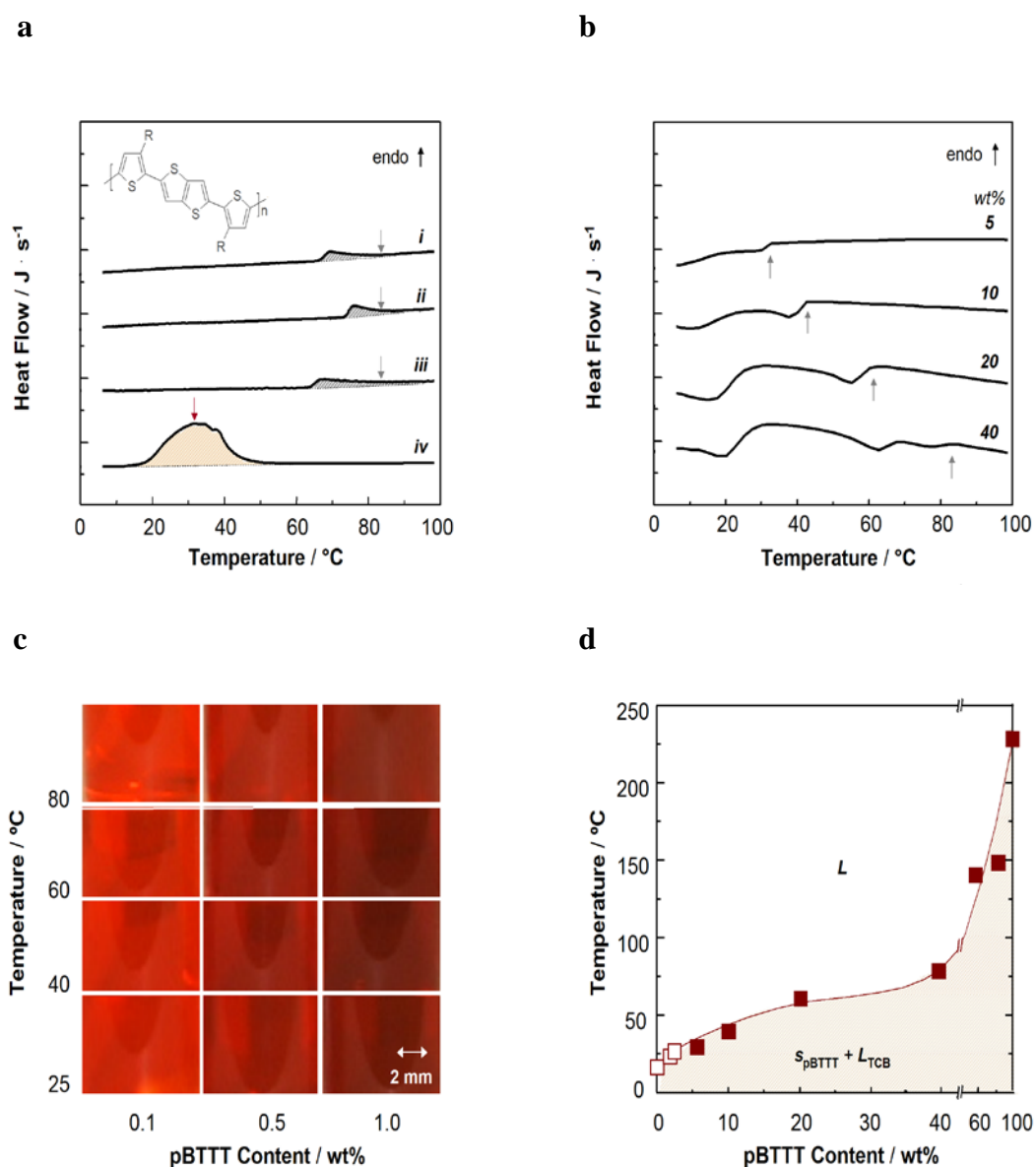
methods promise to reduce - if not entirely eliminate - the need for lithographic patterning steps.

In this chapter, we focus our efforts on ink-jet printing the liquid-crystalline semiconducting polymer, poly(2,5-bis(3-dodecylthiophen-2-yl) thieno [3,2-*b*]thiophene) (pBTTT-C<sub>12</sub>)<sup>17, 18</sup> which has been demonstrated to display hole mobilities  $\mu_{\text{FET}}$  of up to 1 cm<sup>2</sup> V<sup>-1</sup>s<sup>-1</sup> when deposited in an argon-purged atmosphere via spin-coating from hot solutions, followed by optimized annealing procedures. However, pBTTT polymers, which were molecularly tailored for optimizing charge transport and HOMO-LUMO levels, seem to suffer from a number of issues when it comes to ink-jet printing, including low room-temperature solubility in common solvents and thus, the difficulty to formulate printable inks that comprise sufficiently small particles/agglomerates<sup>17, 19</sup> when dispensed into the printing cartridge. In addition, entirely different drying phenomena may occur during solidification of the deposited liquid when compared to, for instance, spin-coating procedures, which can considerably affect the final solid-state microstructure.<sup>20</sup> These issues might severely limit the utility of this interesting class of polymers. Therefore we set out to find suitable solvents that allow preparation of pBTTT-C<sub>12</sub> formulations that fulfil key ink-jet criteria (solution viscosities  $\eta$  of approximately 2 to 20 mPa's; particle diameters  $d < 2 \mu\text{m}$ , and surface tension  $\gamma$  of the droplets of 25 to 50 dynes cm<sup>-1</sup>.<sup>21-25</sup>

## 3.2. Results and Discussions

### 3.2.1. Phase behaviour

In a first set of experiments, the dissolution behaviour of pBTTT-C<sub>12</sub> in a variety of solvents was investigated, including tetralin (THN), indan, 1,2,3,4-tetramethylbenzene (TMB) and 1,2,4-trichlorobenzene (TCB). Differential scanning calorimetry (DSC) analysis revealed for most of these binary systems (0.5 wt% polymer content) endotherms around 70 °C and more (*cf.* Figure 1a; *i*: pBTTT-C<sub>12</sub>/THN, *ii*: pBTTT-C<sub>12</sub>/indan, *iii*: pBTTT-C<sub>12</sub>/TMB), with end-of-peak temperatures indicating full dissolution (highlighted in Figure 1a with grey arrows). Corresponding enthalpies  $\Delta H_{\text{diss}}$  (pBTTT-C<sub>12</sub>) were found to be very similar for all three binaries (respectively, 0.20 J g<sup>-1</sup>, 0.21 J g<sup>-1</sup> and 0.27 J g<sup>-1</sup>; red shaded areas in Figure 1a). In strong contrast, for pBTTT-C<sub>12</sub>/TCB systems (thermogram *iv* in Figure 1a) we observed only a very pronounced, broad endotherm in the temperature range of 20 to 50 °C, which we attribute to the melting of TCB ( $\Delta H_{\text{m}}(\text{TCB}) = 35.80 \text{ J g}^{-1} \gg \Delta H_{\text{diss}}(\text{TCB})$ ) as we first cooled the mixtures to below 0 °C resulting in the solidification of TCB.<sup>26</sup> The dissolution of pBTTT-C<sub>12</sub> in TCB was, however, clearly visible by eye, which resulted in clear, transparent solutions of a dark red colour in the temperature range of 50 – 55 °C for 0.5 wt% pBTTT-C<sub>12</sub>/TCB binaries. Upon further heating, these solutions turned orange at temperatures above 80 °C; a solvatochromic transition that has previously been reported for other thiophene-based polymers.<sup>17, 27</sup> (Note, in our DSC analysis presented in Figure 1a, the dissolution is not discernable as heating from 0 °C first resulted in melting of the TCB, as mentioned above, with the dissolution of pBTTT-C<sub>12</sub> apparently occurring still within the melting range of TCB).



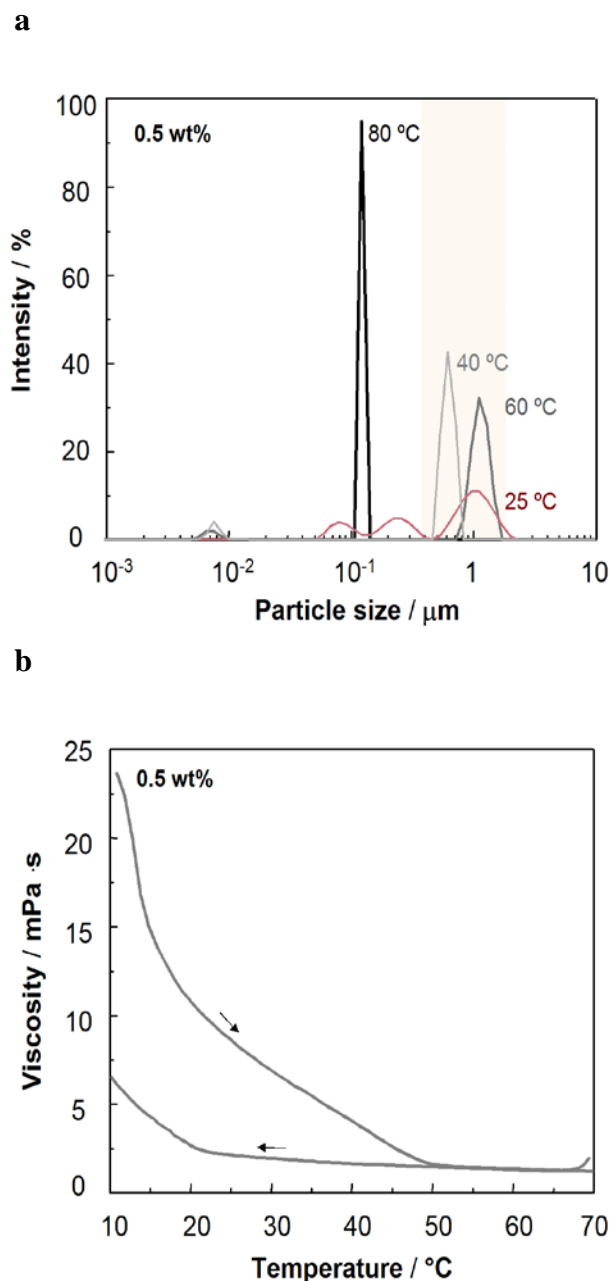
**Figure 1.** (a) Differential scanning calorimetry (DSC) second heating thermograms of poly(2,5-bis(3-dodecylthiophen-2-yl)thieno[3,2-*b*]thiophene (pBTTT-C<sub>12</sub>) (R=C<sub>12</sub>H<sub>25</sub>; see inset) in selected organic solvents: *i*) tetralin (THN), *ii*) indan, *iii*) 1,2,3,4-tetramethyl-benzene (TMB) and *iv*) 1,2,4-trichlorobenzene (TCB) (polymer content = 0.5 wt%). pBTTT-C<sub>12</sub> fully dissolved at temperatures indicated with arrows. (b) Typical DSC second cooling thermograms for pBTTT-C<sub>12</sub>/TCB binaries of a polymer content of, respectively 5, 10, 20 and 40 wt%. On-set of solidification of pBTTT-C<sub>12</sub> is indicated with arrows (deduced from the onset of the relevant exotherms). (c) Photographs of dilute pBTTT-C<sub>12</sub>/TCB solutions, recorded during cooling from 80 °C to room temperature. (d) Corresponding crystallization temperature/composition diagram of the pBTTT-C<sub>12</sub>/TCB binary, as deduced from DSC analysis (■) and visual inspection for more dilute systems (□).

Crystallization temperatures were deduced from the onset of relevant exotherms (also indicated with arrows, Figure 1b). To this end, we focused on pBTTT-C<sub>12</sub>/TCB binaries, as very recently, complementary circuits have been demonstrated using this system.<sup>28</sup> Only for highly concentrated systems (polymer content  $\geq 5$  wt%) clearly discernable exotherms were found. Thus, for more dilute systems, we identified solidification temperatures by visual inspections of such pBTTT-C<sub>12</sub>/TCB solutions during cooling from 80 °C to room temperature (Figure 1c). Reassuringly, no conspicuous aggregation was observed by eye for all binaries of polymer content  $<5$  wt%, with the solutions staying clear and transparent (Figure 1c). In fact, more dilute solutions ( $< 0.1$  wt%) remained orange even when cooling to room temperature, whilst 0.5 and 1.0 wt% solutions adopted a dark red colour.

The differential thermal calorimetry analysis (filled symbols) and the visual observations during cooling of pBTTT-C<sub>12</sub>/TCB reported above (open symbols) allowed us, therefore, to deduce the temperature/composition cooling diagram over a broad range of concentrations of the pBTTT-C<sub>12</sub>/TCB binary (Figure 1d). Clearly, pBTTT-C<sub>12</sub> does not precipitate into visibly large particles even at temperatures below 50 °C for TCB solutions comprising 10 wt% polymer content and less, which promises, for instance, simple and straight-forward transfer of such pBTTT-C<sub>12</sub>/TCB solution into printing cartridges.

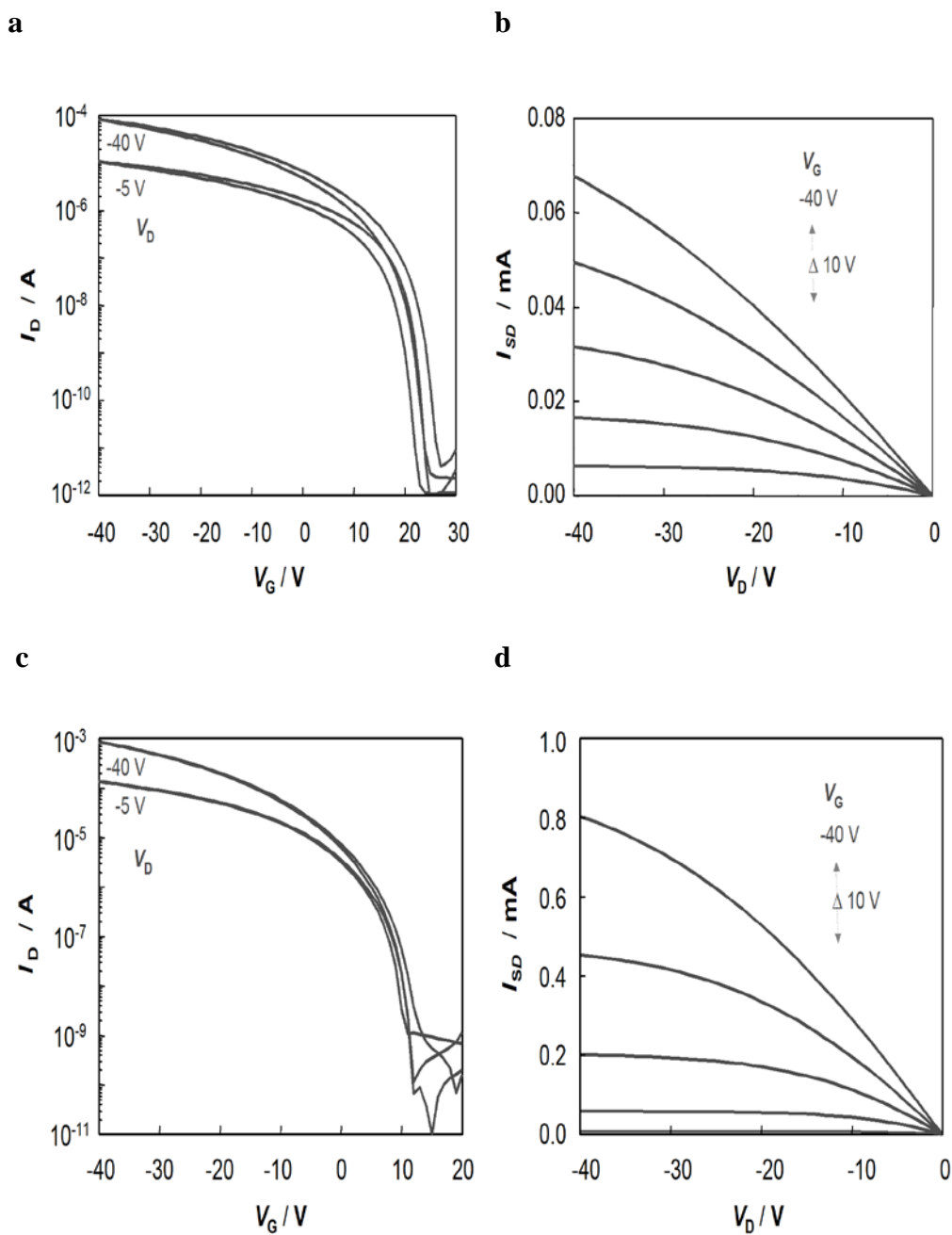
### **3.2.2. pBTTT-C<sub>12</sub> ink properties**

The latter observations were quantified by light-scattering experiments. These revealed that only particles of dimensions of less than 2  $\mu\text{m}$  formed in dilute pBTTT-C<sub>12</sub>/TCB solutions when cooling from 80 °C to room temperature

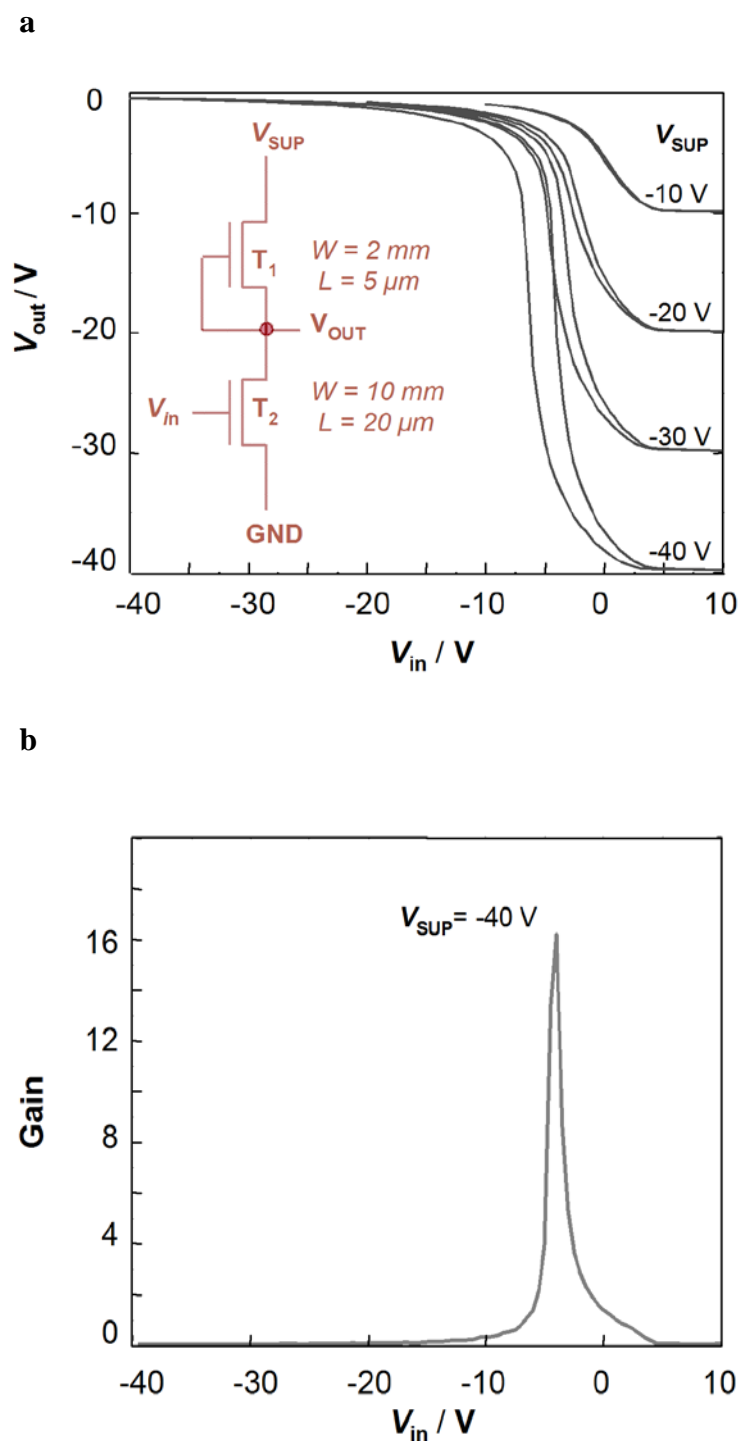


**Figure 2.** (a) Particle size analysis of 0.5 wt% poly(2,5-bis(3-dodecylthiophen-2-yl)thieno[3,2-*b*]thiophene (pBTTT- $C_{12}$ ) in 1,2,4-trichlorobenzene (TCB), during cooling from 80 °C to room temperature, measured at the temperatures indicated. (b) Viscosity of such solutions as a function of temperature.

( $c_{\text{pBTTT-}C_{12}} = 0.5 \text{ wt\%}$ ; Figure 2a), thus, fulfilling general ink-jet requirements. In addition, the room temperature viscosities of 3 to 5 mPa·s for 0.5 wt% pBTTT- $C_{12}$ /TCB solutions were found to be as desired for the ink-jet printing process (Figure 2b).



**Figure 3.** (a) and (b) Transfer and output characteristics of poly(2,5-bis(3-dodecylthiophen-2-yl)thieno[3,2-*b*]thiophene pBTTT-C<sub>12</sub> thin-film field-effect transistors, inkjet-printed from 1,2,4-trichlorobenzene TCB (0.5 wt% pBTTT-C<sub>12</sub>), and for comparison (c) and (d) spin-coated from hot solutions (also 0.5 wt%, in TCB, channel length  $L = 10 \mu\text{m}$ ; channel width  $W = 10 \mu\text{m}$ ).



**Figure 4.** (a) Transfer characteristics of a voltage inverter consisting of two integrated ink-jet printed poly(2,5-bis(3-dodecylthiophen-2-yl)thieno[3,2-*b*]thiophene (pBTTT-C<sub>12</sub>) field-effect transistors (FETs). The channel length ( $L$ ) and width ( $W$ ) used were  $L = 5 \mu\text{m}$  and  $W = 2 \text{ mm}$  for transistor 1 (*i.e.* the load transistor) and  $L = 20 \mu\text{m}$  and  $W = 10 \text{ mm}$  for transistor 2 (*i.e.* the driving transistor). Inset shows the inverter circuitry used. (b) Signal gain as a function of  $V_{\text{IN}}$  for the inverter measured at  $V_{\text{SUP}} = -40 \text{ V}$ .



### 3.2.3. Discrete field-effect transistor devices

We set out to inkjet-print pBTTT-C<sub>12</sub> devices, focusing initially on discrete devices. To this end, bottom-gate/bottom-contact pBTTT-C<sub>12</sub> field-effect transistors were ink-jet printed in light and air from 0.5 wt% TCB solutions onto photolithographically patterned transistor structures. In addition, control devices were fabricated in a nitrogen atmosphere by spin-coating onto identically treated substrates. Typical transfer and output characteristics for the inkjet printed FETs, measured in vacuum (10<sup>-4</sup> mbar), are shown in (Figure 3a). The channel current can be modulated (on/off current ratio) by more than 6 orders of magnitude (Figure 3a). The operating characteristics show negligible hysteresis between forward and backward scans despite the fact that pBTTT-C<sub>12</sub> was printed in light and air. Due to the patterned deposition of the semiconductor, the ink-jet printed devices displayed typically lower current leakage when compared to the spin-coated control FETs. Indeed, the gate-leakage currents improved in the printed FETs by one to two orders of magnitude.

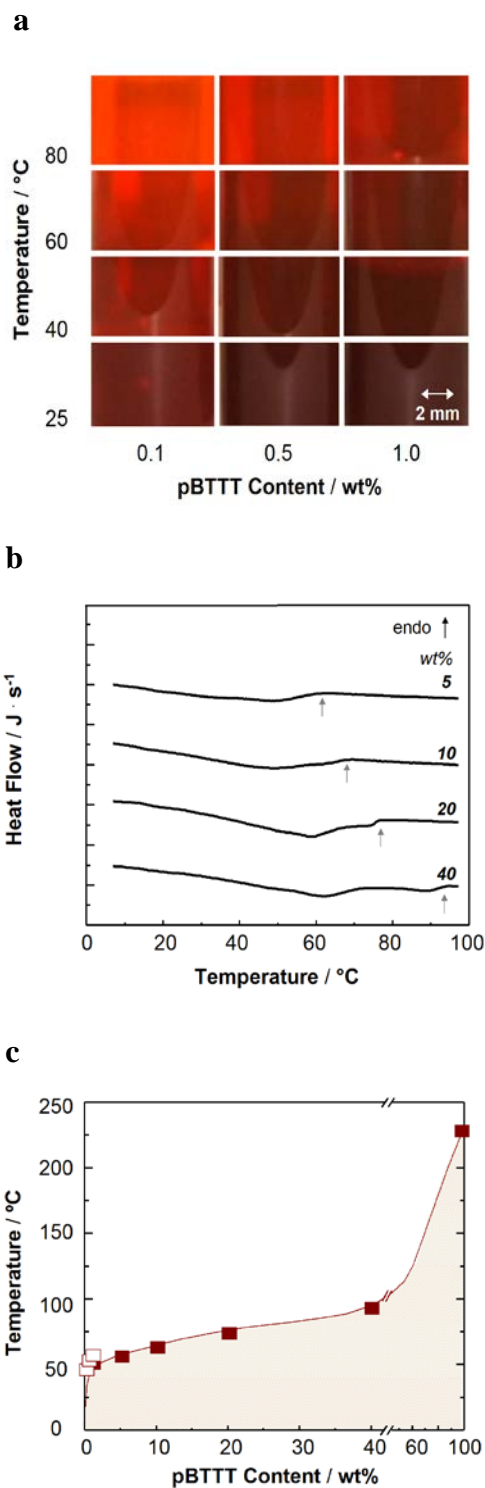
Field-effect mobilities were deduced from the saturation regime ( $V_D = -40$  V) and were found to be in the range of 0.01 to up to 0.1 cm<sup>2</sup> V<sup>-1</sup> s<sup>-1</sup> for the printed structures. Possibly due to the fact the printing was conducted in light and air, these mobilities are somewhat lower than those calculated for the spin-coated, reference devices fabricated in a protective N<sub>2</sub> environment on substrates identical to those used for ink-jetting (0.05 to 0.2 cm<sup>2</sup> V<sup>-1</sup> s<sup>-1</sup>). Nonetheless, the performance of our ink-jet printed devices are sufficiently high as a first demonstration that this technology is suitable also for the

patterned deposition of rigid-rod-like, liquid-crystalline polymer semiconductors, such as pBTTTs.

The larger mobility spread in ink-jetted polymer films indicates that the thin-film architectures at the interface to the dielectric were less homogeneous in the printed transistors. Evidently, the nature of the solvent, substrate temperature during printing, droplet size, drop spacing and the line width have to be controlled carefully in order to realize optimum film forming- and crystallization conditions for the respective polymer; which will be investigated in more detail in future.

#### **3.2.4. Unipolar inverters**

Integration of ink-jet printed discrete devices resulted in unipolar inverter circuits that exhibit high gain (i.e.  $>16$ ) and negligible hysteresis (Figure 4). We note, though, that the operation over two quadrants and the low noise margins are problematic for practical application in electronic circuits. This behaviour is attributed to the large positive threshold voltage and the normally “on” nature of pBTTT transistors. This undesirable feature of our printed inverters can, though, be avoided by optimizing the passivation layer at the dielectric-semiconductor interface to adjust the threshold voltage of discrete FETs.<sup>29</sup>



**Figure 5.** (a) Photographs of dilute poly(2,5-bis(3-dodecylthiophen-2-yl)thieno[3,2-*b*]thiophene pBTTT-C<sub>12</sub>/tetralin solutions, recorded during cooling from 80 °C to room temperature. (b) Typical second cooling thermograms for pBTTT-C<sub>12</sub>/tetralin binaries of a polymer content of, respectively 5, 10, 20 and 40 wt%. Onset of solidification of pBTTT-C<sub>12</sub> is indicated with arrows (deduced from the onset of the relevant exotherms). (c) Corresponding crystallization temperature/composition diagram of the pBTTT-C<sub>12</sub>/tetralin binary, as deduced from DSC analysis (■) and visual inspection for more dilute systems (□).

### 3.3. Conclusions

In summary, we have demonstrated that ink-jet printing is a suitable technique for the patterning of also rigid-rod-like liquid-crystalline semiconducting polymers. To this end, we used 1,2,4-trichlorobenzene as model solvent for pBTTT polymers, yet initial experiments promise that technologically more acceptable solvents, such as tetralin, may also be utilized for this purpose (*cf.* the promising solidification characteristics of pBTTT-C<sub>12</sub> from tetralin solutions; Figure 5). Clearly, a combination of printing and coating techniques will, eventually, be required to pattern the range of materials used in more integrated structures, as well as to realize the various patterns and structures needed in such architectures.

### 3.4. Experimental

#### 3.4.1 Materials

Poly(2,5-bis(3-dodecylthiophen-2-yl)thieno[3,2-*b*]thiophene), (pBTTT-C<sub>12</sub>) was generously supplied by Merck Chemicals ( $M_n = 27.9 \text{ kg mol}^{-1}$ ,  $M_w = 51.4 \text{ kg mol}^{-1}$ ). Tetralin (THN), indan, 1,2,3,4-tetramethylbenzene (TMB) and 1,2,4-trichlorobenzene (TCB) were purchased from Aldrich and used as received.

#### 3.4.2. Sample preparation

Homogeneous pBTTT-C<sub>12</sub> solutions were prepared by dissolving the polymer in the respective solvents at temperatures of 50 - 100 °C, depending on the solvent and concentrations utilized. For FET fabrication, hot TCB solutions

were then either spin-coated onto pre-patterned substrates that were kept at room temperature or inkjet-printed (drop spacing of 25  $\mu\text{m}$ ; see below).

### **3.4.3. Thermal analysis**

Differential scanning calorimetry (DSC) was conducted under  $\text{N}_2$  at a scan rate of 10  $^\circ\text{C min}^{-1}$  with a Mettler Toledo DSC822 instrument. Medium pressure 120  $\mu\text{l}$  Mettler stainless steel crucibles sealed with Viton-O-rings were utilized for this purpose. The sample weight, excluding solvent, was ca. 0.5 - 1 mg. The dissolution temperatures reported refer to end-of-peak temperatures in the second heating DSC thermograms. Crystallization temperatures were deduced from the onset of relevant exotherms (second cooling thermograms).

### **3.4.4. Particle size**

A Malvern instrument Zetasizer (Nano series, ZEN3600), covering a particle size range of 6 nm – 6  $\mu\text{m}$ , was used for the particle size analysis of pBTTT- $\text{C}_{12}$ /TCB binaries. To this end, 0.5 wt% pBTTT- $\text{C}_{12}$  solutions were prepared in the respective solvent by heating the binaries to above the dissolution temperature. 2 ml of these hot solutions were then transferred into glass cuvette cells with a PTFE stopper (10 mm path-length) to occupy about on quarter of the cell total space. Particle sizes were then recorded during cooling the hot solutions to room temperature.

### **3.4.5. Rheology**

The viscosity of pBTTT- $\text{C}_{12}$ /TCB solutions was evaluated with a Thermal Analysis (TA) instrument ARES-G2 Rheometer with an incorporated temperature

system range (-40 to 180 °C). A volume of 5 ml of hot solution (0.5 wt% pBTTT-C<sub>12</sub>) was then dispensed between the top and bottom peltier plates, filling the 2 mm gap. Measurements were carried out as a function of temperature (heating and cooling sweeps).

### **3.5.5. Inkjet printing field-effect transistor devices**

A Dimatix Fujifilm DMP-2831, fitted with a vacuum plate, 16 nozzles, and integrated heated platen (temperature adjustability between 25 °C and 60 °C), was utilized for ink-jet printing pBTTT-C<sub>12</sub> transistors and inverters. Hot pBTTT-C<sub>12</sub>/TCB solutions (0.5 wt% polymer content) were first degassed with helium for 20 mins, before re-heated and dispensed into the disposable printing cartridges (~1 ml volume). Optimum drop spacing was found to be between 25 – 35 μm, which required a drive voltage of 14 to 20 V and a firing frequency of about 5 kHz.

### **3.5.6. Transistor and Inverters Fabrication**

Bottom gate/bottom contact FETs were fabricated employing highly doped Si wafers as gate electrode, 200 nm of thermally grown SiO<sub>2</sub> as gate insulator and photolithographically patterned gold (Au) source/drain electrodes employing 10 nm indium tin oxide (ITO) as the adhesive layer. A monolayer of octadecyltrichlorosilane (OTS) was applied to passivate the SiO<sub>2</sub> surface. Organic semiconductor solutions were prepared in 1,2,4-trichlorobenzene and spin-coated or patterned by ink-jet printing onto the substrates. Spin-coating was performed in nitrogen atmosphere. Ink-jet printing was performed in air using a Dimatrix DMP-2831 keeping the substrates at a temperature of 100 °C. All samples were subsequently annealed at 160 °C for 1 hour in nitrogen atmosphere. Discrete

transistors and inverters were characterized in a probe station under vacuum ( $10^{-4}$  mbar) using an Agilent Semiconductor Parameter Analyzer 4156C. Field-effect mobility was calculated in the saturation regime using the gradual channel approximation employing:<sup>30</sup>

$$\mu_{e,sat} = \frac{L}{C_i W} \cdot \frac{\partial^2 I_D}{\partial V_G^2}. \quad (3.1)$$

### 3.6. References

1. S. R. Forrest, The path to ubiquitous and low-cost organic electronic appliances on plastic, *Nature* **2004**, 428, 911.
2. D. Voss, Cheap and cheerful circuits, *Nature* **2000**, 407, 442.
3. H. Klauk, U. Zschieschang, J. Pflaum, M. Halik, Ultralow-power organic complementary circuits, *Nature* **2007**, 445, 745.
4. I. McCulloch, Thin films - Rolling out organic electronics, *Nat. Mater.* **2005**, 4, 583.
5. M. Muccini, A bright future for organic field-effect transistors, *Nat. Mater.* **2006**, 5, 605.
6. G. Malliaras, R. H. Friend, An organic electronics primer, *Phys. Today* **2005**, 58, 53.
7. F. Garnier, R. Hajlaoui, A. Yassar, P. Srivastava, All-polymer field-effect transistor realized by printing techniques, *Science* **1994**, 265, 1684.
8. Z. N. Bao, Y. Feng, A. Dodabalapur, V. R. Raju, A. J. Lovinger, High-performance plastic transistors fabricated by printing techniques, *Chem. Mater.* **1997**, 9, 1299.

9. Z. N. Bao, J. A. Rogers, H. E. Katz, Printable organic and polymeric semiconducting materials and devices, *J. Mater. Chem.* **1999**, *9*, 1895.
10. H. Sirringhaus, T. Kawase, R. H. Friend, T. Shimoda, M. Inbasekaran, W. Wu, E. P. Woo, High-resolution inkjet printing of all-polymer transistor circuits, *Science* **2000**, *290*, 2123.
11. T. Kawase, T. Shimoda, C. Newsome, H. Sirringhaus, R. H. Friend, Inkjet printing of polymer thin film transistors, *Thin Solid Films* **2003**, *438*, 279.
12. A. C. Arias, S. E. Ready, R. Lujan, W. S. Wong, K. E. Paul, A. Salleo, M. L. Chabiny, R. Apte, R. A. Street, Y. Wu, P. Liu, B. Ong, All jet-printed polymer thin-film transistor active-matrix backplanes, *Appl. Phys. Lett.* **2004**, *85*, 3304.
13. A. Knobloch, A. Manuelli, A. Bernds, W. Clemens, Fully printed integrated circuits from solution processable polymers, *J. Appl. Phys.* **2004**, *96*, 2286.
14. M. L. Chabiny, W. S. Wong, A. C. Arias, S. Ready, R. A. Lujan, J. H. Daniel, B. Krusor, R. B. Apte, A. Salleo, R. A. Street, Printing methods and materials for large-area electronic devices, *Proc. IEEE* **2005**, *93*, 1491.
15. R. A. Street, W. S. Wong, S. E. Ready, I. L. Chabiny, A. C. Arias, S. Limb, A. Salleo, R. Lujan, Jet printing flexible displays, *Mater. Today* **2006**, *9*, 32.
16. P. Calvert, Inkjet printing for materials and devices, *Chem. Mater.* **2001**, *13*, 3299.
17. M. Heeney, C. Bailey, K. Genevicius, M. Shkunov, D. Sparrowe, S. Tierney, I. McCulloch, Stable polythiophene semiconductors incorporating thieno[2,3-b]thiophene, *J. Am. Chem. Soc.* **2005**, *127*, 1078.



18. I. McCulloch, M. Heeney, C. Bailey, K. Genevicius, I. Macdonald, M. Shkunov, D. Sparrowe, S. Tierney, R. Wagner, W. M. Zhang, M. L. Chabiny, R. J. Kline, M. D. McGehee, M. F. Toney, Liquid-crystalline semiconducting polymers with high charge-carrier mobility, *Nat. Mater.* **2006**, *5*, 328.
19. S. A. Wang, J. C. Tang, L. H. Zhao, R. Q. Png, L. Y. Wong, P. J. Chia, H. S. O. Chan, P. K. H. Ho, L. L. Chua, Solvent effects and multiple aggregate states in high-mobility organic field-effect transistors based on poly(bithiophene-alt-thienothiophene), *Appl. Phys. Lett.* **2008**, *93*, 162103.
20. R. D. Deegan, O. Bakajin, T. F. Dupont, G. Huber, S. R. Nagel, T. A. Witten, Capillary flow as the cause of ring stains from dried liquid drops, *Nature* **1997**, *389*, 827.
21. P. G. De Gennes, Wetting: statics and dynamics, *Rev. Mod. Phys.* **1985**, *57*, 827.
22. H. R. Kang, Water-based ink-jet ink .1. Formulation, *J. Imaging Sci.* **1991**, *35*, 179.
23. H. R. Kang, Water-based ink-jet ink .2. Characterization, *J. Imaging Sci.* **1991**, *35*, 189.
24. H. R. Kang, Water-based ink-jet ink .3. Performance studies, *J. Imaging Sci.* **1991**, *35*, 195.
25. P. Brookes, J. Canisius, M. Goncalves-Miskiewicz, M. Heckmeier, M. James, D. Mueller, K. Patterson, D. Sparrowe, S. Tierney, Ink Jet printable organic semiconducting materials and formulations - Combining printability, high performance and air stability, *Nip24/Digital Fabrication*

2008: 24th International Conference on Digital Printing Technologies, Technical Program and Proceedings **2008**, 927.

26. C. R. Weast, M. J. Astle, *Handbook of Chemistry and Physics*, CRC PRESS. Inc., Boca Raton **1980 - 1981**.
27. O. Inganas, W. R. Salaneck, J. E. Osterholm, J. Laakso, Thermochromic and solvatochromic effects in poly(3-hexylthiophene), *Synth. Met.* **1988**, 22, 395.
28. T. N. Ng, S. Sambandan, R. Lujan, A. C. Arias, C. R. Newman, H. Yan, A. Facchetti, Electrical stability of inkjet-patterned organic complementary inverters measured in ambient conditions, *Appl. Phys. Lett.* **2009**, 94, 233307.
29. C. Celle, C. Suspene, J. P. Simonato, S. Lenfant, M. Ternisien, D. Vuillaume, Self-assembled monolayers for electrode fabrication and efficient threshold voltage control of organic transistors with amorphous semiconductor layer, *Org. Electron.* **2009**, 10, 119.
30. D. Hong, G. Yerubandi, H. Q. Chiang, M. C. Spiegelberg, J. F. Wager, Electrical modelling of thin-film transistors, *Crit. Rev. Solid State Mater. Sci.* **2008**, 33, 101.

## Chapter 4

### Solid-State Processing of Organic Semiconductors

#### 4.1. Introduction

The term "plastic crystals" is generally used to refer to crystalline solids that feature a remarkably high molecular mobility in certain solid states and, hence, typically are characterized by relatively small entropy of fusion, often accompanied by a comparatively high melting temperature.<sup>1-3</sup> Classical examples of such materials are CBr<sub>4</sub>, C<sub>2</sub>Cl<sub>6</sub>, pentaerythritol, cyclohexane, camphor, *etc.* – generally species that originally were classified by Timmermans in the 1930's as "globular".<sup>1-3</sup> More recently, selected organic salts that are attracting attention as solid-state conductors in applications such as lithium batteries also have been demonstrated to feature plastic crystalline phases.<sup>4-6</sup> The high molecular mobility in such solids results in a high plasticity, similar to that observed in many metals.<sup>7</sup> This characteristic is not restricted to small molecular organic compounds, but is also observed in certain polymers. A major, commercially exploited case-in-point is that of poly(tetrafluoroethylene) (PTFE, better known as Teflon<sup>®</sup>).<sup>8, 9</sup> This uniquely hydrophobic polymer is typically of ultra-high molecular weight ( $M_w > 5 \cdot 10^{57}$  kg mol<sup>-1</sup>) and, as a consequence, is of ultra-high viscosity. PTFE is, therefore considered to be non-melt-processable, nor is it soluble in common solvents. However, this widely employed polymer is routinely processed in the *solid* state at temperatures of 200 °C below its melting point, often assisted by a

lubricant in a process known as paste extrusion.<sup>9</sup> Similarly, it has been demonstrated that selected grades of ultra-high molecular weight polyethylene (UHMW PE) can be processed into useful shapes simply by compression molding below their melting temperature, for instance into mechanically coherent films, and transformed by tensile deformation – also in the solid state – into ultra-high strength fibers and tapes.<sup>10</sup>

Recognizing that molecular mobility in the solid state allows for major rearrangement of the constituent molecules without losing their order – indeed, frequently enhancing it – and, thus, permits shaping these materials at temperatures well below their melting points without the need for solvents or to create a vapor phase, in this chapter, we embarked on a study to explore whether such solid-state processing concepts are applicable to organic semiconducting species. These materials currently are under scrutiny for a broad range of (opto-) electronic applications, including field-effect transistors (FETs), organic photovoltaic (OPV) devices and the like,<sup>11-13</sup> which typically are fabricated from the vapor phase, dilute solutions or melt. These processes require either inefficient vacuum deposition techniques,<sup>14</sup> derivatisation of the semiconducting species with solubilizing side chains, which can compromise their properties,<sup>15</sup> or use of complex precursor routes.<sup>16-18</sup> Processing such materials in their solid state should offer significantly simplified fabrication schemes that are compatible with large-scale, roll-to-roll manufacturing methods of high yield, such as calendaring, lamination and rolling. In addition, solid-state forming might be applicable to “intractable”, non-melt-processable and/or non-soluble materials as the example of PTFE illustrates.

## 4.2. Results and discussions

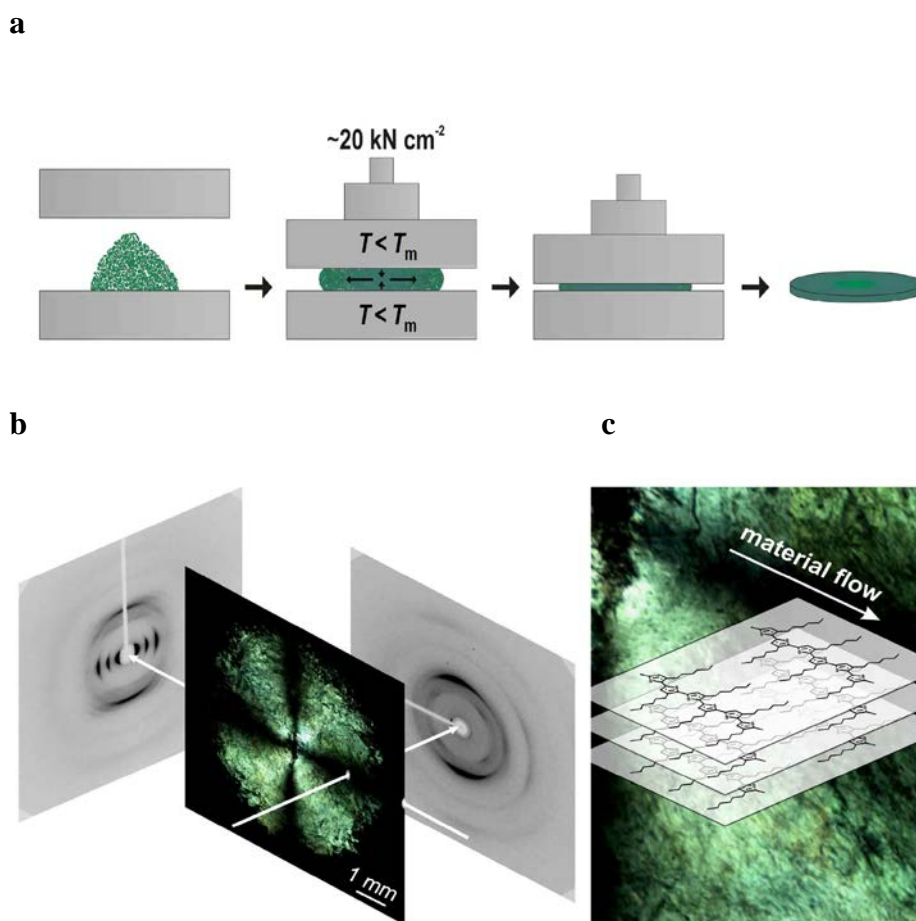
### 4.2.1. Thin-film fabrication

Solid-state processing of conjugated small molecular-, oligomeric- and polymeric compounds was conducted as schematically indicated in Figure 1a. Solid, powdered material was placed in a hot press, followed by compression molding well below the melting temperatures of the species, typically at pressures of approximately  $10\text{-}30\text{ kN cm}^{-2}$ , which is somewhat above the range reported by Michels to cause flow of the above mentioned classical plastic crystals.<sup>2, 3, 19</sup>

### 4.2.2. Microstructure

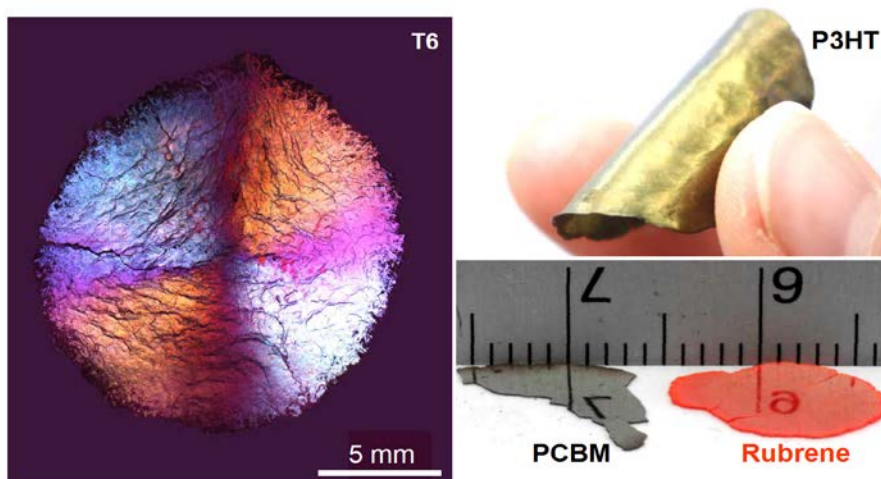
The simple solid-state processing procedure in most cases yielded highly ordered, mechanically coherent films with controlled thicknesses typically in the range of  $20\text{-}200\text{ }\mu\text{m}$ , both for small molecules and polymers. The high degree of order is evidenced by the polarized reflected light optical micrographs of, for instance, solid-state processed poly(3-hexylthiophene) (P3HT) and  $\alpha$ -sexithiophene (6T), that featured a distinct Maltese cross across the entire film (Figure 1 and 2)– which typically were of  $2\text{-}5\text{ cm}$  in diameter – indicating a major radial molecular flow occurred in the compression molding procedure. This suggests that the solid-state processing method does not bear any resemblance to standard sintering procedures.

The latter conclusion was supported by wide-angle X-ray diffraction (WAXD) (Figure 1b) conducted on solid-state pressed P3HT films. Indeed, the



**Figure 1.** (a) Schematic illustration of the solid-state compression molding process of organic semiconductors. (b) Polarized optical reflection micrograph and wide-angle X-ray diffraction of a solid-state molded poly(3-hexylthiophene), taken perpendicular to, and in the plane of the film. (c) Molecular arrangement of the P3HT macromolecules, as deduced from optical microscopy and wide-angle X-ray diffraction.

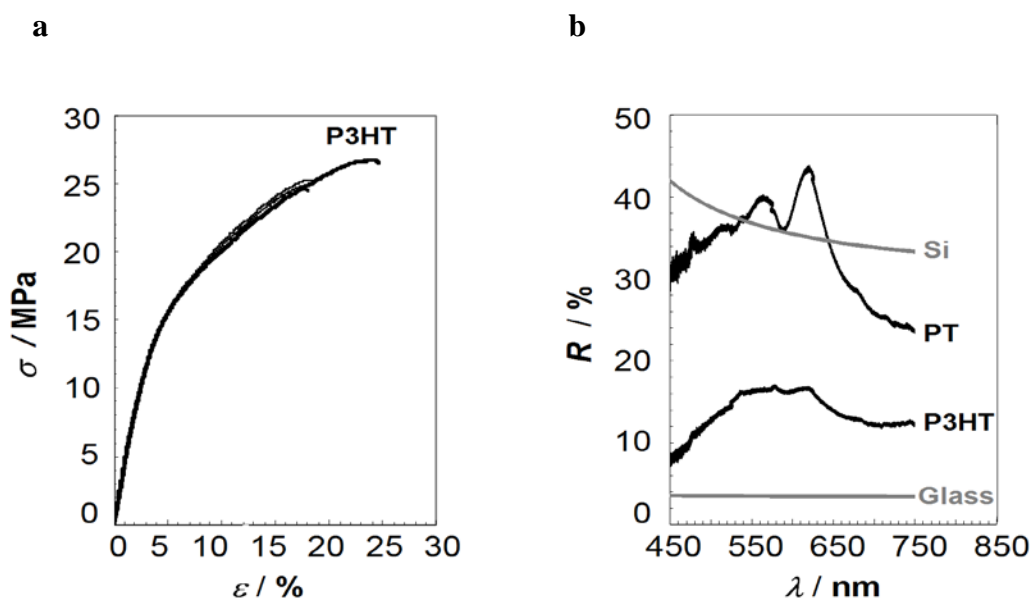
diffraction patterns taken, respectively, through and parallel to the film's plane revealed that in the solid-state processed films the macromolecules are highly ordered radially *and* with their side chains arranged perpendicularly to the surface of the films, as schematically depicted in Figure 1c. (Interestingly, this arrangement is orthogonal to the orientation found in so-called friction-transfer films<sup>20</sup> of the same polymer<sup>21</sup>).



**Figure 2.** Optical properties of solid-state processed organic functional materials. *Left panel:* Optical reflection micrograph taken between crossed polarizers of a solid-state molded  $\alpha$ -sexithiophene (T6) film. *Right panel (top):* Image of a solid-state processed poly(3-hexylthiophene), P3HT ( $M_w = 246 \text{ kg mol}^{-1}$ ) structure, illustrating that flexible, tough films of good mechanical toughness can be produced. *Right panel (bottom):* Reflection of an aluminum ruler in ([6,6]-phenyl C<sub>61</sub>-butyric acid methyl ester) (PCBM) (left) and rubrene (right) films, illustrating their mirror-like characteristics.

#### 4.2.3. Mechanical properties

Certain solid-state compression molded films displayed also a remarkable mechanical robustness and toughness even when produced hundreds of degrees below their melting points. For instance, free-standing flexible films were obtained with P3HT of a molecular weight of  $M_w = 246 \text{ kg mol}^{-1}$  (Figure 2, right panel/top) that featured average values of the Young's modulus,  $E$ , of 0.5 GPa, stress at break,  $\sigma$ , of 18 MPa and remarkably large elongation at break,  $\epsilon$ , of 20 % (*cf.* stress/strain tests in Figure 3a). Such mechanical characteristics are in contrast with inorganics and small molecular-weight compounds that typically fail at an elongation well below 1 %. Therefore, this processing method clearly permits the production of truly flexible electronic components.

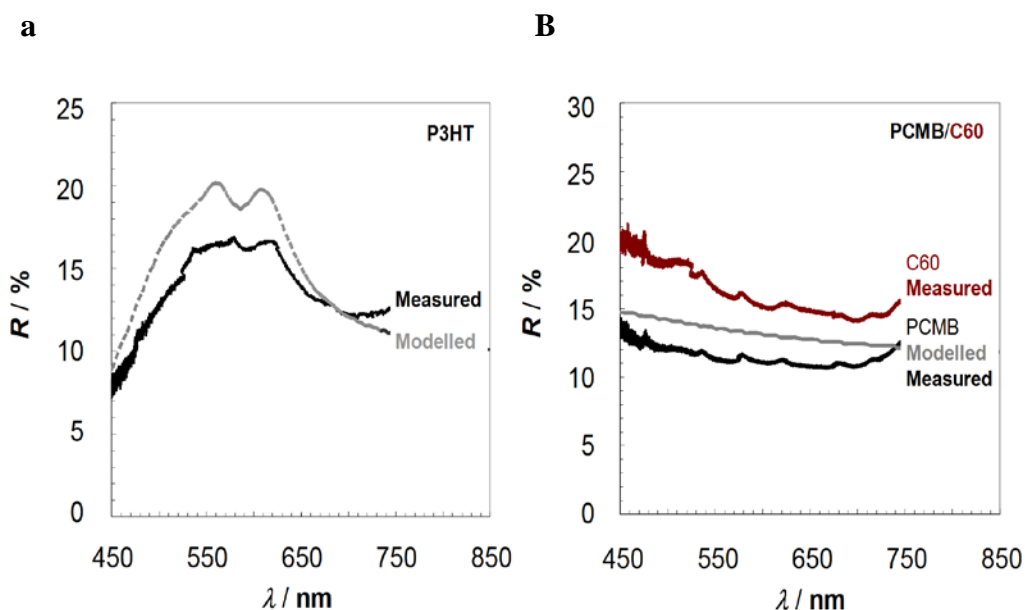


**Figure 3.** (a) Stress-strain ( $\sigma - \varepsilon$ ) curves of three solid-state processed poly(3-hexylthiophene), P3HT, tapes, recorded at room temperature. (b) Normal incidence reflectivity,  $R$ , measured with a confocal optical system calibrated using silicon wafers, of unsubstituted polythiophene (PT); for comparison, data for P3HT, silicon and glass are also shown ( $R_{\text{Si}}$  and  $R_{\text{Glass}}$  are modeled).

#### 4.2.4. Reflectivity

A number of solid-state compression-molded films we prepared featured a mirror-like appearance (*cf.* the ([6,6]-phenyl C<sub>61</sub>-butyric acid methyl ester), [60]PCBM, and rubrene structures in Figure 2; right panel/bottom) and certain structures displayed a high degree of reflectivity. For example, the solid-state molded “intractable” polythiophene (PT) was found to exhibit a reflectivity,  $R$ , reaching > 35 % (determined at normal incidence with a confocal optical system; Figure 3b), which is comparable to the reflectivity of a silicon wafer. These high reflectivity values of PT span across the whole visible spectral range, and exceed by more than two fold values found for most organic compounds. For instance, the reflectivities of P3HT and C60 peak are only around 17 % (Figure 3b and 4a,b). Evidently, the lack of side chains in PT seems to allow for a higher density of the active moieties compared to the substituted polymer, which resulted in an





**Figure 4.** (a) Normal incidence reflectivity for poly(3-hexylthiophene) and (b) fullerene C<sub>60</sub> and [6,6]-phenyl C<sub>61</sub>-butyric acid methyl ester, [60]PCBM. A comparison is given for measured (black lines) and modelled (grey lines) reflectivities. For the modelling, we have used the optical constants deduced for thin spin-coated films (Ref. 22).

enhanced refractive index. In fact, the unsubstituted polythiophene displays a specific gravity,  $\rho_{PT} = 1.52 \text{ g cm}^{-3}$  higher than poly(3-hexylthiophene),  $\rho_{P3HT} = 1.17 \text{ g cm}^{-3}$ , which is in agreement with the theoretical densities calculated for these two polymers from the respective crystallographic lattice parameters.<sup>23-26</sup>

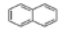


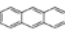


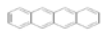




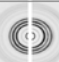
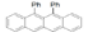





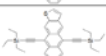


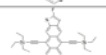


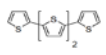


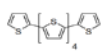
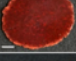

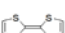


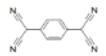


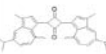
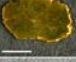

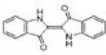





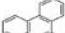






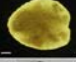










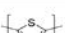


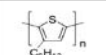


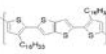


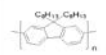


Interestingly, such compact packing also results in a relative increase in refractive index,<sup>27</sup> which indeed is comparable to inorganic semiconductors. For instance, in case of PT, preliminary spectroscopic ellipsometry revealed refractive indices of up to 2.8 (at 625 nm) which are in the range predicted by Yang and Jenekhe,<sup>28</sup> for which we here present experimental confirmation. The solid-state processed films have a large surface roughness, resulting in scattering of the incident light. As a consequence the measured values might be slightly underestimated. Films with smoother surfaces may, therefore, exhibit larger reflectivities than those reported here. In addition, we like to note that this good match between

the reflectivities for spin-coated films and solid-state processed films indicates that, from an optical point of view, films fabricated by the two techniques exhibit comparable properties; *i.e.*, solid-state processing does not have detrimental effects on the optical properties of semiconducting materials. Combined with the fact that the electric properties are also preserved, the good optical properties suggest that this protocol is potentially applicable for a broad range of optoelectronics applications. In addition and without doubt, the above also demonstrates that solid-state processing offers a unique opportunity to fabricate functional thin films from compounds of so far elusive film-forming capabilities (*e.g.*, when processed from solution or the melt).<sup>28</sup>

#### **4.2.5. Applicability of solid state processing**

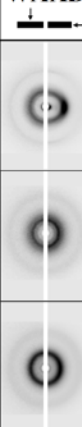
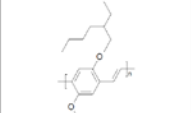
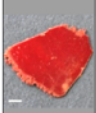

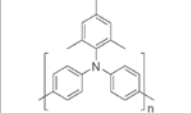

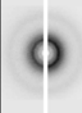
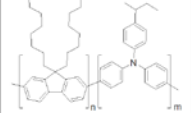
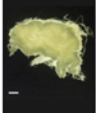
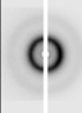
In order to explore the applicability and potential limits of the solid-state processing technology, we investigated a large number of semiconducting organic species, including a wide variety of small-molecular compounds, oligomers and polymers currently investigated for applications in organic- and plastic electronics. Their chemical structures, melting,  $T_m$ , and processing,  $T_p$ , temperatures, as well as WAXD patterns taken perpendicular to, and in the plane of solid-state molded films of selected materials used in this study, are presented in Table 1. As we can conclude from many of the diffraction patterns – and in agreement with our above observations on P3HT and 6T – solid-state compression molding involved major radial flow of the materials, often resulting in high degrees of anisotropic order, which is remarkable considering that these materials were processed at temperatures far below their respective melting points.

**Table 1.** Small molecular organic compounds, oligomers and polymers investigated for their applicability for solid-state processing procedures. Their chemical structures, melting-,  $T_m$ ,  $\Delta S_m$  and processing-,  $T_p$  temperature, as well as WAXD patterns taken perpendicular to (left), and in the plane (right), of solid-state molded films are presented.

Compound	Structure	$T_m$ (°C)	$\Delta S_m^\circ$ (J mol <sup>-1</sup> K <sup>-1</sup> )	$T_p$ (°C)	Film (scale-bar:2mm)	WAXD
Naphthalene		81	50	25		
Anthracene		217	58	100 150		
Tetracene		347	64	150 250		
Pentacene		>350	- <sup>a</sup>	250 300		
Rubrene		331	77	170 250		
TIPS-Pentacene		>260	- <sup>a</sup>	25 100		
TES-ADT		123 154	35 <sup>b</sup> 36	25		
diF-TESADT		195	84	25 100		
$\alpha$ -Quarterthiophene		212	83	100 150		
$\alpha$ -Sexithiophene		299	71	150		
Tetrathiafulvalene		120	42	25		
TCNQ		291	71	150		
Squaraine		>250	- <sup>a</sup>	100 150		
Indigo		>300	- <sup>a</sup>	250		
Perylene (EPPTC)		>350	- <sup>a</sup>	250		
Triphenylene		198	50	120		
CuPh		>300	- <sup>a</sup>	200		
Alq <sub>3</sub>		414	75	250		
C60		>350	- <sup>a</sup>	250 300		
PCBM		282	35	150 250		
Carbon Nanotubes		>350	- <sup>a</sup>	150 200		
Polythiophene		>300	- <sup>a</sup>	250		
P3HT		248	14 (33 <sup>c</sup> )	100 150		
PBTTT-C <sub>16</sub>		51 142 244	14 <sup>b</sup> 48 <sup>b</sup> 1	100 150		
PFO		137	11.1 (64 <sup>c</sup> )	100 150		

<sup>a</sup> degradation/sublimation prior to/during melting  
<sup>b</sup> crystalline/crystalline-, crystalline/mesophase- or mesophase/mesophase-transitions  
<sup>c</sup> calculated with literature value for the extrapolated enthalpy of melting of 100% crystalline material P3HT<sup>29</sup>, PFO<sup>30</sup>

**Table 2.** Solid-state compression molding was found to be applicable also to some polymers of low – if any – crystallinity, including poly[2-methoxy-5-(2'-ethyl-hexyloxy)-1,4-phenylene vinylene] (MEH-PPV;  $M_w = 350 \text{ kg mol}^{-1}$ ), poly[(9,9-dioctylfluoronyl-2,7-diyl)-co-(4,4'-(N-(4-butylphenyl) diphenylamine)] (TFB,  $M_w = 31 \text{ kg mol}^{-1}$ ) and poly(bis(4-phenyl)2,3,4-trimethylphenyl)amine (PTAA;  $M_w = 17.5 \text{ kg mol}^{-1}$ ). Chemical structures, processing,  $T_p$ , temperature, and WAXD patterns taken perpendicular to (left), and in the plane (right) are presented.

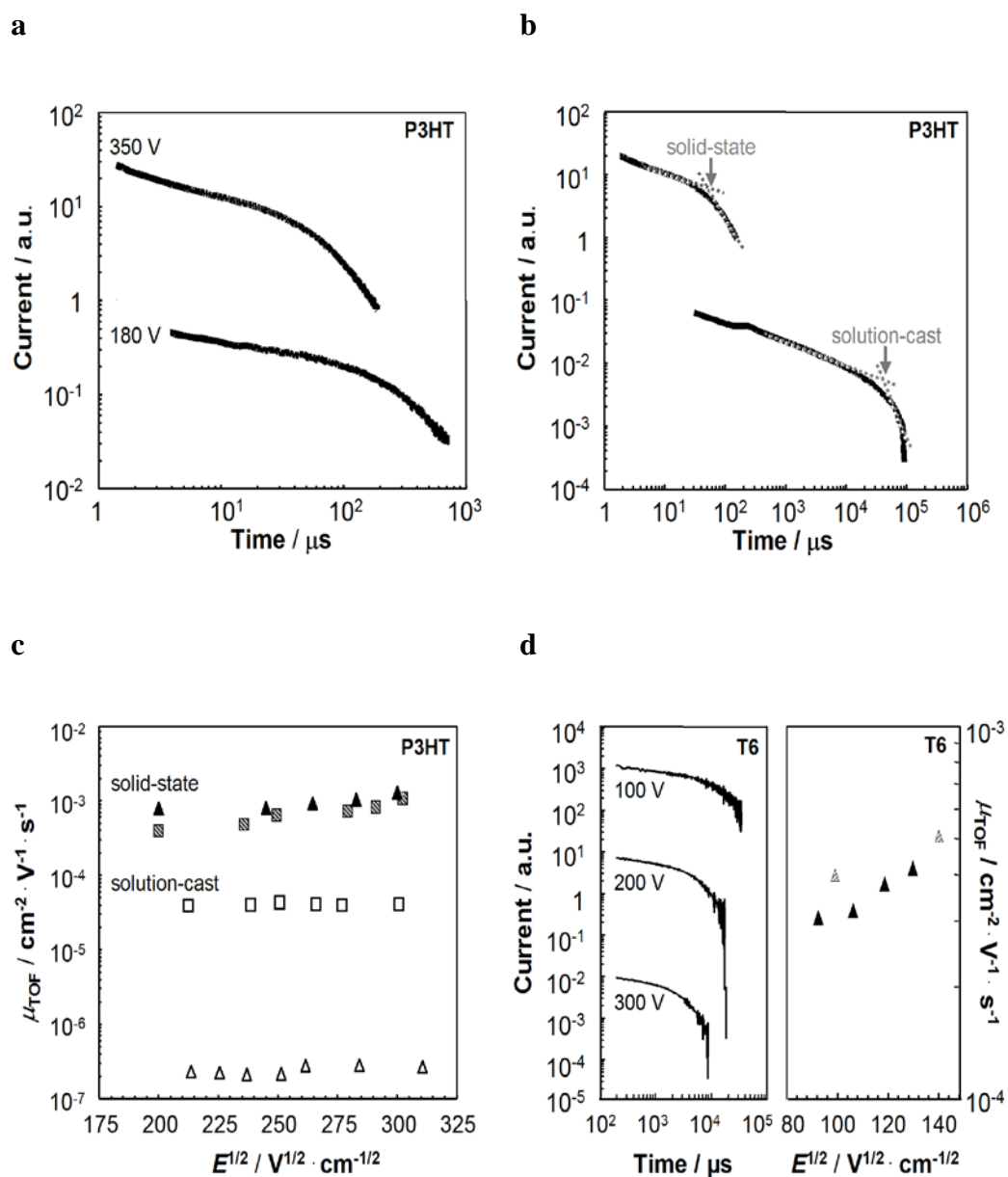
Compound	Structure	$T_p$ (°C)	Film (scale-bar:2mm)	WAXD 
MEH-PPV		50		
PTAA		50		
TFB		50		

Also included in Table 1, where accessible, are values of the entropy of fusion,  $\Delta S_m^\circ$ , which are deemed to be indicative of plastic crystal behaviour when found to be below 5 e.u. ( $\text{cal deg}^{-1} \text{ mol}^{-1}$ ) – as strictly empirically advanced by Timmermans,<sup>1-3</sup> and in the modern literature expressed as  $\Delta S_m^\circ < 20 \text{ J K}^{-1} \text{ mol}^{-1}$ . Many of the materials investigated here do not fit that criterion, but this discrepancy more recently was observed also for a number of plastic crystalline organic salts.<sup>4</sup> In the case of polymers, as is customary,  $\Delta S_m^\circ$  is presented per mole repeat unit.<sup>31</sup> It should be noted, however, that uncertainty exists about the degree of crystallinity of some of the compounds, which naturally affects the relevance of the values given in Table 1. However our solid-state compression molding was found to also be applicable to some polymers of low – if any – crystallinity, for which  $\Delta S_m^\circ$  could not be sensibly deduced. These materials are listed in Table 2.

#### 4.2.6. Bulk charge transport

In order to investigate whether or not solid-state processing deteriorated the electronic properties of the semiconductors, time-of-flight (TOF) photoconductivity experiments were conducted, which allow determination of *bulk* charge transport across thin-film architectures. For this purpose a typical small molecular compound (6T) and two polymeric species, *i.e.* P3HT and the liquid-crystalline poly(2,5-bis(3-hexadecylthiophen-2-yl)thieno[3,2-*b*]thiophene), pBTTT-C<sub>16</sub>, were selected. P3HT was chosen as it permitted us to readily create solid-state processed- as well as conventional solution-cast films, affording a direct comparison of the electronic characteristics resulting from the different fabrication techniques.

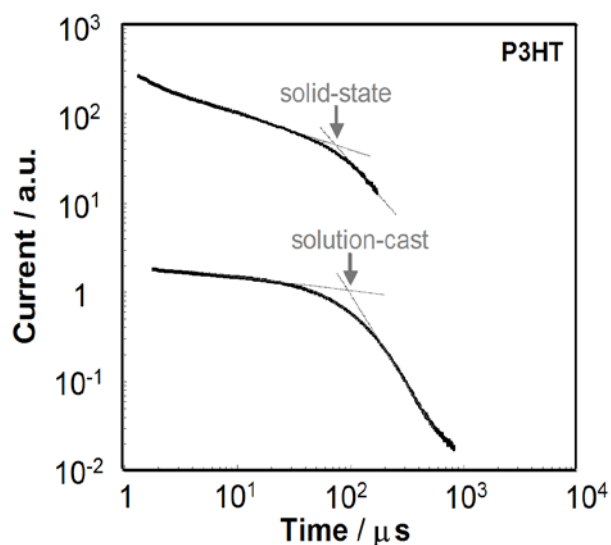
Encouragingly, as for many polymer semiconductors, clear but dispersive hole photocurrent transients were found in time-of-flight (TOF) photoconductivity measurements conducted on solid-state molded P3HT structures with thickness of 50  $\mu\text{m}$  and more (usually 1-5  $\mu\text{m}$  thick films are employed in TOF). This is evident from the data shown in Figure 5a (inflection point arrival time  $t_{\text{tr}}$  is indicated by arrows). The pre- and post-transit power laws (gradients) deduced from these transients followed  $I \propto t_{\text{tr}}^{-(1-\alpha_1)}$  and  $I \propto t_{\text{tr}}^{-(1+\alpha_2)}$  respectively, as it is expected in case of dispersive charge-transport, where  $I$  is the photocurrent and  $\alpha_1$  and  $\alpha_2$  are constants.<sup>32</sup> Hole transport scaled with bias (*i.e.*, electric field strength), which illustrates that the charge carriers created traversed the entire film. Furthermore, an intriguing observation is that solid-state processed P3HT structures displayed significantly enhanced bulk charge transport properties compared to solution-cast films, in agreement with previous studies that unidirectional



**Figure 5.** (a) Time-of-flight (TOF) photoconductivity measurements on solid-state molded poly(3-hexylthiophene) (P3HT) architectures. Typical hole photocurrent transients measured under vacuum at two different voltages (thickness of P3HT film,  $d = 45 \mu\text{m}$ ). (b) Comparison of P3HT films processed either in the solid state or from solution ( $E \sim 10^5 \text{ V cm}^{-1}$ ). (c) Corresponding Poole-Frenkel plots of solid-state molded (filled symbols) and solution-cast (open symbols) P3HT structures (triangles: P3HT of  $M_w = 246 \text{ kg mol}^{-1}$ ; squares:  $M_w = 60 \text{ kg mol}^{-1}$ ). (d) TOF photoconductivity measurements on sexithiophene (6T). *Left panel:* Photocurrents measured at different bias across solid-state molded  $\alpha$ -sexithiophene, 6T (film thickness,  $d = 200 \mu\text{m}$ ). *Right panel:* Field-dependence of bulk charge-carrier mobility of solid-state processed 6T structures (filled symbols:  $d = 200 \mu\text{m}$ , grey symbols:  $d = 175 \mu\text{m}$ ).

orientation of the macromolecular chains can result in improved bulk charge transport.<sup>33</sup> Indeed, charge carrier mobilities  $\mu_{\text{TOF}}$  in solid-state molded P3HT (246 kg mol<sup>-1</sup>) was determined to be  $1 \cdot 10^{-3} \text{ cm}^2 \text{ V}^{-1} \text{ s}^{-1}$ ; which is more than three orders of magnitude higher than that measured for the unannealed solution-processed material of the same molecular weight that featured  $\mu_{\text{TOF}}$  in the range of  $1 \cdot 10^{-7}$  to  $1 \cdot 10^{-6} \text{ cm}^2 \text{ V}^{-1} \text{ s}^{-1}$  (Figure 5b). The latter, relatively low mobility value is consistent with previously reported values for high-molecular-weight P3HT.<sup>34</sup> However, as shown in Figure 5c and Figure 6, also for P3HT of lower molecular weight (60 kg mol<sup>-1</sup>), for which typically higher  $\mu_{\text{TOF}}$  are reported,<sup>34</sup> solid-state processing induced enhancement of bulk charge-carrier mobility when compared with solution-cast structures, further substantiating the beneficial aspects of our method. Similar observations were made with pBTTT-C<sub>16</sub> (solid-state pressed at 100 °C; Figure 7), for which bulk charge carrier mobilities increased by about one order of magnitude with respect to solution-cast structures ( $\mu_{\text{TOF}}^{\text{solid-state}} = 1 \cdot 10^{-4} - 5 \cdot 10^{-4} \text{ cm}^2 \text{ V}^{-1} \text{ s}^{-1}$ , compared to room temperature  $\mu_{\text{TOF}}^{\text{solution-cast}} = 5 \cdot 10^{-6} - 5 \cdot 10^{-5} \text{ cm}^2 \text{ V}^{-1} \text{ s}^{-1}$ ).<sup>35</sup> Interestingly,  $\mu_{\text{TOF}}$  was found to be essentially field-independent for solid-state processed pBTTT-C<sub>16</sub>, indicating reduced energetic disorder then in case of solution-cast structures, which usually displayed a distinct field dependence.

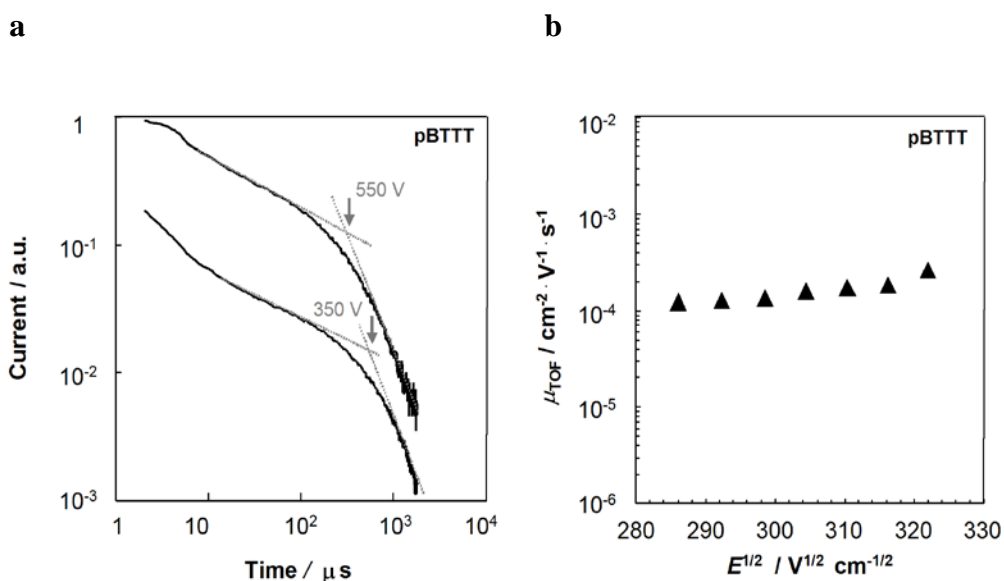
Good bulk charge transport, even across films of more than 150  $\mu\text{m}$  thickness, was found also for solid-state molded 6T (Figure 5d) – a material that is known to be difficult to characterize with TOF, typically requiring special techniques.<sup>36</sup> Charge-carrier mobilities up to  $5 \cdot 10^{-4} \text{ cm}^2 \text{ V}^{-1} \text{ s}^{-1}$  were deduced from the photocurrents, which exceeds by two orders of magnitude a previously reported value ( $5 \cdot 10^{-6} \text{ cm}^2 \text{ V}^{-1} \text{ s}^{-1}$ ) for vapour deposited films. In agreement with the



**Figure 6.** TOF photocurrent transients of poly(3-hexylthiophene) P3HT of  $M_w$  of  $60 \text{ kg mol}^{-1}$ . A comparison is shown between solution-cast (film thickness  $d = 5 \text{ }\mu\text{m}$ , measured at a voltage  $V = 55 \text{ V}$ ) and solid-state pressed structures ( $d = 50 \text{ }\mu\text{m}$ ,  $V = 450 \text{ V}$ ).

previous study, a pronounced field-dependence of the mobility was observed (Figure 5d/right panel).<sup>36</sup> We note, though, that in our preliminary investigations no efforts were yet made to optimize the crystal polymorph, crystal orientation and texture with respect to charge transport pathway of this small molecular semiconductor. In addition, we like to again emphasize that the TOF mobilities for solid-state processed P3HT, pBTTT- $\text{C}_{16}$  and 6T were deduced from photocurrents measured in structures that were 10 to 100 times thicker than usual architectures investigated in time-of-flight photoconductivity measurements, which generally are of a thickness of  $1\text{-}5 \text{ }\mu\text{m}$ . In contrast to our data on solid-state structures, for thick architectures, one normally would expect lower charge-carrier mobilities than for thin structures, as a result of the inherent reduction in the average drift velocity over time due to the dispersive nature of the charge transport in organic semiconductors.

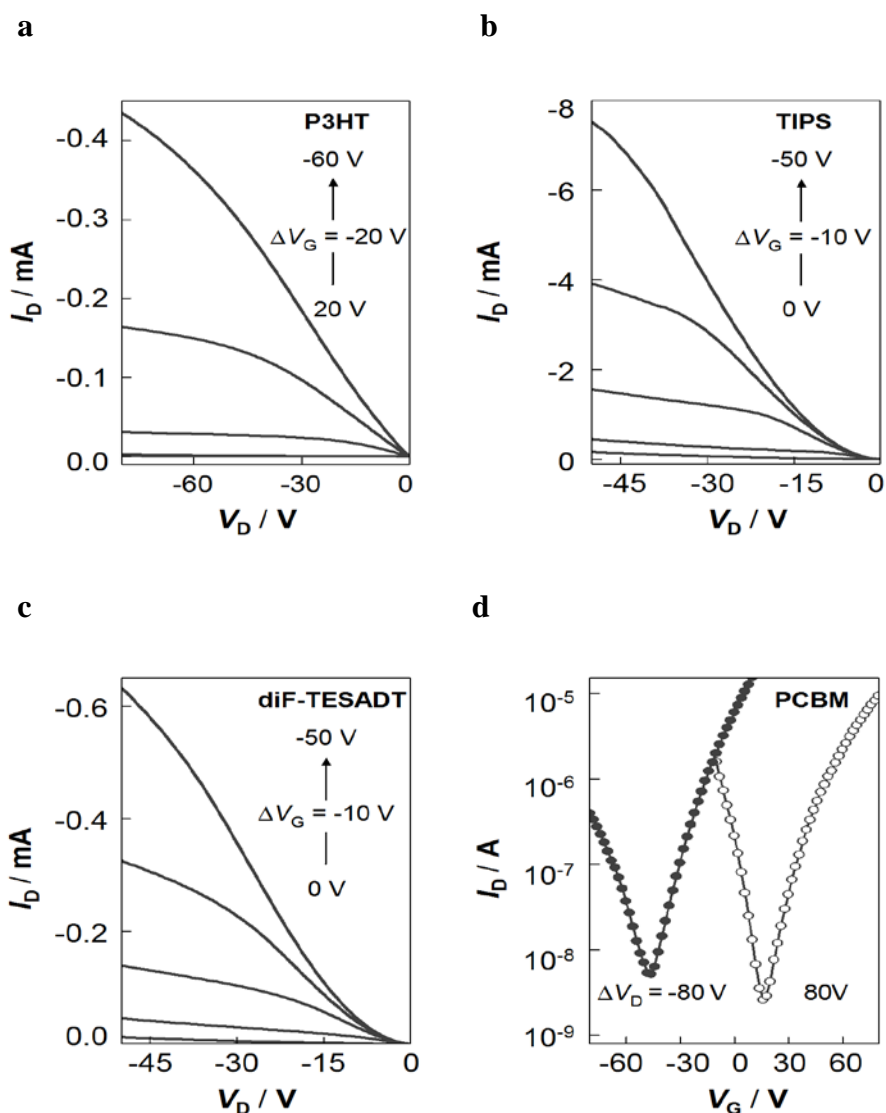




**Figure 7.** (a) Time-of-flight (TOF) photoconductivity measurements on solid-state molded poly(2,5-bis(3-hexadecylthiophen-2-yl)thieno[3,2-*b*]thiophene) (pBTTT-C<sub>16</sub>). Typical hole photocurrent transients recorded under vacuum at two different voltages (film thickness,  $d = 45 \mu\text{m}$ ). (b) Field-dependence of bulk charge-carrier mobility (Poole-Frenkel plot).

#### 4.2.7. Field-effect transistors

Having established that solid-state processing of organic semiconductors did not adversely affect their electronic characteristics measured in TOF experiments, we proceeded to examine whether this method – even in its non-optimized, crude version – would affect the often more sensitive interfacial charge transport characteristics. For this purpose, we fabricated field-effect transistors by directly molding solid-state pressed films onto bottom-gate/bottom-contact architectures, employing a range of small molecular semiconducting compounds, in addition to the same P3HT batch ( $246 \text{ kg mol}^{-1}$ ) as used for the TOF measurements reported above. Promisingly transistors based on solid-state processed P3HT, 6,13-bis(tri-isopropylsilylethynyl) pentacene (TIPS), di-fluoro 5,11-bis(tri-ethyl silylethynyl) anthra-di-thiophene (diF-TESADT), [60]PCBM all demonstrated a pronounced field-effect (current modulation by application of  $V_G$



**Figure 8.** Field-effect transistor (output) characteristics of (a) solid-state processed P3HT, (b) 6,13-bis(triisopropylsilylethynyl) pentacene (TIPS), (c) difluoro-5,11-bis(triethyl silylethynyl) anthra dithiophene (diF-TESADT) and ([6,6]-phenyl C<sub>61</sub>-butyric acid methyl ester) [60]PCMB. (d) Transfer characteristics of devices fabricated with solid-state molded [60]PCBM.

Figure 8a,c). The devices based on [60]PCBM additionally exhibited ambipolar transport – *i.e.* transport of holes and/or electrons – even though compression molding was conducted in light and air (Figure 8d). Generally only a minor hysteresis between the gate voltage,  $V_G$ , scans in the forward and reverse directions was observed, which illustrates that sufficiently adequate interfaces between the

**Table 3.** Device performance of thin-film field-effect transistors based on solid-state processed active layers of poly(3-hexylthiophene) (P3HT), 6,13-bis(tri-isopropylsilylethynyl) pentacene (TIPS), difluoro 5,11-bis(triethyl silylethynyl) anthradithiophene (diF-TESADT) and ([6,6]-phenyl C<sub>61</sub>-butyric acid methyl ester) ([60]PCBM).

Compound	Pressure/ Temperature (kN cm <sup>-2</sup> /°C)	Transistor Parameters			
		Hole mobility $\mu_n$ (cm <sup>2</sup> V <sup>-1</sup> s <sup>-1</sup> )	Electron mobility $\mu_e$ (cm <sup>2</sup> V <sup>-1</sup> s <sup>-1</sup> )	On/Off current ratio (-)	Threshold voltage $V_T$ (V)
P3HT	30 / 150	0.1	-	10 <sup>3</sup>	20
TIPS	10 / 100	0.001	-	10 <sup>2</sup>	9
diF-TESADT	10 / 100	0.03	-	10 <sup>2</sup>	8
[60]PCBM	30 / 150	0.0001	0.001	10 <sup>5</sup>	<i>n</i> -type: +20 <i>p</i> -type: -50

respective semiconductor and the gate dielectric were created when compression molding the active layer in its solid-state onto the pre-structured FET substrates.

Table 3 summarizes the processing conditions and transistor parameters extracted from the operating characteristics of Figure 8, which illustrate that we were able to obtain field-effect carrier mobilities that are comparable with – or at least often approaching – those recorded for fully optimized solution-processed films based on the same FET geometry,<sup>37-40</sup> despite the fact that solid-state processing of all four compounds studied here has not yet been optimized. Indeed the mobility value for P3HT (0.1 cm<sup>2</sup> V<sup>-1</sup> s<sup>-1</sup>) is essentially equivalent to the highest reported in the literature,<sup>37</sup> which required a tedious fabrication process. This is a rather surprising result if one considers the strongly injection limited nature of the source/drain (S/D) contacts, as evident from the non-linear dependence of  $I_D$  on  $V_D$  at low bias (Figure 8a,c). The latter suggest that higher

mobilities may be achieved by improving the carrier injection through, for instance, the use of different S/D electrodes such as platinum (Pt).

### **4.3. Conclusions**

In summary, we advanced solid-state processing of a broad spectrum of organic semiconducting species as an efficient alternative to vacuum deposition, solution- or melt-processing technologies and precursor routes. We demonstrated that bulk carrier mobilities derived from TOF studies did not deteriorate, but in some cases, actually, were significantly enhanced when compared to conventionally processed structures. Advantageously, interfacial charge transport both for electrons and holes was not affected, despite processing the organic semiconductors in light and air. Indeed, our data illustrate that the solid-state technology – even in the present embryonic state – can be employed to fabricate FETs. Clearly, there is ample room for improvement, notably in enhancing the physical interface between the active species and substrates – most importantly the gate dielectric and source/drain electrodes in case of FET structures – especially when bearing in mind that deformation of plastic crystals is critically influenced by temperature and the magnitude of pressure and rate at which it is applied.<sup>1</sup> With respect to reducing the thickness of the films, which is critical in certain device configurations, the initial particle size of the solid semiconductors will need to be adjusted.

It is evident that the simple nature of the solid-state fabrication process can be more broadly exploited. For instance, the present processing scheme can be applied to otherwise intractable and/or insoluble solids as illustrated here with

amongst others,  $\alpha$ -sexithiophene, pentacene and most prominently, unsubstituted polythiophene, PT. Solid-state molding should also allow simple deposition of adjacent *p*- and *n*-channel FETs in one single step, which opens up entirely new and facile manufacturing pathways for the fabrication of complementary logic circuits, a much sought-after technology for the fabrication of large-scale organic integrated circuits. In addition, blends and layered structures may readily be created, without the difficulty to identify orthogonal solvents for the different species – a bottleneck often encountered today in, for example, photovoltaic cell manufacturing. Expansion of the present compression molding method can naturally be achieved by common rolling and calendering technologies, such as those applied in metal manufacturing and lamination, which are likely to lead to additional order and orientation of the semiconducting species.<sup>7</sup>

## 4.4. Experimental

### 4.4.1 Materials

Materials were purchased from various suppliers and were used as received. From *Aldrich*: naphthalene, pentacene,  $\alpha$ -quarterthiophene,  $\alpha$ -sexithiophene, tetracyanoquinodimethane (TCNQ), 2,4-di-3-guaiazulenyl-1,3-dihydroxy-cyclo-butenediylum dihydroxide bis(inner salt) (squaraine), triphenylene, indigo, tris-(8-hydroxyquinoline) aluminum (Alq<sub>3</sub>), copper-(II)-phthalocyanine (CuPh), C<sub>60</sub>, poly[2-methoxy-5-(2'-ethyl-hexyloxy)-1,4-phenylene vinylene] (MEH-PPV;  $M_w = 350 \text{ kg mol}^{-1}$ ), poly(bis(4-phenyl)2,3,4-trimethylphenyl)amine-(PTAA;  $M_w = 17.5 \text{ kg mol}^{-1}$ ); from *Acros Organic*: anthracene; from *Fluka Analytical*: tetracene, tetrathiafulvalene; from *Sensient*

*SynTec Imaging Technologies GmbH*: (2,9-di-(pent-3-yl)-anthra [2,1,9-def:6,5,10-d'e'f']di-isoquinoline-1,3,8,10-tetrone) (EPPTC); from *Solenne*: ([6,6]-phenyl C<sub>61</sub>-butyric acid methyl ester) ([60]-PCBM); from *Bucky USA*: singlewall carbon nanotubes; from *American Dye Source Inc.*: poly(9,9-di-octyl-fluoronyl-2,7-diyl) (PFO,  $M_w = 29 \text{ kg mol}^{-1}$ ), poly[(9,9-di-octyl-fluoronyl-2,7-diyl)-co-(4,4'-(N-(4-butyl-phenyl))di-phenylamine)] (TFB,  $M_w = 31 \text{ kg mol}^{-1}$ ). 6,13-Bis(tri-isopropylsilylethynyl)-pentacene (TIPS),<sup>41</sup> 5,11-bis(tri-ethyl silylethynyl) anthra-dithiophene (TESADT),<sup>42</sup> di-fluoro 5,11-bis(tri-ethyl silylethynyl) anthra-dithiophene (diF-TESADT)<sup>43</sup> and poly(2,5-bis(3-hexadecylthiophen-2-yl)thieno[3,2-*b*]thiophene) (pBTTT-C<sub>16</sub>;  $M_w = 55.5 \text{ kg mol}^{-1}$ )<sup>44</sup> were synthesized according to literature procedures. Polythiophene (PT) and poly(3-hexylthiophene) (P3HT;  $M_w = 246 \text{ kg mol}^{-1}$ ) were synthesized in analogy to the procedure reported by McCullough<sup>45</sup> using low catalyst loadings in refluxing THF.

#### 4.4.2. Solid-state compression molding

The as-received materials were first sandwiched between two cleaned glass slides and PTFE release films, and then pressed at temperatures  $T_p < T_m$  (see Table 1) at an applied force of  $\sim 10 - 30 \text{ kN m}^{-2}$  using a Rondol Technology hot press. Resulting films were of a thickness of 20-200  $\mu\text{m}$  (measured with a micrometer) depending on grain size of material and molding conditions. In the case of field-effect transistor (FET) fabrication, the pressed films were cut to smaller dimension to fit the source-drain channel length and width, and were then pressed at room temperature at  $1 - 2 \text{ kN m}^{-2}$ . Similarly, for TOF measurements, solid-state molded material was either pressed between ITO-coated glass slides

(P3HT, pBTTT-C<sub>16</sub>) or aluminum electrodes were evaporated on either side of a self supporting film (6T).

#### **4.4.3. Thermal analysis**

Melting temperatures,  $T_m$ , and enthalpies of fusion,  $\Delta H_m$ , were determined with a Mettler DSC822e differential scanning calorimeter (DSC). Samples of 1-10 mg sealed in aluminum crucibles were heated under nitrogen at a scanning rate of 10 °C min<sup>-1</sup> from 25 °C to – where applicable – a temperature of at least 25 °C above  $T_m$ . Melting temperatures reported here refer to the maximum in the endothermic peaks; entropies of fusion  $\Delta S_m^\circ$  were calculated as  $\Delta H_m / T_m$ .

#### **4.4.4. Wide-angle X-ray diffraction**

Wide-angle X-ray diffraction (WAXD) studies were performed on an Oxford Diffraction Xcalibur™ XP (Abingdon, UK) instrument, using a Mo-K $\alpha$  source ( $\lambda = 0.7093 \text{ \AA}$ ) operating at -50 V and 40 mA. Patterns were recorded with an Oxford Diffraction Onyx CCD detector at a distance of 130 mm.

#### **4.4.5. Optical microscopy**

Optical microscopy was carried out with a Leica DMRX polarising microscope equipped with a Leica DFC 480 Camera.

#### **4.4.6. Mechanical properties**

Mechanical testing was performed at room temperature with an Instron Tensile Tester (Model 5864) at a cross-head speed of 5 mm min<sup>-1</sup>. Strips of a

width of 2 mm and gauge length 10 mm were cut from the centre of a pressed film of a thickness of  $\sim 210 \mu\text{m}$ .

#### **4.4.7. Reflectivity measurements**

To measure normal incidence reflectivity, a confocal LabRam HR 800 instrument (Jobin-Yvon/Horiba) was employed, with light, coming from a halogen lamp, being focused into a small area of the sample using an Olympus BX41 microscope (fitted with a long distance, small aperture 10x objective). The reflected light was collected through the same objective and directed to a spectrometer which spatially separated the different light wavelengths into different pixels of a Peltier cooled charge coupled device (CCD). As reference, a Therlabs BB1EO2 mirror with  $>99 \%$  reflectivity over the measured spectral range was employed. The system was calibrated using silicon wafers; the reported reflectivities have less than 5 % uncertainty, *i.e.*  $<2 \%$  in the reflectivity values reported. Measurements were taken at several spots throughout the samples to check film homogeneity.

#### **4.4.8. Density measurements**

Densities of the P3HT and PT were characterized by helium gas pycnometry at ambient with a Quantachrome Micro-Ultracycnometer-1000 equipped with a Nanocell. Amounts of  $\sim 80 \text{ mg}$  each polymer were employed and Pulse Mode was applied for purging the cell prior to the measurements. The instrument was operated in the Multi Run Mode and density values were determined by averaging over 10 runs. The theoretical specific densities  $\rho^{\text{calc}}$  were calculated using lattice parameters given in Refs. 23-26 (for P3HT:



$\rho_{\text{P3HT}}^{\text{calc}} = 1.10$  to  $1.13 \text{ g cm}^{-3}$ , depending on the crystal structure proposed) and Ref. 26 (for PT;  $\rho_{\text{PT}}^{\text{calc}} = 1.63 \text{ g cm}^{-3}$ ).

#### 4.4.9. Time-of-flight photoconductivity measurements

All photoconduction experiments were performed in a vacuum chamber (typical pressure  $10^{-5}$  mbar, unless noted differently) at room temperature. The optical excitation was provided by either the 6 ns, 532 nm wavelength output of a frequency doubled insert model Nd:YAG laser (P3HT, pBTTT) or its 6 ns, 355 nm frequency tripled output (6T), as the materials studied here display an absorption peak close to this wavelength. All measurements were carried out under DC bias from a low noise power supply. The laser pulse intensity was kept sufficiently low. As a consequence, the photogenerated charge was less than 10 % of the charge stored across the sample ( $C \cdot V$ , where  $C$  is the sample capacitance and  $V$  the applied potential), avoiding space-charge effects that would result in a non-uniform electric field. The transient current was measured as a voltage drop across a range of load resistors (ranging from  $47 \Omega$  for fast signals to  $83 \text{ k}\Omega$  for very slow signals) at the input of a buffer amplifier whose output was connected to an Agilent Infinium digitizing oscilloscope. Signal averaging (typically over 128 pulses) and background subtraction were performed in order to minimize both random and coherent radio frequency noise. Charge carrier mobilities  $\mu_{\text{TOF}}$  were calculated using the expression:

$$\mu_{\text{TOF}} = d^2/V \cdot t_{\text{tr}} \quad (4.1)$$

where  $d$  is the sample thickness and  $t_{tr}$  the inflection point arrival time obtained from a double logarithmic plot of the photocurrent transient, and  $V$  the applied voltage. The electronic response time of the circuit  $\tau$  was at all times kept well below the time base of the measurement.

#### **4.4.10. Fabrication and characterization of field-effect transistors**

Field-effect transistors were fabricated with heavily doped Si<sup>++</sup> wafers as the global gate electrode with a 200 nm thermally oxidized SiO<sub>2</sub> layer as the gate dielectric. Using conventional photolithography, gold source and drain electrodes were defined in a bottom-contact configuration with channel length,  $L$ , and width,  $W$ , in the range of 1-60  $\mu$ m and 1-10 mm, respectively. A 10 nm-thin titanium adhesion layer for the gold was used on SiO<sub>2</sub>. The SiO<sub>2</sub> layer was treated with the primer hexamethyldisilazane (HMDS) prior to semiconductor deposition in order to passivate its surface. The semiconductor layer was deposited using the solid-state processing method described above. Electrical characterization was performed using an HP 4156C semiconductor parameter analyzer. All measurements were performed at room temperature in high-vacuum ( $10^{-5}$  mbar) or under N<sub>2</sub> at atmospheric pressure.

#### **4.5. References**

1. J. N. Sherwood, *Ed. The Plastically Crystalline State* Wiley, London **1979**.
2. J. Timmermans, Plastic crystals: a historical review, *J. Phys. Chem. Solids* **1961**, *18*, 1.
3. J. Timmermans, Un nouvel etat mesomorphe les cristaux organiques plastiques, *J. Chim. Phys.* **1938**, *35*, 331.

4. P. J. Alarco, Y. Abu-Lebdeh, M. Armand, Highly conductive, organic plastic crystals based on pyrazolium imides, *Solid State Ionics* **2004**, *175*, 717.
5. D. R. MacFarlane, M. Forsyth, Plastic crystal electrolyte materials: new perspectives on solid state ionics, *Adv. Mater.* **2001**, *13*, 957.
6. D. R. MacFarlane, J. H. Huang, M. Forsyth, Lithium-doped plastic crystal electrolytes exhibiting fast ion conduction for secondary batteries, *Nature* **1999**, *402*, 792.
7. C. Y. Barlow, N. Hansen, *Materials Processing Handbook*, CRC Press, Boca Raton **2007**.
8. H. W. Starkweather, Melting and crystalline transitions in normal perfluoroalkanes and poly(tetrafluoroethylene), *Macromolecules* **1986**, *19*, 1131.
9. S. Ebnesajjad, *Fluoroplastics*, Plastic Design Library, Norwich, NY **2000**.
10. B. P. Rotzinger, H. D. Chanzy, P. Smith, High-strength high modulus polyethylene - synthesis and processing of ultrahigh molecular-weight virgin powders, *Polymer* **1989**, *30*, 1814.
11. B. de Boer, A. Facchetti, Semiconducting polymeric materials, *Polymer Reviews* **2008**, *48*, 423.
12. S. Allard, M. Forster, B. Souharce, H. Thiem, U. Scherf, Organic semiconductors for solution-processable field-effect transistors (OFETs), *Angew. Chem. Int. Ed.* **2008**, *47*, 4070.
13. T. W. Kelley, P. F. Baude, C. Gerlach, D. E. Ender, D. Muyres, M. A. Haase, D. E. Vogel, S. D. Theiss, Recent progress in organic electronics: materials, devices, and processes, *Chem. Mater.* **2004**, *16*, 4413.

14. S. R. Forrest, Ultrathin organic films grown by organic molecular beam deposition and related techniques, *Chem. Rev.* **1997**, *97*, 1793.
15. Z. N. Bao, A. J. Lovinger, Soluble regioregular polythiophene derivatives as semiconducting materials for field-effect transistors, *Chem. Mater.* **1999**, *11*, 2607.
16. J. H. Edwards, W. J. Feast, A new synthesis of poly(acetylene), *Polymer* **1980**, *21*, 595.
17. P. T. Herwig, K. Mullen, A soluble pentacene precursor: synthesis, solid-state conversion into pentacene and application in a field-effect transistor, *Adv. Mater.* **1999**, *11*, 480.
18. A. Afzali, C. D. Dimitrakopoulos, T. O. Graham, Photosensitive pentacene precursor: synthesis, photothermal patterning, and application in thin-film transistors, *Adv. Mater.* **2003**, *15*, 2066.
19. A. Michels, *Bull. Soc. Chim. Belg.* **1948**, *57*, 575.
20. J. C. Wittmann, P. Smith, Highly oriented thin-films of poly(tetrafluoroethylene) as a substrate for oriented growth of materials, *Nature* **1991**, *352*, 414.
21. S. Nagamatsu, W. Takashima, K. Kaneto, Y. Yoshida, N. Tanigaki, K. Yase, Backbone arrangement in "friction-transferred" regioregular poly(3-alkylthiophene)s, *Macromolecules* **2003**, *36*, 5252.
22. M. Campoy-Quiles, J. Nelson, D. D. C. Bradley, P. G. Etchegoin, Dimensionality of electronic excitations in organic semiconductors: a dielectric function approach, *Phys. Rev. B* **2007**, *76*, 195206.
23. M. Brinkmann, P. Rannou, Effect of molecular weight on the structure and morphology of oriented thin films of regioregular poly(3-hexylthiophene)

- grown by directional epitaxial solidification, *Adv. Funct. Mater.* **2007**, *17*, 101.
24. T. J. Prosa, M. J. Winokur, J. Moulton, P. Smith, A. J. Heeger, X-ray structural studies of poly(3-alkylthiophenes) - an example of an inverse comb, *Macromolecules* **1992**, *25*, 4364.
  25. K. Tashiro, M. Kobayashi, T. Kawai, K. Yoshino, Crystal structural change in poly(3-alkylthiophene)s induced by iodine doping as studied by an organized combination of X-ray diffraction, infrared/Raman spectroscopy and computer simulation techniques, *Polymer* **1997**, *38*, 2867.
  26. S. Bruckner, W. Porzio, The structure of neutral polythiophene - an application of the Rietveld method, *Makromol. Chem. Macromol chem physic* **1988**, *189*, 961.
  27. E. Hecht, A. Zajac, *Optics*, Addison Wesley Publishing Company, Reading, MA **1997**.
  28. C. J. Yang, S. A. Jenekhe, Group-contribution to molar refraction and refractive-index of conjugated polymers, *Chem. Mater.* **1995**, *7*, 1276.
  29. S. Malik, A. K. Nandi, Crystallization mechanism of regioregular poly(3-alkylthiophene)s, *J. Polym. Sci., Part B: Polym. Phys.* **2002**, *40*, 2073.
  30. S. H. Chen, C. H. Su, A. C. Su, Y. S. Sun, U. Jeng, S. A. Chen, Gibbs-Thomson analysis of crystalline poly(9,9-di-n-octyl-2,7-fluorene), *J. Appl. Crystallogr.* **2007**, *40*, S573.
  31. P. J. Flory, *Principle of Polymer Chemistry* Cornell University Press, New York **1953**.

32. A. J. Mozer, N. S. Sariciftci, A. Pivrikas, R. Osterbacka, G. Juska, L. Brassat, H. Bassler, Charge carrier mobility in regioregular poly(3-hexylthiophene) probed by transient conductivity techniques: a comparative study, *Phys. Rev. B* **2005**, *71*, 035214.
33. M. Redecker, D. D. C. Bradley, M. Inbasekaran, E. P. Woo, Mobility enhancement through homogeneous nematic alignment of a liquid-crystalline polyfluorene, *Appl. Phys. Lett.* **1999**, *74*, 1400.
34. A. M. Ballantyne, L. Chen, J. Dane, T. Hammant, F. M. Braun, M. Heeney, W. Duffy, I. McCulloch, D. D. C. Bradley, J. Nelson, The effect of poly(3-hexylthiophene) molecular weight on charge transport and the performance of polymer : fullerene solar cells, *Adv. Funct. Mater.* **2008**, *18*, 2373.
35. M. A. Baklar, S. Barard, D. Sparrowe, R. Wilson, I. McCulloch, M. Heeney, T. Kreouzis, N. Stingelin, Origin of mobility enhancement in liquid-crystalline polymer semiconductors, *Submitted* **2010**.
36. S. C. Jain, M. Willander, V. Kumar, *Semiconductors and Semimetals: Conducting Organic Materials and Devices*, Elsevier/Academic Press, Amsterdam **2007**.
37. J. F. Chang, B. Q. Sun, D. W. Breiby, M. M. Nielsen, T. I. Solling, M. Giles, I. McCulloch, H. Sirringhaus, Enhanced mobility of poly(3-hexylthiophene) transistors by spin-coating from high-boiling-point solvents, *Chem. Mater.* **2004**, *16*, 4772.
38. S. K. Park, T. N. Jackson, J. E. Anthony, D. A. Mourey, High mobility solution processed 6,13-bis(triisopropyl-silylethynyl) pentacene organic thin film transistors, *Appl. Phys. Lett.* **2007**, *91*, 063514.

39. S. K. Park, D. A. Mourey, S. Subramanian, J. E. Anthony, T. N. Jackson, High-mobility spin-cast organic thin film transistors, *Appl. Phys. Lett.* **2008**, *93*, 43301.
40. T. D. Anthopoulos, C. Tanase, S. Setayesh, E. J. Meijer, J. C. Hummelen, P. W. M. Blom, D. M. de Leeuw, Ambipolar organic field-effect transistors based on a solution-processed methanofullerene, *Adv. Mater.* **2004**, *16*, 2174.
41. J. E. Anthony, J. S. Brooks, D. L. Eaton, S. R. Parkin, Functionalized pentacene: improved electronic properties from control of solid-state order, *J. Am. Chem. Soc.* **2001**, *123*, 9482.
42. M. M. Payne, S. A. Odom, S. R. Parkin, J. E. Anthony, Stable, crystalline acenedithiophenes with up to seven linearly fused rings, *Org. Lett.* **2004**, *6*, 3325.
43. S. Subramanian, S. K. Park, S. R. Parkin, V. Podzorov, T. N. Jackson, J. E. Anthony, Chromophore fluorination enhances crystallization and stability of soluble anthradithiophene semiconductors, *J. Am. Chem. Soc.* **2008**, *130*, 2706.
44. I. McCulloch, M. Heeney, C. Bailey, K. Genevicius, I. Macdonald, M. Shkunov, D. Sparrowe, S. Tierney, R. Wagner, W. M. Zhang, M. L. Chabinyc, R. J. Kline, M. D. McGehee, M. F. Toney, Liquid-crystalline semiconducting polymers with high charge-carrier mobility, *Nat. Mater.* **2006**, *5*, 328.
45. R. S. Loewe, S. M. Khersonsky, R. D. McCullough, A simple method to prepare head-to-tail coupled, regioregular poly(3-alkylthiophenes) using grignard metathesis, *Adv. Mater.* **1999**, *11*, 250.





## Chapter 5

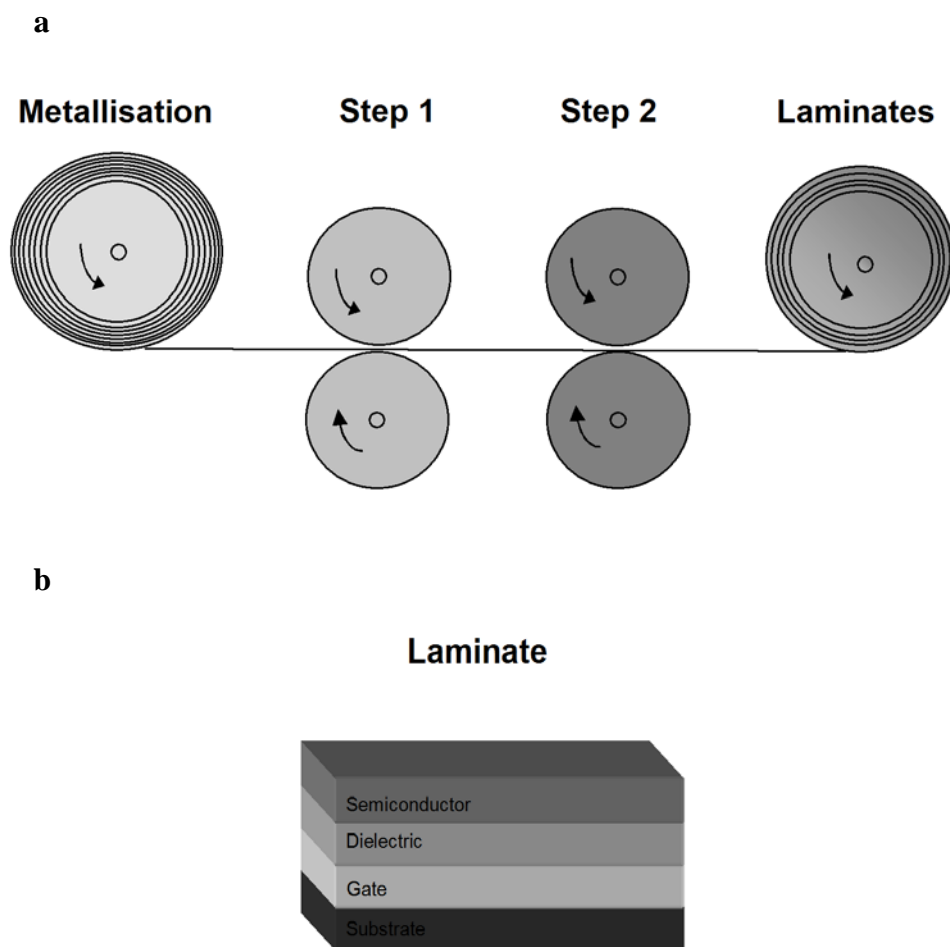
### Outlook

The possibility of processing organic semiconductors into functional structures of well defined molecular order offers new exciting opportunities in the area of plastic electronics. In this thesis we explored the potential of ink-jet printing and elucidating structure/property relationships of liquid-crystalline polymers to produce high mobility structures. In addition, this thesis illustrates the potential of solid-state processing of organic semiconductors which allows fabrication of a large variety of useful structures; and a multitude of scientific and technical products may readily be explored in future. This outlook envisages to broaden the range of processes that are in reach with the processing strategies described in this thesis, and potential applications are discussed.

#### **5.1. Roll-to-roll coating of electronic products**

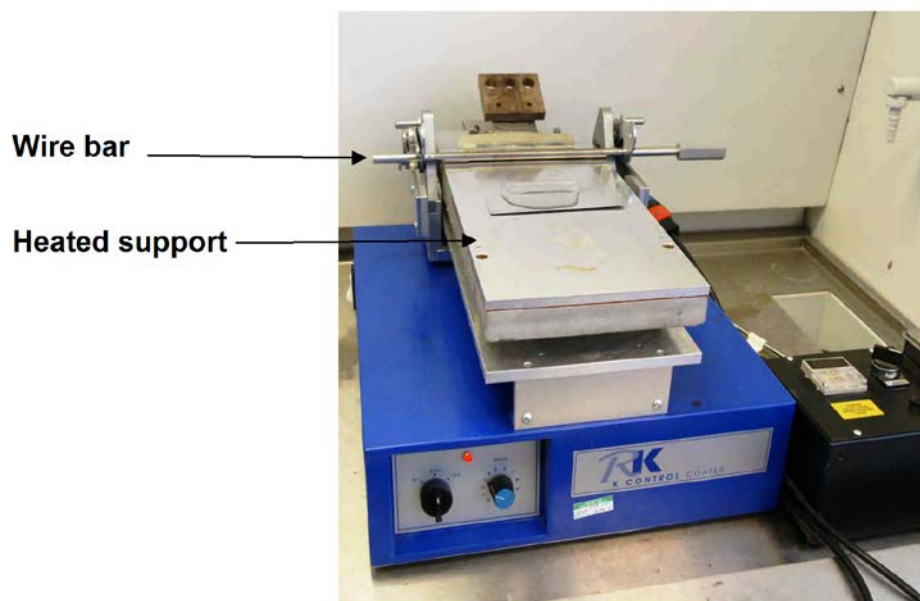
##### **5.1.1. Foil stamping and lamination**

It is clear that high-throughput roll-to-roll methods have to be adopted for rendering manufacturing of large-area organic electronic products economically viable. Inexpensive low-temperature deposition and patterning techniques are therefore attracting increasing interest as alternative candidates to the spin-coating procedures typically used on laboratory-scale for the fabrication of organic



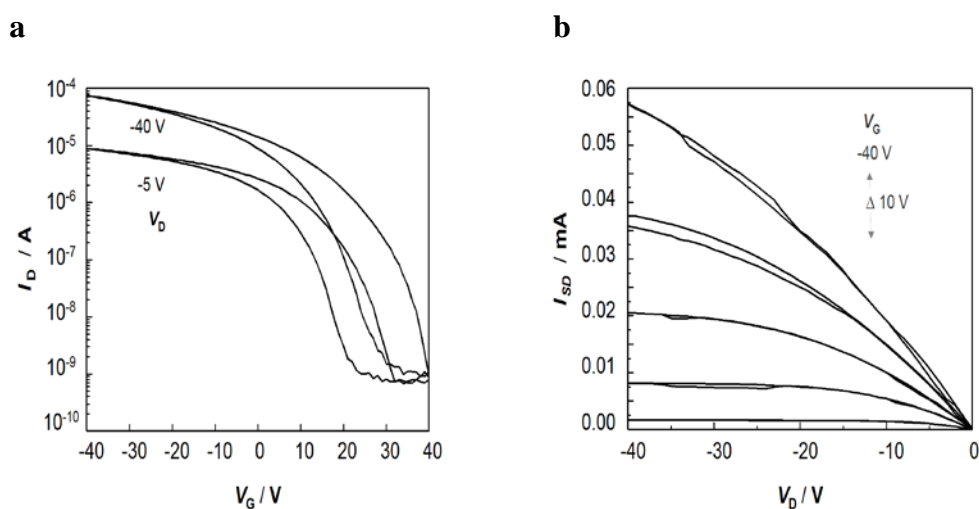
**Figure 1.** (a) Schematic illustration of the production of organic thin-film-transistors by roll-to-roll methodologies. The process involves producing novel laminates of gate metal, dielectric (step 1) and semiconductor (step 2) homogeneously over a carrier substrate. The production of the laminate requires suitable materials that can be processed as thin films, and which have the requisite mechanical and electrical properties. (b) Wire-bar coating may be exploited to produce the laminates of a dielectric material, semiconductor or a semiconducting blend of adjusted mechanical properties onto vacuum metalized substrates. A patterned stamping process could be subsequently used to transfer the laminate from the carrier substrate onto the patterned source/drain electrodes on a roll-to-roll scale. This manufacturing process is based on ongoing activities within the frame work of a TSB-funded project: DT/F006144/2 (DECAF).

semiconducting devices. These processing schemes promise to be readily up-scalable and are compatible with flexible substrates and large-area fabrication at low cost per unit area.<sup>1,2</sup>



**Figure 2.** Photograph of the RK Print desk-top wire-bar coater used in this thesis.

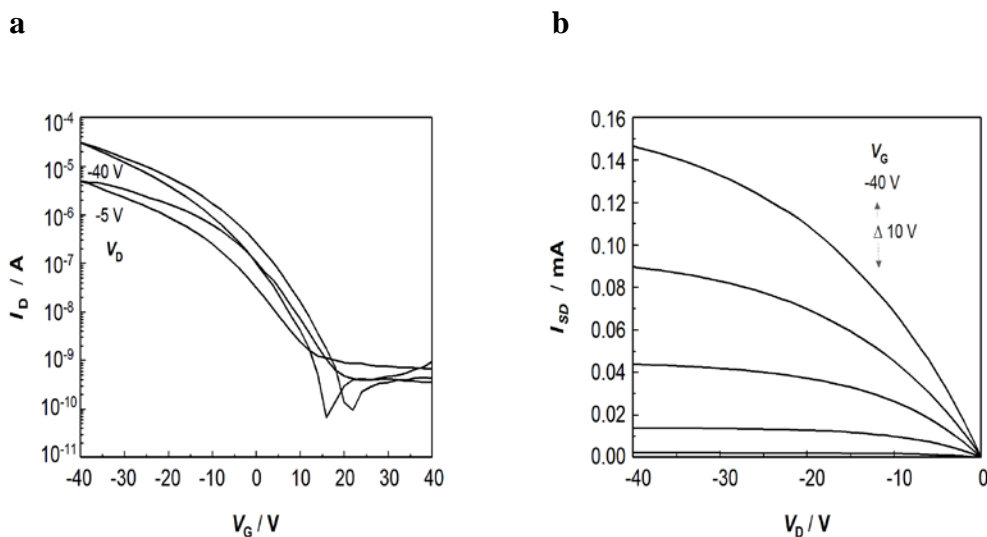
In this thesis, we explored ink-jet printing of the liquid-crystalline polymer poly(2,5-bis(3-dodecylthiophen-2-yl)thieno[3,2-*b*]thiophenes) pBTTT-C<sub>12</sub>, which allows precise deposition of well-defined semiconducting patterns. However, ink-jet printing is a series process, thus not ideal for the manufacturing of large-area products at high throughput. pBTTT formulations, as already discussed in chapter 3, should therefore be adjusted so that they are also applicable to roll-to-roll procedures. This would allow, for instance, multi-layer architectures to be realized by exploiting lamination techniques (schematically depicted in Figure 1a). Consequently self-aligned architectures can be produced by using a patterned stamping process to transfer the laminate (Figure 1b) onto the patterned source-drain electrodes, thus achieving direct registration. This would be a process stream similar to those employed for, e.g., the manufacture of security features used in credit cards and banknotes.<sup>3</sup> Wire-bar coating techniques<sup>4,5</sup> (Figure 2) may be exploited for this purpose, especially for the fabrication of multi-layer structures.



**Figure 3.** (a) and (b) Transfer and output characteristics of poly(3-hexylthiophene) (P3HT) ( $M_w = 60 \text{ kg mol}^{-1}$ ) bottom gate/bottom contact thin-film field-effect transistors (channel length  $L = 10 \text{ }\mu\text{m}$ ; channel width  $W = 10 \text{ mm}$ ), wire-bar coated from a 1.0 wt% xylene solution.

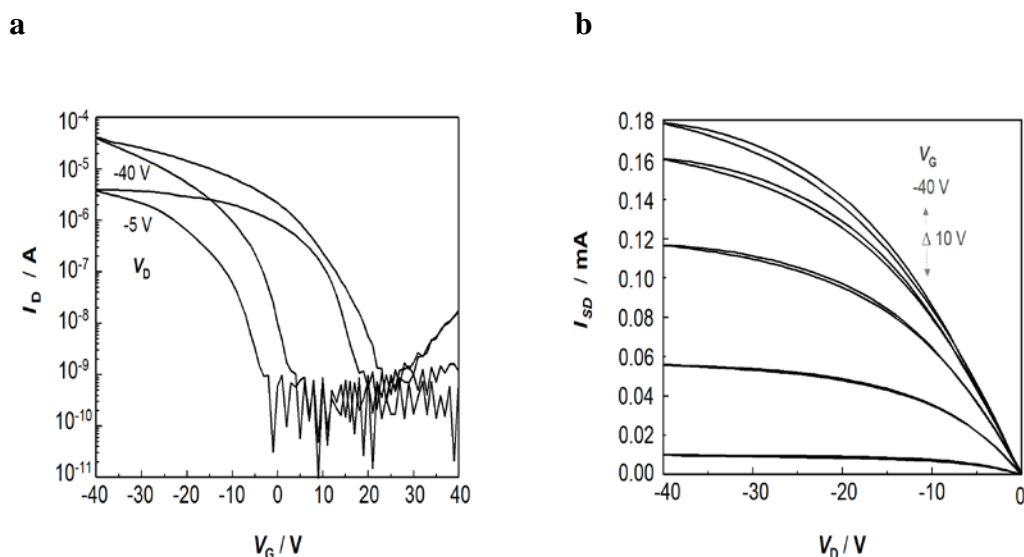
Indeed, this methodology is commonly employed for deposition of coatings for a wide range of applications, including labels, office products and flexible packaging. Most interestingly for use in electronics manufacturing, wire-bar coating is generally uncomplicated to scale-up to roll-to-roll production methods such as reverse gravure coating, without compromising control of the thickness of the deposited layers across the entire substrate area. In addition, wire-bar coating has the advantage that it permits straight-forward processing also at elevated temperatures ( $T > 100 \text{ }^\circ\text{C}$ ), in contrast to inkjet printing methods, which often are limited to deposition temperatures below  $80 \text{ }^\circ\text{C}$ .

Reassuringly, initial studies on wire-bar coating of regio-regular poly(3-hexylthiophene) (rr-P3HT) layers onto pre-patterned Si/SiO<sub>2</sub> to fabricate discrete devices demonstrated field-effect transistors (FETs) of a performance very similar to spin-coated structures (Figure 3a,b). Indeed, hole mobilities of  $10^{-2} \text{ cm}^2 \text{ V}^{-1} \text{ s}^{-1}$  and on/off ratios of  $10^5$  were achieved, despite the fact that the devices were fabricated



**Figure 4.** (a) and (b) Transfer and output characteristics of poly(2,5-bis(3-dodecylthiophen-2-yl)thieno[3,2-*b*]thiophene) (pBTTT-C<sub>12</sub>) ( $M_w = 51.4 \text{ kg mol}^{-1}$ ) thin-film field-effect transistors (top gate/ top contact; channel length  $L = 20 \mu\text{m}$ ; channel width  $W = 10 \text{ mm}$ ), spin-coated from a 1.0 wt% 1,2,4-trichlorobenzene solution.

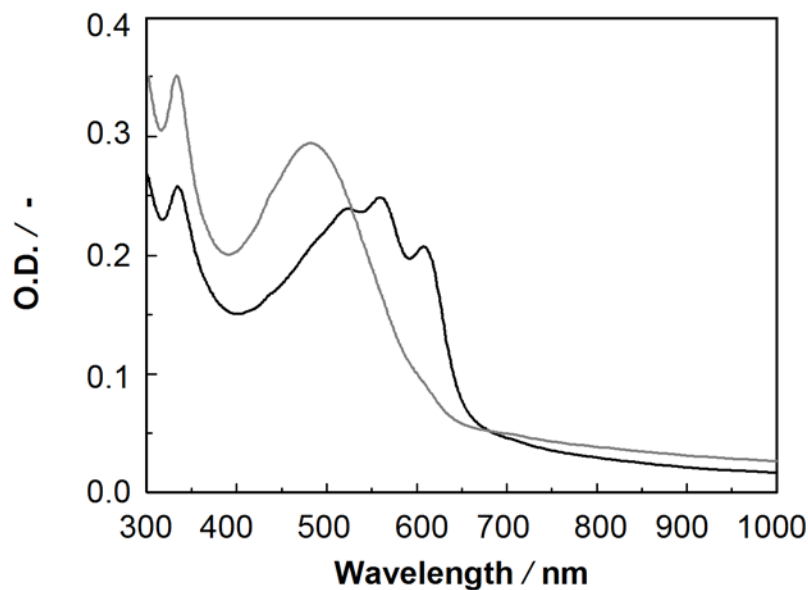
in light and air [NB. the FETs were measured in N<sub>2</sub> environment, after annealing in vacuum at 80 °C for 4 hours]. Therefore, it is evident that the wire-bar coating process may be readily extendable to poly(2,5-bis(3-alkylthiophen-2-yl)thieno[3,2-*b*]thiophene (pBTTT) formulations which possess better electronic performances than (rr-P3HT) as discussed in this thesis (chapter 1 and 3), especially when considering deposition at elevated temperatures is possible. Indeed, in a preliminary series of experiments, we fabricated top-gate/bottom-contact pBTTT-C<sub>12</sub> FET devices on flexible polyethylene terephthalate (PET) substrates by spin-coating from a 1.0 wt% 1,2,4-trichlorobenzene (TCB) solution. Poly(vinyl phenol) (PVP) was thereby utilized as the gate dielectric. The resulting FET structures for these spin-coated devices displayed promising transfer and output characteristics (Figure 4a,b), with hole mobilities of  $10^{-2} \text{ cm}^2 \text{ V}^{-1} \text{ s}^{-1}$  and on/off ratios of up to  $10^4$ , despite having been processed at ambient conditions.



**Figure 5.** (a) and (b) Transfer and output characteristics of poly(3-hexythiophene):high-density polyethylene (P3HT:HDPE), (50:50) thin-film field-effect transistors (channel length  $L = 10 \mu\text{m}$ ; channel width  $W = 10 \text{mm}$ ), wire-bar coated from 1.0 wt% xylene solution.

Furthermore, wire-bar coating also allows deposition of blends of the semiconducting material with, for instance, an insulating commodity polymer. This allows to control the processing parameters such as solution viscosity and the mechanical properties of the resulting architectures.<sup>6</sup> The latter becomes particularly relevant when considering fabrication of organic electronic products by lamination processes as already discussed earlier (Figure 1a,b). Blending can contribute to maintain the mechanical integrity within the multilayer architecture, thus preventing shorts.

Reassuringly the electronic properties seem not seriously affected by the blending (see Figure 5).<sup>6-9</sup> Indeed, preliminary FET characteristics of P3HT:high-density polyethylene (HDPE) blends using a 50:50 weight ratio wire-bar coated onto pre-patterned transistors displayed field-effect mobilities of  $10^{-2} \text{cm}^2 \text{V}^{-1} \text{s}^{-1}$  and on/off ratios reaching  $10^4$  despite fabrication was conducted in light and air



**Figure 6.** Ultraviolet–visible (UV-vis) absorption spectra of poly(3-hexylthiophene):[6,6]-phenyl C<sub>61</sub>-butyric acid methyl ester (P3HT:[60]PCBM), (50:50) blend, deposited on a microscopy glass slide, spin-coated (grey) and wire-bar coated (black) P3HT films from 1 wt% xylene solution.

(Figure 5a,b). Clearly, there is ample room for expanding this process, thus opening new pathways for the manufacturing of organic electronic applications. A thorough understanding of the solution phase behaviour, as discussed in Chapter 3, will be highly useful for this purpose.

### 5.1.2. Large-area fabrication of organic solar cells

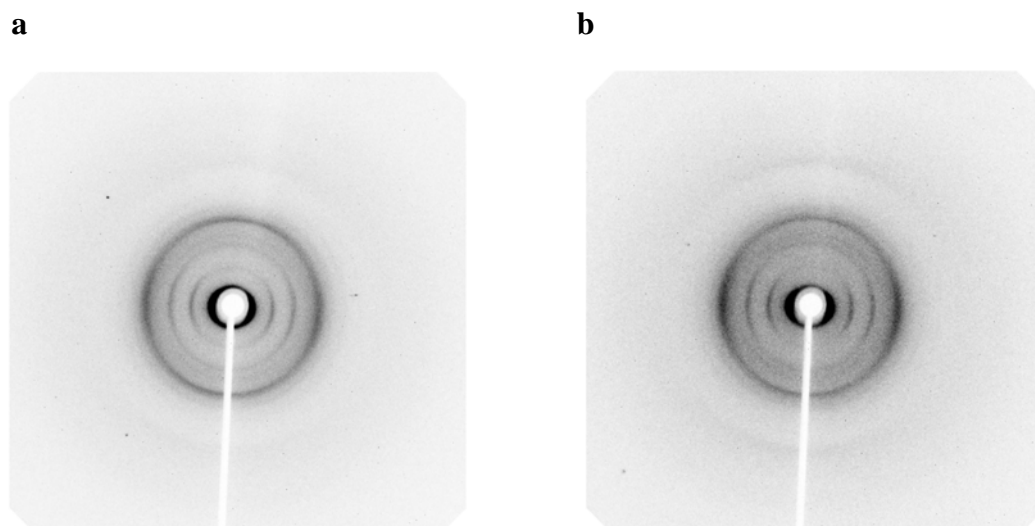
Organic solar cells represent a very promising and rapidly developing technology that has recently received considerable attention from academia as well as industry.<sup>10-18</sup> Organic solar cells promise to provide inexpensive, mechanically flexible products, processed at low temperatures with up-scalable roll-to-roll fabrication procedures. This is in strong contrast to inorganic-based solar cells where, typically, the deposition of the active components requires high temperature and vacuum fabrication steps. Clearly, to render OPV technology attractive, further studies are necessary to improve the overall power conversion

efficiency of current organic solar cells. Among other things, the materials chemistry needs to be tailored in order to produce stable materials that can better match the solar spectrum. Some progress has been realized in this regard.<sup>19-21</sup> Improvements in device engineering are also required to enhance the process of light harvesting, for instance TiO<sub>x</sub> layers may be used as optical spacers to better absorb and distribute the incoming light.<sup>22,23</sup> Finally optimising the materials processing protocols should allow to better control film thicknesses and, thus, film homogeneity over larger areas. In this thesis, focus was directed towards realising processes that allow high through-put methods compatible with roll-to-roll manufacturing such as reverse gravure coating, blade coating, slot-die coating and spray coating.<sup>11,24-26</sup>

In order to build on the work presented in this thesis, we explored the option to use wire-bar coating technologies for the deposition of OPV formulations. Clearly, for this purpose, the importance of solvent selection and solubility of the active materials is even more significant compared to FET formulations, as the active layer is comprised of at least two semiconducting components. Thus minute changes in processing conditions can have significant affect on the resulting microstructure, which in turn will strongly influence the device photovoltaic performance.<sup>27</sup>

Interestingly, UV-vis absorption spectra of films of P3HT: [6,6]-phenyl C<sub>61</sub>-butyric acid methyl ester [60]PCBM 50:50 blends wire-bar coated at 80 °C were similar to those observed for spin-coated and then heat-treated structures.<sup>12,28</sup> This indicates that good molecular aggregation (i.e. intermolecular order<sup>29</sup>) was realized





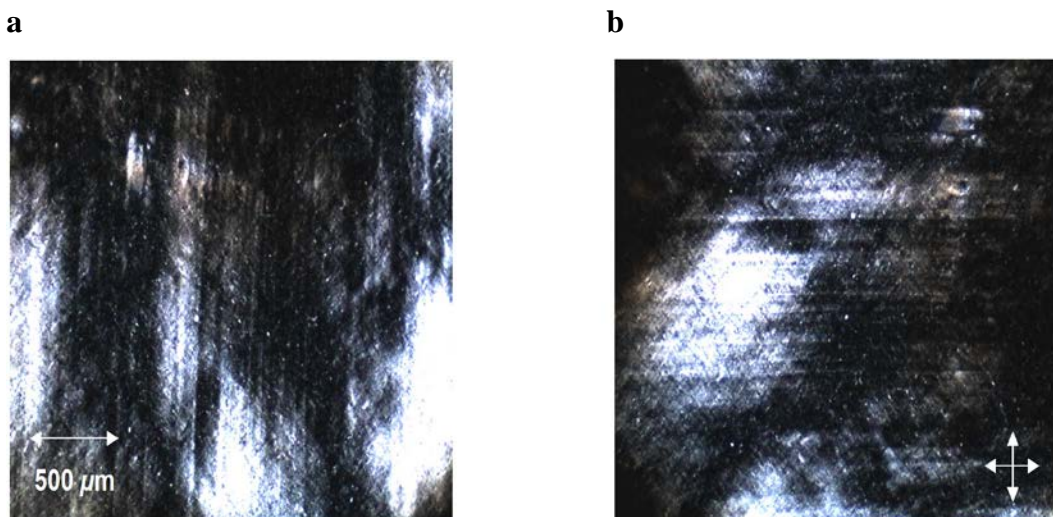
**Figure 7.** Wide-angle X-ray diffraction of rolled poly(3-hexylthiophene) P3HT ( $60 \text{ kg mol}^{-1}$ ) film of  $30 \mu\text{m}$  thickness. The sample was rolled at room temperature. (a) X-ray beam in plane parallel to the film rolling direction, and (b) perpendicular to the film.

in such wire-bar coated films, even without employing post-treatment procedures, such as annealing (Figure 6). However, further investigations on the effect of the wire-bar coating procedure on charge photo-generation and recombination is required. These may be assessed in transient absorption (TAS) and photoluminescent quenching measurements.

## 5.2. Rolling

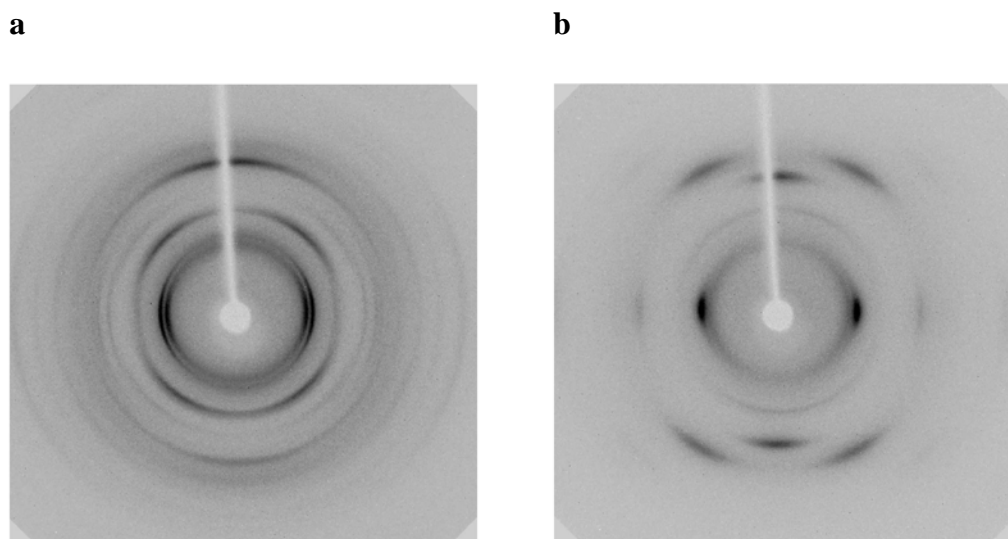
### 5.2.1. Polymer semiconductors

We have shown in Chapter 4 that solid-state processing often allows excellent control over the morphology and final microstructure of organic semiconducting structures. Such molecular order in the organic components employed in devices is most desirable since this normally facilitates molecule-to-molecule hopping of charge-carriers by improved lateral packing (e.g.  $\pi$ -stacking).



**Figure 8.** (a) and (b) Polarized optical micrographs of solid-state pressed poly(vinylidene fluoride) (PVDF) between cross polarizer showing the presence of preferred orientation.

In this context, it is interesting to note that molecular order may be further improved by inducing uniaxial orientation of the macromolecules. For this purpose the solid-state processing technology may be extended to rolling and calendering procedures, which are known to frequently induce a certain degree of ‘texture’ (i.e. anisotropic molecular order).<sup>30</sup> In addition, film thickness of such solid-state structures may be reduced to an extent which will be significantly influenced by the temperature, magnitude of pressure and the rate at which pressure is applied. Promisingly, preliminary rolling experiments permitted fabrication of P3HT films of a thickness of  $\sim 4 \mu\text{m}$  only (which is a factor of 10 thinner when compared to the structures generally obtained by simple solid-state processing). However, so far only limited uniaxial orientation has been obtained, as it is evident from the wide-angle X-ray (WAXS) data of a rolled P3HT thin film shown in Figure 7.



**Figure 9.** (a) Wide-angle X-ray (WAXS) patterns of a melt-processed poly(vinylidene fluoride) (PVDF) films. (b) WAXS patterns of a PVDF film stretched four times, showing a strong molecular anisotropy.

### 5.2.2. Ferroelectric polymers

Interestingly, solid-state processing routes can also be applied to other functional polymers, such as poly(vinylidene fluoride) (PVDF). PVDF is a promising material for use in ferroelectric applications; however, the paraelectric crystal form is the more stable crystal phase compared to the interesting ferroelectric polymorph. In fact, the ferroelectric form can usually only be obtained through tedious stretch alignment, which produces structures that are not easy to integrate e.g. into device architectures. Therefore the use of PVDF structures in ferroelectric applications such as on-chip cooling and temperature sensors for regulators and electronics,<sup>31,32</sup> has been restricted and the significantly more expensive copolymer poly(vinylidene fluoride)–(trifluoroethylene) (PVDF-TrFE) has frequently been utilized for this purpose.<sup>33</sup>

We can envisage adopting the solid-state processing technique as revealed in Chapter 4 of this thesis to solid-state roll PVDF in order to induce the chain alignment necessary for inducing the desired ferroelectric polymorph. This may open up routes to produce in a most simple fashion ferroelectric architectures with the significantly cheaper PVDF. Encouragingly, initial experiments showed that PVDF – as well as PVDF-TrFE copolymers – can be processed in the solid-state below their melting temperatures, resulting in ordered structures as evident in polarized optical microscopy (Figure 8a,b). Comparisons with stretched-aligned PVDF structures are now required (Figure 9a,b) to gain the capability to optimize the solid-state technology for PVDF processing.

### 5.3. References

1. J. R. Sheats, Manufacturing and commercialization issues in organic electronics, *J. Mater. Res.* **2004**, *19*, 1974.
2. R. A. Street, W. S. Wong, S. E. Ready, I. L. Chabinyk, A. C. Arias, S. Limb, A. Salleo, R. Lujan, Jet printing flexible displays, *Mater. Today* **2006**, *9*, 32.
3. R. L. van Renesse, *Optical Document Security*, Artech House, Boston **2005**.
4. A. A. Tracton, *Coatings Technology (Fundamentals, Testing and Processing Techniques)*, CRC Press, Boca Raton **2007**.
5. R. Hanumanthu, L. E. Scriven, Coating with patterned rolls and rods, *Tappi J.* **1996**, *79*, 126.
6. C. Muller, S. Goffri, D. W. Breiby, J. W. Andreasen, H. D. Chanzy, R. A. J. Janssen, M. M. Nielsen, C. P. Radano, H. Sirringhaus, P. Smith, N.

- Stingelin-Stutzmann, Tough, semiconducting polyethylene-poly(3-hexylthiophene) diblock copolymers, *Adv. Funct. Mater.* **2007**, *17*, 2674.
7. S. Goffri, C. Muller, N. Stingelin-Stutzmann, D. W. Breiby, C. P. Radano, J. W. Andreasen, R. Thompson, R. A. J. Janssen, M. M. Nielsen, P. Smith, H. Sirringhaus, Multicomponent semiconducting polymer systems with low crystallization-induced percolation threshold, *Nat. Mater.* **2006**, *5*, 950.
  8. P. Wolfer, C. Muller, P. Smith, M. A. Baklar, N. Stingelin-Stutzmann,  $\alpha$ -Quaterthiophene-polyethylene blends: phase behaviour and electronic properties, *Synthetic Metals* **2007**, *157*, 827.
  9. M. B. Madec, D. Crouch, G. R. Llorente, T. J. Whittle, M. Geoghegan, S. G. Yeates, Organic field effect transistors from ambient solution processed low molar mass semiconductor-insulator blends, *J. Mater. Chem.* **2008**, *18*, 3230.
  10. C. J. Brabec, Organic photovoltaics: technology and market, *Sol. Energy Mater. Sol. Cells* **2004**, *83*, 273.
  11. C. J. Brabec, J. R. Durrant, Solution-processed organic solar cells, *MRS Bull.* **2008**, *33*, 670.
  12. D. Chirvase, J. Parisi, J. C. Hummelen, V. Dyakonov, Influence of nanomorphology on the photovoltaic action of polymer-fullerene composites, *Nanotechnology* **2004**, *15*, 1317.
  13. K. M. Coakley, M. D. McGehee, Conjugated polymer photovoltaic cells, *Chem. Mater.* **2004**, *16*, 4533.
  14. G. Dennler, M. C. Scharber, C. J. Brabec, Polymer-fullerene bulk-heterojunction solar cells, *Adv. Mater* **2009**, *21*, 1323.

15. Y. L. Loo, I. McCulloch, Progress and challenges in commercialization of organic electronics, *MRS Bull.* **2008**, *33*, 653.
16. A. C. Mayer, S. R. Scully, B. E. Hardin, M. W. Rowell, M. D. McGehee, Polymer-based solar cells, *Mater. Today* **2007**, *10*, 28.
17. S. E. Shaheen, D. S. Ginley, G. E. Jabbour, Organic-based photovoltaics, toward low-cost power generation, *MRS Bull.* **2005**, *30*, 10.
18. V. Shrotriya, Polymer power, *Nat. Photonics* **2009**, *3*, 447.
19. D. Muhlbacher, M. Scharber, M. Morana, Z. G. Zhu, D. Waller, R. Gaudiana, C. Brabec, High photovoltaic performance of a low-bandgap polymer, *Adv. Mater* **2006**, *18*, 2931.
20. R. Kroon, M. Lenes, J. C. Hummelen, P. W. M. Blom, B. De Boer, Small bandgap polymers for organic solar cells (polymer material development in the last 5 years), *Polym. Rev.* **2008**, *48*, 531.
21. J. A. Hauch, P. Schilinsky, S. A. Choulis, R. Childers, M. Biele, C. J. Brabec, Flexible organic P3HT : PCBM bulk-heterojunction modules with more than 1 year outdoor lifetime, *Sol. Energy Mater. Sol. Cells* **2008**, *92*, 727.
22. S. H. Park, A. Roy, S. Beaupre, S. Cho, N. Coates, J. S. Moon, D. Moses, M. Leclerc, K. Lee, A. J. Heeger, Bulk heterojunction solar cells with internal quantum efficiency approaching 100%, *Nat. Photonics* **2009**, *3*, 297.
23. A. Roy, S. H. Park, S. Cowan, M. H. Tong, S. N. Cho, K. Lee, A. J. Heeger, Titanium suboxide as an optical spacer in polymer solar cells, *Appl. Phys. Lett.* **2009**, *95*, 013302.

24. L. Blankenburg, K. Schultheis, H. Schache, S. Sensfuss, M. Schrodner, Reel-to-reel wet coating as an efficient up-scaling technique for the production of bulk-heterojunction polymer solar cells, *Sol. Energy Mater. Sol. Cells* **2009**, *93*, 476.
25. Y. H. Chang, S. R. Tseng, C. Y. Chen, H. F. Meng, E. C. Chen, S. F. Horng, C. S. Hsu, Polymer solar cell by blade coating, *Org. Electron.* **2009**, *10*, 741.
26. J. M. Ding, A. D. Vornbrock, C. Ting, V. Subramanian, Patternable polymer bulk heterojunction photovoltaic cells on plastic by rotogravure printing, *Sol. Energy Mater. Sol. Cells* **2009**, *93*, 459.
27. C. Muller, T. A. M. Ferenczi, M. Campoy-Quiles, J. M. Frost, D. D. C. Bradley, P. Smith, N. Stingelin-Stutzmann, J. Nelson, Binary organic photovoltaic blends: A simple rationale for optimum compositions. *Adv. Mater.* **2008**, *20*, 3510.
28. N. Camaioni, L. Garlaschelli, A. Geri, M. Maggini, G. Possamai, G. Ridolfi, Solar cells based on poly(3-alkyl)thiophenes and [60]fullerene: a comparative study, *J. Mater. Chem.* **2002**, *12*, 2065.
29. J. Clark, C. Silva, R. H. Friend, F. C. Spano, Role of intermolecular coupling in the photophysics of disordered organic semiconductors: Aggregate emission in regioregular polythiophene, *Phys. Rev. Lett.* **2007**, *98*, 206406.
30. C. Y. Barlow, N. Hansen, *Materials Processing Handbook*, CRC Press, Boca Raton **2007**.

31. B. Neese, Y. Wang, B. Chu, K. Ren, S. Liu, Q. M. Zhang, C. Huang, J. West, Piezoelectric responses in poly(vinylidene fluoride/hexafluoro propylene) copolymers, *Appl. Phys. Lett.* **2007**, *90*, 242917.
32. B. Neese, B. J. Chu, S. G. Lu, Y. Wang, E. Furman, Q. M. Zhang, Large electrocaloric effect in ferroelectric polymers near room temperature, *Science* **2008**, *321*, 821.
33. K. Asadi, D. M. de Leeuw, B. de Boer, P. W. M. Blom, Organic non-volatile memories from ferroelectric phase-separated blends, *Nat. Mater.* **2008**, *7*, 547.



## Appendix I

### **$\alpha$ -Quaterthiophene-polyethylene blends: phase behaviour and electronic properties**

#### **A1.1. Introduction**

In recent years, there has been increasing interest in organic semiconductors, as these materials promise low-cost fabrication of, *e.g.*, discrete thin-film field-effect transistors (FETs),<sup>1-3</sup> light-emitting diodes (LEDs),<sup>4, 5</sup> organic photovoltaic (OPV) cells,<sup>6</sup> sensors,<sup>7, 8</sup> as well as more integrated structures such as radio-frequency identification tags (RFIDs).<sup>9-11</sup> Both, small molecules and polymers have been investigated for this purpose, with the former usually exhibiting superior electronic properties and the latter generally allowing use of more straight-forward processing methods. In this work, we focus on small molecular species as they display well-defined conjugation lengths and provide simple model systems for elucidating relevant structure-property correlations, especially with respect to their electronic behaviour.

One promising class of semiconducting small molecules are the thiophene homologues,<sup>12</sup> in part due to the rich chemistry of the aromatic thiophene ring, which allows a wide variety of systems to be synthesized. This permits design and tuning of the semiconducting properties of these materials.<sup>13, 14</sup> For instance,

charge-carrier mobilities determined in field-effect transistor configuration,  $\mu_{\text{FET}}$ , of the simple, unsubstituted oligomers increase with conjugation length, apparently saturating around  $10^{-1} \text{ cm}^2 \text{ V}^{-1} \text{ s}^{-1}$  for molecules that comprise six thiophene groups or more (see Table 1).

Generally, oligothiophenes are processed via relatively cumbersome vapour deposition techniques.<sup>15-20</sup> Melt- and solution-based pathways are less common due to the comparatively high melting temperatures, limited solubility at ambient as well as low viscosities of these species, which restricts growth of continuous thin films over large areas.<sup>21, 22</sup> Some issues in melt- and solution-processing of  $\alpha$ -quaterthiophene (4T) are addressed below; in particular, the use of 4T in blends with the insulating linear (high-density) polyethylene. The addition of a high molecular weight polymer to the small-molecular oligothiophene is expected, among other things, to increase solution- and melt-viscosity, which provides, for example, improved film-forming characteristics. Furthermore, highly desirable mechanical (solid-state) properties will be imparted to these two-component systems if tough polymers (such as polyethylene, PE) are utilized for this purpose. This has recently been demonstrated with poly(3-hexylthiophene) (P3HT):PE blends and diblock co-polymers.<sup>23, 24</sup> Importantly, in these studies, it was reported that  $\mu_{\text{FET}}$  was not significantly affected by the presence of the insulator at a PE weight fraction as high as 97 wt% in blends and 90 wt% in block co-polymers. Compared to these systems that are comprised of two macromolecular species, oligothiophene:polyethylene (*i.e.* small-molecular: polymeric) binaries provide additional insight into such crystalline:crystalline semiconducting:insulating organic blends, for instance, as shown here, the

influence of the rate of solidification on microstructures induced and the dependence of the resulting electronic characteristics of these materials systems on the latter.













## **A1.2. Results and discussions**

### **A1.2.1. Phase behaviour of $\alpha$ -quaterthiophene**

Among existing (non-substituted) oligothiophenes,  $\alpha$ -quaterthiophene offers a good trade-off between electronic properties and processability in terms of the material's melting temperature and solubility. Bi- and terthiophene, for instance, would provide good solubility and low melting temperatures,  $T_m$ , but their short conjugation length results in poor semiconducting properties/device performance. Oligothiophenes comprising five thiophene units and more, on the other hand, although interesting for their superior electronic characteristics, display inconveniently high melting temperatures in excess of 250 °C (*cf.* Table 1).

Differential scanning calorimetry (DSC) of  $\alpha$ -quaterthiophene indicates that melt processing requires also relatively elevated temperatures >215 °C, with sublimation commencing at similar temperatures (see Figure 1a). This allows, accordingly, only a relatively small processing window. However, in contrast to its higher homologues, 4T permits relatively straight-forward solution processing. For instance, for concentrations up to ~10 wt%, dissolution temperatures <~140 °C of this species are found in common benign non-chlorinated solvents such as decalin, with corresponding crystallization temperatures of  $T_c$  <110 °C (see, e.g. crystallization /composition diagram of 4T and decalin in Figure 2). Such solutions

**Table 1.** Melting temperatures,  $T_m$ , and charge-carrier mobilities,  $\mu_{\text{FET}}$ , of oligothiophenes and one of its polymeric derivatives, as well as appearance of selected solids and solutions.

Species	Abbreviation	$T_m / ^\circ\text{C}$	$\mu_{\text{FET}} / \text{cm}^2\text{V}^{-1}\text{s}^{-1}$	Solid	Solution <sup>1)</sup>	Reference
$\alpha$ -bithiophene	2T	34 <sup>2)</sup>	--			
$\alpha$ -terthiophene	3T	95 <sup>2)</sup>	--			25
$\alpha$ -quaterthiophene	4T	213 <sup>2)</sup>	$0.1 - 6 \cdot 10^{-3}$			15, 16
$\alpha$ -quinquethiophene	5T	253	$0.6 - 5 \cdot 10^{-2}$			17, 18, 26
$\alpha$ -sexithiophene	6T	298 <sup>2)</sup>	$2.5 - 8 \cdot 10^{-2}$		--	18, 19
$\alpha$ -septithiophene	7T	328	$1 \cdot 10^{-1}$		--	18, 26
$\alpha$ -octithiophene	8T	370	$0.7 - 3 \cdot 10^{-1}$		--	15, 20, 27
poly(3-hexylthiophene) <sup>3)</sup>	P3HT	220 <sup>2)</sup>	$0.6 - 1.2 \cdot 10^{-1}$			23, 28, 29

<sup>1)</sup> solvent: decalin at  $T = 140^\circ\text{C}$

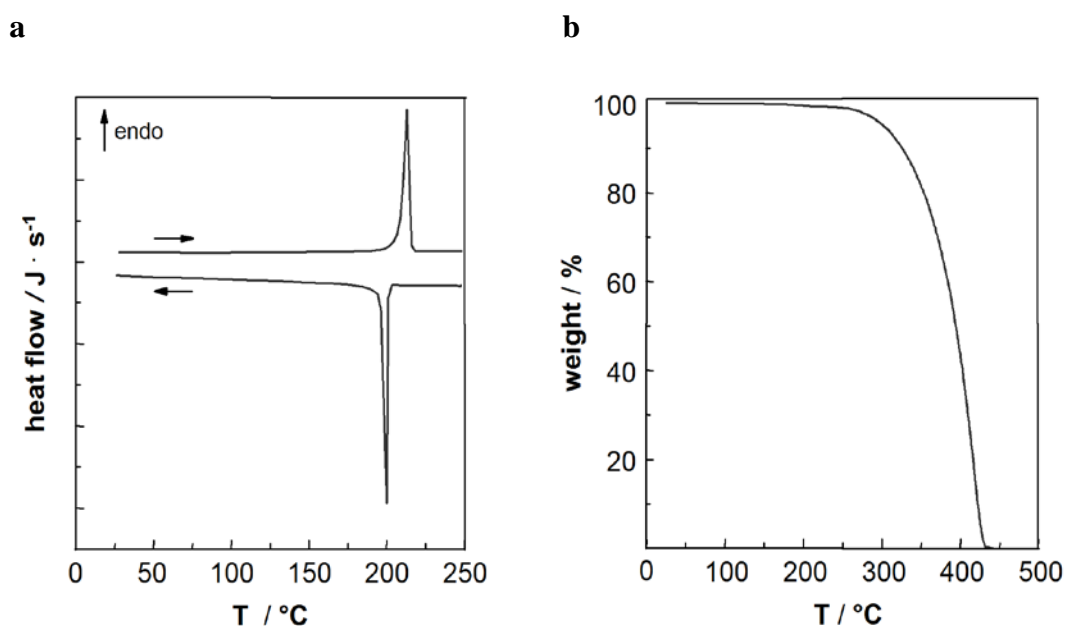
<sup>2)</sup> deduced from DSC second heating thermograms (this chapter)

<sup>3)</sup>  $M_w = 22 \text{ kg mol}^{-1}$

were found to be rather thermally stable (as confirmed by nuclear magnetic resonance (NMR) -data - not shown), which is contrary to those of other conjugated oligomers, such as the polycyclic tetracene and pentacene.<sup>30</sup>

### A1.2.2. Phase behaviour of 4T:HDPE blends

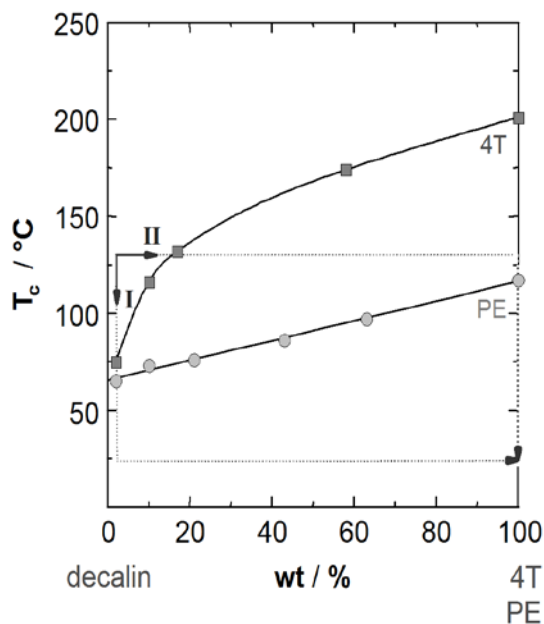
Blends of 4T and high-density polyethylene (HDPE) formed homogenous dilute solutions in decalin at elevated temperatures (see Experimental). In contrast to the P3HT:PE binaries described in Refs. 23 and 24, for which two different solidification sequences can be induced (*i.e.* P3HT crystallizing prior to PE and *vice versa*), we found that 4T exhibits a higher crystallization temperature than PE at all concentrations explored and, accordingly, invariably crystallized prior to the



**Figure 1.** (a) Differential scanning calorimetry (DSC) and (b) thermo-gravimetric analysis (TGA) of  $\alpha$ -quaterthiophene (4T) (heating/cooling rate =  $10\text{ }^{\circ}\text{C min}^{-1}$ ) from which we can deduce the DSC peak melting temperature  $T_m = 213\text{ }^{\circ}\text{C}$ , enthalpy of fusion  $\Delta H_m = 119\text{ J g}^{-1}$ , crystallization temperature  $T_c = 201\text{ }^{\circ}\text{C}$  and enthalpy of crystallization  $\Delta H_c = -118\text{ J g}^{-1}$ .

polymer. Conveniently, this was reported to be the crystallization sequence most favourable to yield high-mobility, low-percolation threshold systems.<sup>23,24</sup>

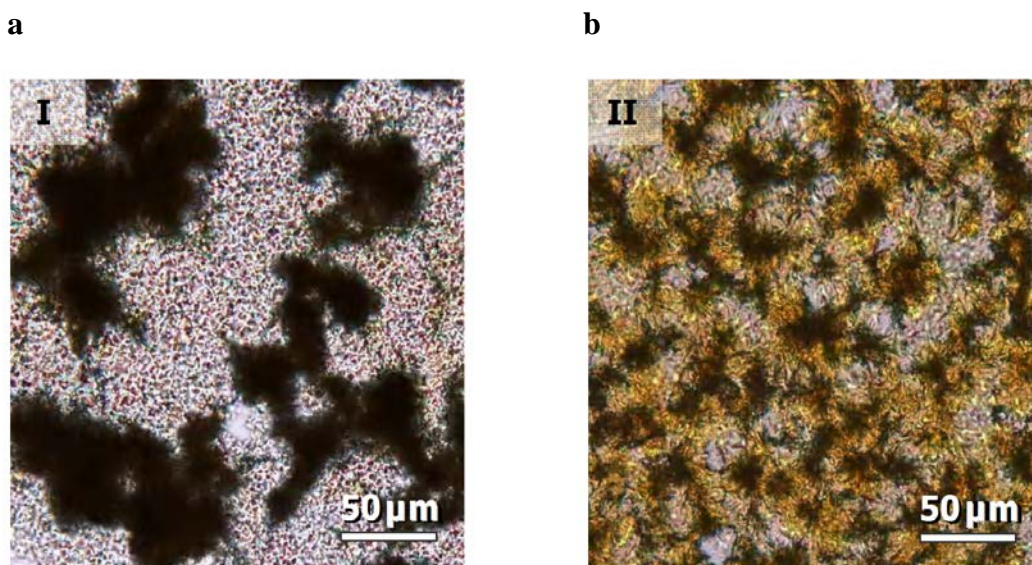
Hence, the 4T:HDPE blends allowed us to explore the influence of different rates of solidification on the microstructures induced and, in turn, their influence on the electronic properties of the blends. For this purpose we followed the two processing pathways indicated in Figure 2. In path I, hot solutions of the two components were cast at ambient, followed by solvent evaporation at that same temperature, causing the materials to slowly crystallize from dilute solution. “Flash”-removal of the solvent was conducted at elevated temperature of  $\sim 130\text{ }^{\circ}\text{C}$  (path II), which resulted in faster crystallization of 4T from the more concentrated viscous liquids, followed by solidification of the polymer. Casting and solvent removal at ambient resulted in coarse microstructures, while 4T:HDPE films



**Figure 2.** Crystallization temperature/composition diagrams of  $\alpha$ -quaterthiophene (4T):decalin and high-density polyethylene HDPE:decalin binaries (superimposed) constructed with peak crystallization temperatures determined from differential scanning calorimetry DSC second cooling thermograms. In path I, a dilute solution was cooled to room temperature, followed by slow solvent removal at ambient, whereas in path II the solvent was rapidly evaporated at  $\sim 130$  °C, followed by cooling to room temperature.

produced at elevated temperatures (*i.e.* fast solvent removal) featured a distinctly finer and more homogenous distribution of the semiconductor (Figure 3).

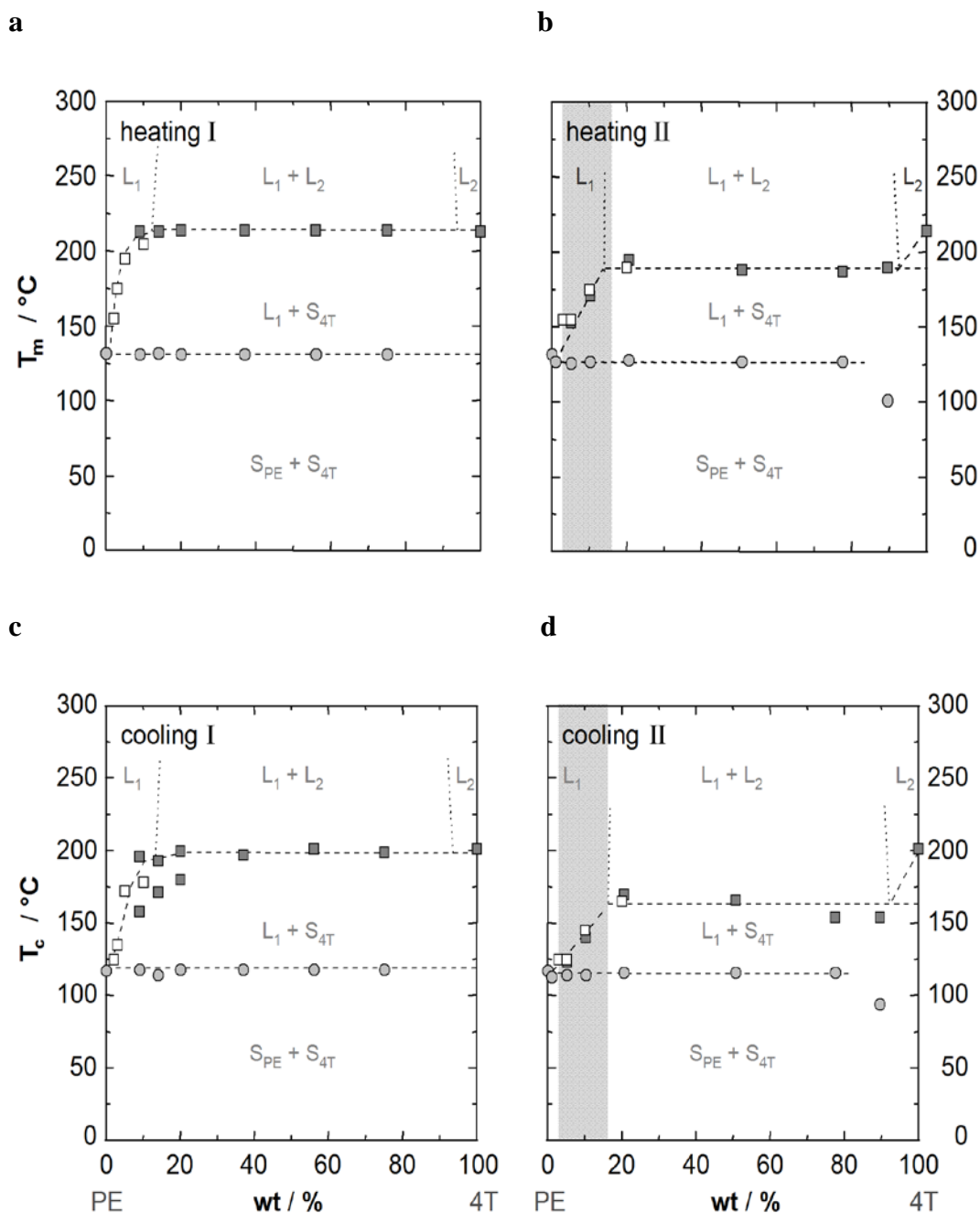
A significant influence of the rate of solidification was also found on the phase behaviour of binary 4T:HDPE mixtures (see Figure 4a,d). All temperature/composition diagrams indicate simple monotectic phase behaviour with a miscibility gap of the two components over a wide range of temperatures and compositions (N.B. A partial miscibility of the two blend components has previously been reported<sup>31</sup>). However, the melting-, dissolution- and crystallization- temperatures of the semiconducting species were significantly affected by the manner in which the 4T:HDPE blends were produced. Considerably



**Figure 3.** Optical micrographs (unpolarized transmitted light) of 50:50  $\alpha$ -quaterthiophene:polyethylene (4T:PE) blends processed via (a) pathway (I) and (b) (II). The darker regions correspond to  $\alpha$ -quaterthiophene.

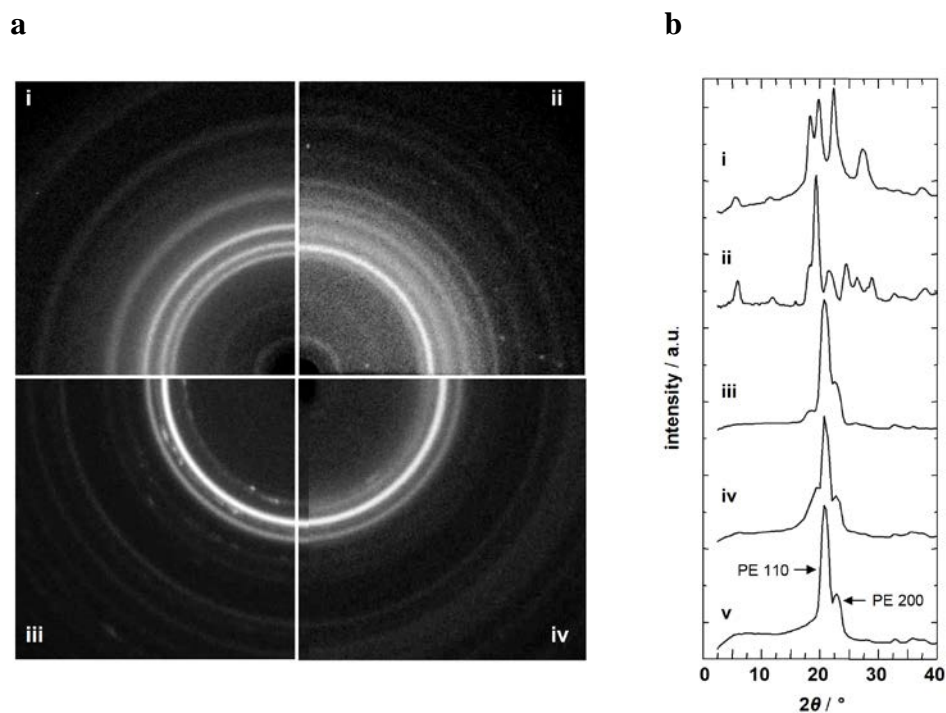
lower values of both,  $T_m$  and  $T_c$  of 4T were recorded in blends obtained by casting at elevated temperatures, consistent with a smaller crystal and domain size of this species (*cf.* Figure 3).

As the processing pathway selected is likely to affect also molecular order known to potentially influence semiconducting properties of conjugated species<sup>18,19</sup> – wide-angle X-ray diffraction (WAXD) was performed on the differently processed 4T:HDPE blends, as well as neat 4T and HDPE references (Figure 5a,b). For the binary mixtures, diffractions resulting from both individual components were observed (Figure 5a,b). Neat 4T crystallized as the low temperature polymorph when processed according to path I and as the high temperature version via route II,<sup>32</sup> as was also found for 4T in the blends with HDPE (*cf.* Figure 5a,b). For  $\alpha$ -oligothiophenes of even number of thiophene units,



**Figure 4.** Binary non-equilibrium temperature/composition diagrams of  $\alpha$ -quaterthiophene:high-density polyethylene 4T:HDPE blends. Heating via (a) pathway I, and (b) pathway II. (c) and (d) Cooling under conditions allowing respectively slow (I) and fast solidification (II). The diagrams were constructed from differential scanning calorimetry DSC peak temperatures observed in first heating and cooling thermograms (full symbols) and optical microscopy (open symbols).  $L_1$ ,  $L_2$  denote liquid phases and  $S_{4T}$ ,  $S_{PE}$  solid 4T and polyethylene.



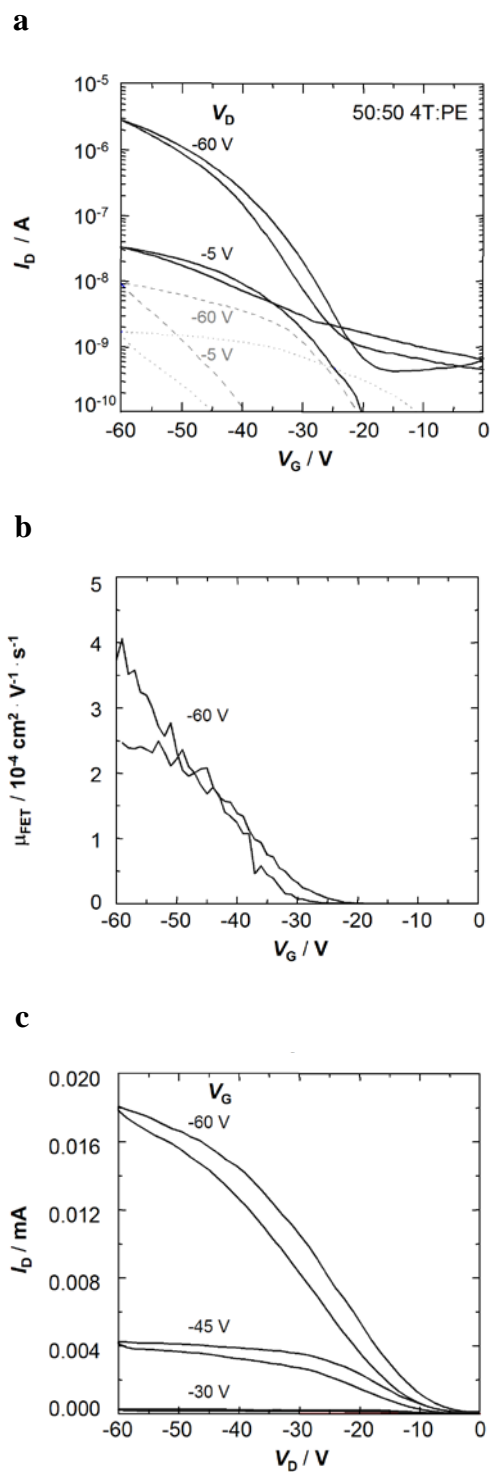


**Figure 5.** (a) and (b) Wide-angle X-ray diffraction patterns that were radially integrated of neat 4T processed following i: path (I), ii: path (II) and 10:90  $\alpha$ -quaterthiophene:high-density polyethylene 4T:HDPE binaries obtained via iii: path (I), iv: path (II) and HDPE (v).

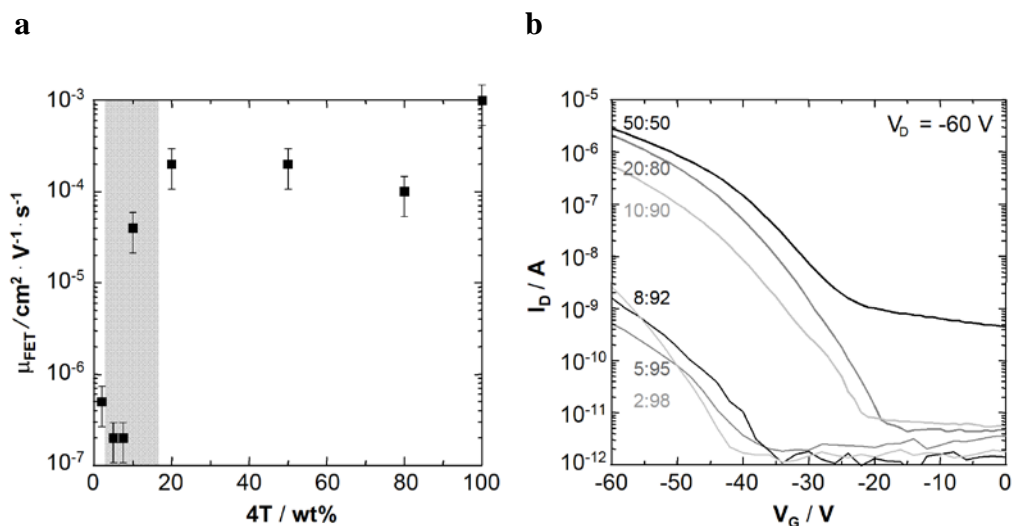
however, charge-transport characteristics were reported to be little affected by the polymorph,<sup>18</sup> and, hence, here of lesser concern.

### A1.2.3. Electronic properties of 4T:HDPE blends

In a first set of experiments, electronic properties of thin films of 4T:HDPE blends were examined in the bottom-gate/bottom-contact FET-configuration. Small source-drain currents were recorded in transistors based on 4T:HDPE produced by slow solvent removal at ambient. Mobilities in such films were estimated to be less than  $10^{-6} \text{ cm}^2 \text{ V}^{-1} \text{ s}^{-1}$ .



**Figure 6.** (a) Transfer characteristics of bottom-gate bottom-contact field-effect transistors FET comprising a 50:50  $\alpha$ -quaterthiophene:high-density polyethylene 4T:HDPE blend ( $L = 5 \mu\text{m}$ ;  $W = 10 \text{mm}$ ) fabricated by rapid solvent evaporation at  $\sim 130 \text{ }^\circ\text{C}$  (solid lines) and slow solidification, at ambient (dashed lines). (b) Corresponding charge-carrier mobility and (c) output characteristics of a FET comprising an active layer cast at  $\sim 130 \text{ }^\circ\text{C}$ .



**Figure 7.** (a) Field-effect mobility and (b) transfer characteristics of  $\alpha$ -quaterthiophene:high-density polyethylene 4T:HDPE blends cast at  $\sim 130$  °C as function of composition.

In sharp contrast, clean FET characteristics were observed for devices comprising 4T:HDPE layers produced at elevated temperatures. In fact, current modulations of  $10^3$  and charge-carrier mobilities of  $\sim 1 \cdot 10^4 \text{ cm}^2 \text{ V}^{-1} \text{ s}^{-1}$  were measured for blends comprising 10 wt% 4T or more, exemplarily shown in Figure 6 for 50:50 4T:HDPE solidified in this manner. This is comparable with  $\mu_{\text{FET}}$  values reported for vapour-deposited neat  $\alpha$ -quaterthiophene.<sup>15, 16</sup> Note, however, the sub-linear dependence of source-drain current,  $I_{\text{D}}$ , on source-drain bias,  $V_{\text{D}}$ , observed in the output characteristics at small  $V_{\text{D}}$ , and the relatively small  $I_{\text{D}}$  at  $V_{\text{D}} = -5 \text{ V}$  in the transfer characteristic, both suggesting limited charge injection (Figure 6a,c). No significant dependence on channel length was observed for devices of  $L = 5 \mu\text{m}$  and  $20 \mu\text{m}$ .

Electronic characteristics deteriorated rapidly when the semiconductor content in 4T:HDPE binaries was reduced to  $< \sim 10$  wt%. Charge-carrier mobilities of  $< 10^{-6} \text{ cm}^2 \text{ V}^{-1} \text{ s}^{-1}$  were obtained for these devices, and a distinct shift of the

threshold voltage,  $V_T$ , of  $\sim 15$  V was observed (see Figure 7a,b). This indicates that a barrier may have formed preventing efficient injection of charge carriers from the source-drain electrodes into the active layers that comprised larger concentrations of insulator.

### **A1.3. Conclusions**

A FET performance comparable to that of neat 4T was recorded with devices based on 4T:HDPE binaries that were processed via path II *and* (at elevated temperatures) featured liquid-liquid phase separation. In contrast, blends in which the two components were miscible in the liquid state (grey-shaded concentration regimes in Figures 4 and 7) showed rapidly deteriorating charge-transport with decreasing semiconductor content, with device performance similar to that found for FETs based on active layers displaying large-scale phase separation, as induced by solidification path I.

### **A1.4. Experimental**

#### **A1.4.1. Materials**

$\alpha$ -Quaterthiophene ( $M_w = 0.34$  kg mol<sup>-1</sup>,  $T_m = 213$  °C,  $T_c = 201$  °C) was purchased from Sigma-Aldrich and linear high-density polyethylene ( $M_w = 10^2$  kg mol<sup>-1</sup>,  $T_m = 132$  °C,  $T_c = 117$  °C) was supplied by DSM (Stamylan 7048).

#### **A1.4.2. Sample preparation**

For thermal analysis and X-ray diffraction studies,  $\alpha$ -quaterthiophene: polyethylene blends were mixed by co-dissolving the materials in decalin (Fluka;

used as received) (~1 wt% total material content) at a temperature of ~140 °C, followed by solvent evaporation at ambient (path I) or at ~130 °C (path II). The latter temperature was selected to be above the crystallization temperature  $T_c$  of polyethylene, but below that of 4T (*cf.* Figure 2). Thin films of blends of different compositions were cast from ~1 wt% solutions (total content) at ambient or ~130 °C, onto glass slides for optical microscopy and onto doped silicon-silicon oxide (Si/SiO<sub>2</sub>) substrates treated with octadecyltrichlorsilane (OTS) for FET studies. The thickness of these films was 5 - 10  $\mu\text{m}$ .

#### **A1.4.3. Thermal analysis**

Thermo-gravimetric analysis (TGA) and differential scanning calorimetry (DSC) were conducted under N<sub>2</sub> atmosphere at a scan rate of 10 °C min<sup>-1</sup> with a Mettler Toledo TGA/SDTA851<sup>e</sup> and a Mettler Toledo DSC 822<sup>e</sup> instrument, respectively. For DSC analysis of  $\alpha$ -quaterthiophene and polyethylene in decalin, medium pressure 120  $\mu\text{l}$  Mettler stainless steel crucibles sealed with Viton O-rings were utilized. The sample weight, including solvent, was ~50 mg. For characterization of the dried 4T:HDPE blends, amounts of about 5 mg were sealed in Al standard 40  $\mu\text{l}$  crucibles.

#### **A1.4.4. Optical microscopy**

Optical microscopy was carried out with a Leica DMRX polarizing microscope equipped with a Mettler Toledo FP82HT hot stage. For construction of the sections of the binary phase diagrams at low concentrations of one component, blend films were heated and cooled at 10 °C min<sup>-1</sup> in the hot stage and

the transition temperatures were deduced from appearance/disappearance of birefringence of the respective crystalline phases.

#### **A1.4.5. Wide-angle X-ray diffraction**

Wide-angle X-ray diffraction patterns of different 4T:HDPE blends were recorded with an Xcalibur PX instrument (Oxford Diffraction) using MoK $\alpha$ -radiation source ( $\lambda = 0.7093 \text{ \AA}$ ).

#### **A1.4.6. Field-effect transistors**

Bottom-gate/bottom-contact FETs were fabricated in a N<sub>2</sub> atmosphere on highly doped Si-wafers with a thermally grown 230 nm SiO<sub>2</sub> layer; the two layers served as the gate electrode and gate insulator, respectively. Prior to application of the semiconductor, the Si-wafers were surface-treated with octadecyltrichlorosilane according to the following procedure. Si/SiO<sub>2</sub> substrates were cleaned in an ultrasonic bath with acetone, water and isopropyl alcohol (in this sequence) and exposed to UV-light for 20 min. Subsequently, the substrates were heated to 60 °C for 15 to 20 min in a mixture of toluene and (OTS) (3:7 ratio). Finally, the OTS-treated Si/SiO<sub>2</sub> was cleaned in hexane, acetone and isopropyl alcohol, followed by drying with nitrogen. Gold (Au) source and drain electrodes (30 nm thick) were defined by standard photolithography (channel lengths,  $L = 5 \mu\text{m}$  and  $20 \mu\text{m}$ ; channel width,  $W = 10 \text{ mm}$ ).

Electronic characterization of the FETs was conducted in a N<sub>2</sub> atmosphere with a HP4155B semiconductor parameter analyzer. Field-effect mobilities were calculated from transfer characteristics (saturation regime) employing the relation:

$$\frac{\delta I_D(V_G)}{dV_G} = \frac{C_i \cdot W}{L} \mu_{FET}(V_G, V_D) \cdot (V_G - V_0) \quad (\text{A1.1})$$

where  $I_D$  is the source-drain current (saturation regime),  $V_G$  and  $V_D$  gate and source-drain voltage, respectively,  $C_i$  the insulator capacitance,  $W$  and  $L$  the channel width and length, and  $V_0$  the turn-on voltage.<sup>33</sup>

### A1.5. References

1. G. Horowitz, Organic field-effect transistors, *Adv. Mater.* **1998**, *10*, 365.
2. H. E. Katz, Z. N. Bao, S. L. Gilat, Synthetic chemistry for ultrapure, processable, and high-mobility organic transistor semiconductors, *Acc. Chem. Res.* **2001**, *34*, 359.
3. H. Sirringhaus, N. Tessler, R. H. Friend, Integrated optoelectronic devices based on conjugated polymers, *Science* **1998**, *280*, 1741.
4. J. H. Burroughes, D. D. C. Bradley, A. R. Brown, R. N. Marks, K. Mackay, R. H. Friend, P. L. Burns, A. B. Holmes, Light-emitting-diodes based on conjugated polymers, *Nature* **1990**, *347*, 539.
5. P. Furuta, J. Brooks, M. E. Thompson, J. M. J. Frechet, Simultaneous light emission from a mixture of dendrimer encapsulated chromophores: a model for single-layer multichromophoric organic light-emitting diodes, *J. Am. Chem. Soc.* **2003**, *125*, 13165.
6. W. U. Huynh, J. J. Dittmer, W. C. Libby, G. L. Whiting, A. P. Alivisatos, Controlling the morphology of nanocrystal-polymer composites for solar cells, *Adv. Funct. Mater.* **2003**, *13*, 73.

7. B. Crone, A. Dodabalapur, A. Gelperin, L. Torsi, H. E. Katz, A. J. Lovinger, Z. Bao, Electronic sensing of vapors with organic transistors, *Appl. Phys. Lett.* **2001**, *78*, 2229.
8. T. Someya, H. E. Katz, A. Gelperin, A. J. Lovinger, A. Dodabalapur, Vapor sensing with  $\alpha$ ,  $\omega$ -dihexylquarterthiophene field-effect transistors: the role of grain boundaries, *Appl. Phys. Lett.* **2002**, *81*, 3079.
9. A. R. Brown, A. Pomp, C. M. Hart, D. M. de Leeuw, Logic gates made from polymer transistors and their use in ring oscillators, *Science* **1995**, *270*, 972.
10. B. Crone, A. Dodabalapur, Y. Y. Lin, R. W. Filas, Z. Bao, A. LaDuca, R. Sarpeshkar, H. E. Katz, W. Li, Large-scale complementary integrated circuits based on organic transistors, *Nature* **2000**, *403*, 521.
11. C. J. Drury, C. M. J. Mutsaers, C. M. Hart, M. Matters, D. M. de Leeuw, Low-cost all-polymer integrated circuits, *Appl. Phys. Lett.* **1998**, *73*, 108.
12. C. D. Dimitrakopoulos, P. R. L. Malenfant, Organic thin film transistors for large area electronics, *Adv. Mater.* **2002**, *14*, 99.
13. J. Nakayama, T. Konishi, M. Hoshino, Preparation of thiophene oligomers, *Heterocycles* **1988**, *27*, 1731.
14. B. Bäuerle, *Handbook of oligo- and polythiophenes : the synthesis of oligothiophenes*, Wiley-VCH, New York **1999**.
15. G. Horowitz, R. Hajlaoui, D. Fichou, A. El Kassmi, Gate voltage dependent mobility of oligothiophene field-effect transistors, *J. Appl. Phys.* **1999**, *85*, 3202.



16. H. E. Katz, L. Torsi, A. Dodabalapur, Synthesis, material properties, and transistor performance of highly pure thiophene oligomers, *Chem. Mater.* **1995**, *7*, 2235.
17. X. M. Hong, H. E. Katz, A. J. Lovinger, B. C. Wang, K. Raghavachari, Thiophene-phenylene and thiophene-thiazole oligomeric semiconductors with high field-effect transistor on/off ratios, *Chem. Mater.* **2001**, *13*, 4686.
18. S. Nagamatsu, K. Kaneto, R. Azumi, M. Matsumoto, Y. Yoshida, K. Yase, Correlation of the number of thiophene units with structural order and carrier mobility in unsubstituted even- and odd-numbered  $\alpha$ -oligothiophene films, *J. Phys. Chem. B* **2005**, *109*, 9374.
19. B. Servet, G. Horowitz, S. Ries, O. Lagorsse, P. Alnot, A. Yassar, F. Deloffre, P. Srivastava, R. Hajlaoui, P. Lang, F. Garnier, Polymorphism and charge-transport in vacuum-evaporated sexithiophene films, *Chem. Mater.* **1994**, *6*, 1809.
20. M. E. Hajlaoui, F. Garnier, L. Hassine, F. Kouki, H. Bouchriha, Growth conditions effects on morphology and transport properties of an oligothiophene semiconductor, *Synth. Met.* **2002**, *129*, 215.
21. M. Melucci, M. Gazzano, G. Barbarella, M. Cavallini, F. Biscarini, P. Maccagnani, P. Ostojic, Multiscale self-organization of the organic semiconductor  $\alpha$ -quinquethiophene, *J. Am. Chem. Soc.* **2003**, *125*, 10266.
22. H. Akimichi, K. Waragai, S. Hotta, H. Kano, H. Sakaki, Field-effect transistors using alkyl substituted oligothiophenes, *Appl. Phys. Lett.* **1991**, *58*, 1500.

23. S. Goffri, C. Muller, N. Stingelin-Stutzmann, D. W. Breiby, C. P. Radano, J. W. Andreasen, R. Thompson, R. A. J. Janssen, M. M. Nielsen, P. Smith, H. Sirringhaus, Multicomponent semiconducting polymer systems with low crystallization-induced percolation threshold, *Nat. Mater.* **2006**, *5*, 950.
24. C. Muller, S. Goffri, D. W. Breiby, J. W. Andreasen, H. D. Chanzy, R. A. J. Janssen, M. M. Nielsen, C. P. Radano, H. Sirringhaus, P. Smith, N. Stingelin-Stutzmann, Tough, semiconducting polyethylene-poly(3-hexylthiophene) diblock copolymers, *Adv. Funct. Mater.* **2007**, *17*, 2674.
25. F. Garnier, G. Horowitz, X. Z. Peng, D. Fichou, Structural basis for high carrier mobility in conjugated oligomers, *Synth. Met.* **1991**, *45*, 163.
26. J. Nakayama, S. Murabayashi, M. Hoshino, Preparation of an  $\alpha$ ,  $\beta$ -type of terthiophenes and septithiophenes, *Heterocycles* **1987**, *26*, 2599.
27. D. Fichou, M. P. Teulade-Fichou, G. Horowitz, F. Demanze, Thermal and optical characterization of high purity  $\alpha$ -octithiophene, *Adv. Mater.* **1997**, *9*, 75.
28. J. F. Chang, J. Clark, N. Zhao, H. Sirringhaus, D. W. Breiby, J. W. Andreasen, M. M. Nielsen, M. Giles, M. Heaney, I. McCulloch, Molecular-weight dependence of interchain polaron delocalization and exciton bandwidth in high-mobility conjugated polymers, *Phys. Rev. B* **2006**, *74*, 115318.
29. J. F. Chang, B. Q. Sun, D. W. Breiby, M. M. Nielsen, T. I. Solling, M. Giles, I. McCulloch, H. Sirringhaus, Enhanced mobility of poly(3-hexylthiophene) transistors by spin-coating from high-boiling-point solvents, *Chem. Mater.* **2004**, *16*, 4772.

30. A. Maliakal, K. Raghavachari, H. Katz, E. Chandross, T. Siegrist, Photochemical stability of pentacene and a substituted pentacene in solution and in thin films, *Chem. Mater.* **2004**, *16*, 4980.
31. H. Kuhn, R. Eckert, Deutsches Patentamt, Auslegeschrift 1119546, *Germany*, **1961**.
32. D. Fichou, Structural order in conjugated oligothiophenes and its implications on opto-electronic devices, *J. Mater. Chem.* **2000**, *10*, 571.
33. A. R. Brown, C. P. Jarrett, D. M. de Leeuw, M. Matters, Field-effect transistors made from solution-processed organic semiconductors, *Synth. Met.* **1997**, *88*, 37.



## Appendix II

### Efficient, stable *bulk* charge transport in crystalline / crystalline semiconductor-insulator blends

#### A2.1. Introduction

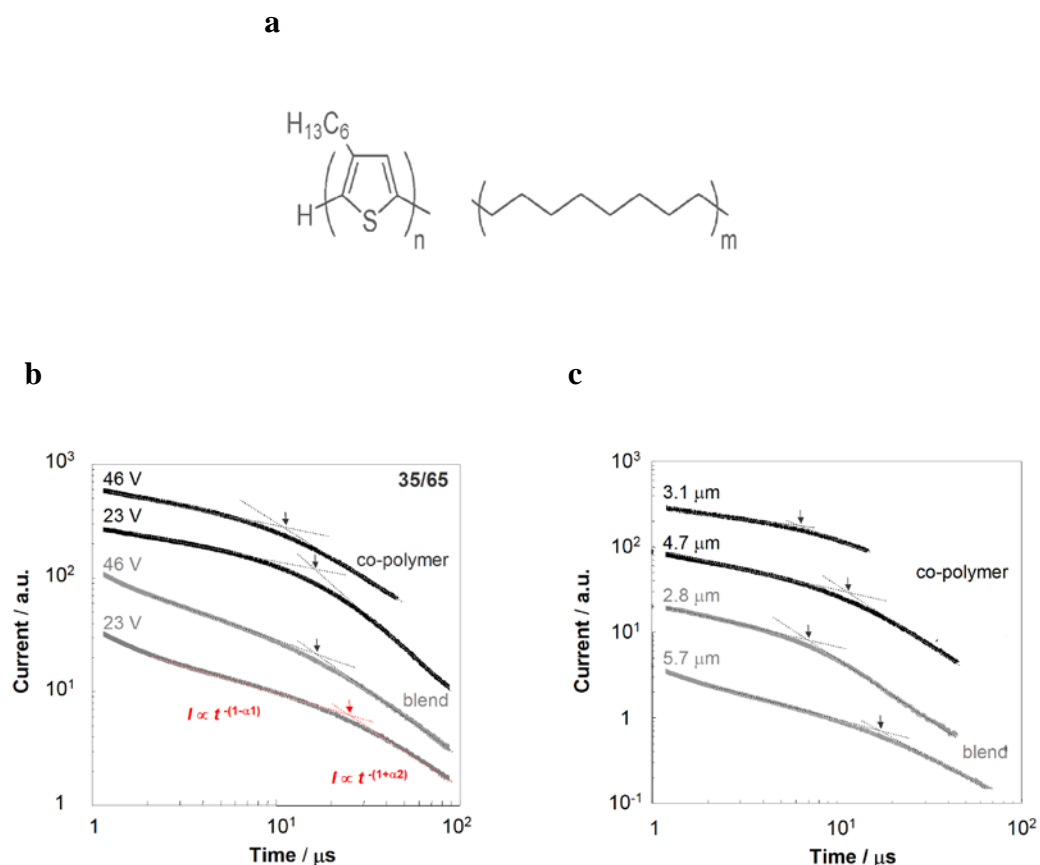
Recently, the potential of organic semiconductor/insulator multi-component systems has been demonstrated with a broad variety of structures ranging from polymer/polymer,<sup>1-5</sup> polymer/small molecule<sup>6</sup> and small molecule/small molecule blends,<sup>7</sup> to [block-] copolymer architectures.<sup>8-12</sup> In general, the main focus has been on the use of such blends and copolymers in field-effect transistor applications, as these materials systems promise the possibility to preferentially segregate the organic semiconductor on the surface of the active layer in contact with the gate dielectric.<sup>2, 3, 13, 14</sup> Such a vertical phase separation often enhances device performance as field-effect transistors (FETs) critically depend on the active semiconductor/gate-dielectric interface – indeed, charge transport occurs essentially in the semiconductor's first few molecular layers at the active layer/gate dielectric interface.<sup>15, 16</sup> However, in various devices other than FET structures, bulk charge transport is often more critical for achieving good electronic performance than interfacial phenomena, for instance, in organic photovoltaic (OPV) cells, based on bulk-heterojunction<sup>17, 18</sup> and the other photoconductor applications. As a consequence, systems that combine good bulk

charge transport with desirable characteristic such as strength and toughness, are much sought after, e.g. for the realization of mechanically- robust, large- area photovoltaic products.

## **A2.2. Results and discussions**

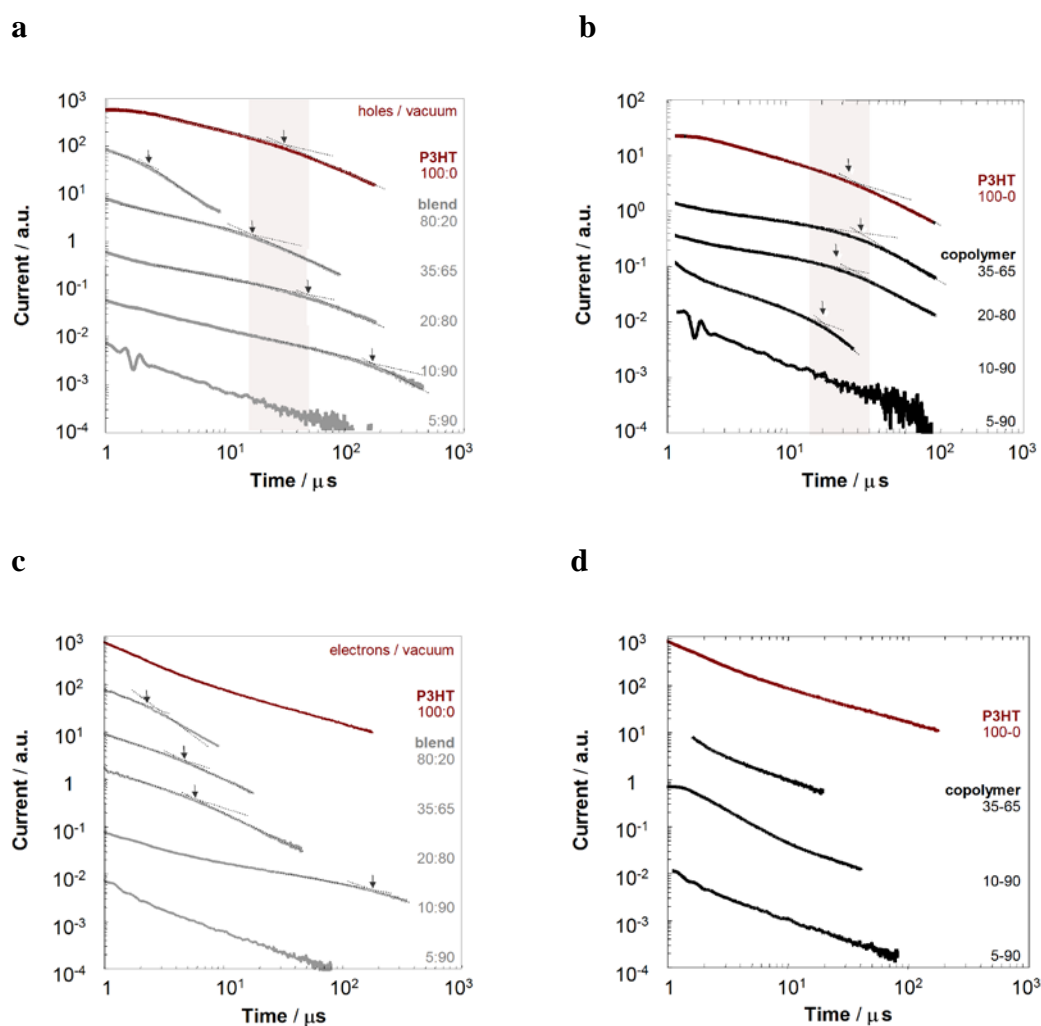
### **A2.2.1. Bulk charge transport**

We set out to investigate thin films of semiconductor/insulator blends and the effect of high-density polyethylene (HDPE) content on bulk charge transport of a broad range of crystalline/crystalline poly(3-hexylthiophene) P3HT:HDPE (see Figure 1a, chemical structures) combinations; and for comparison also of related diblock copolymers. In a first set of time-of-flight photoconduction experiments with 35:65 wt% P3HT:HDPE blends and copolymers, we find clean, dispersive hole photocurrent transients that are very similar to those previously reported for 100 % P3HT (Figure 1b,c).<sup>19</sup> The appearance of inflection point arrival times,  $t_{tr}$  (indicated by arrows), shows that the charge-carriers are traversing the entire film thickness, whilst the pre- and post-transit power laws (gradients) that are deduced from these transients follow, respectively,  $I \propto t_{tr}^{-(1-\alpha_1)}$  and  $I \propto t_{tr}^{-(1+\alpha_2)}$ , is as expected for dispersive charge transport ( $I$  being the photocurrent measured; and  $\alpha_1$  and  $\alpha_2$  being constants).<sup>20</sup> Hole transport scales with bias (*i.e.*, electric field strength) and thickness at the same field strength, even at a content of 65 wt% of the insulating polymer (both in blends and diblock copolymers) (Figure 1c). Clearly, carrier range corresponds to the sample thickness.<sup>21, 22</sup>



**Figure 1.** (a) Chemical structure of poly(3-hexylthiophene) P3HT (right) and high-density polyethylene HDPE (left). Bulk transport in both P3HT:HDPE systems based on diblock copolymers<sup>23</sup> (synthesized according to Ref. 11), and blends (Ref. 1) has been investigated here. (b) Typical hole photocurrent transients measured under vacuum of 35:65 wt% P3HT:HDPE thin-film architectures (film thickness,  $d = 5.7 \mu\text{m}$  and  $4.7 \mu\text{m}$  for, respectively, the blend and copolymer architectures), scaling with electric field. Inflection point arrival time,  $t_{\text{tr}}$  (indicated by the arrows), increases from  $\sim 10 \mu\text{s}$  to  $\sim 20 \mu\text{s}$  (for the copolymer) as the potential is reduced from 46 V to 23 V. Similar behaviour is observed for the blend. (c) Arrival time scaling with sample thickness at constant electric field strength ( $\sim 10^5 \text{ V cm}^{-1}$ ). The arrival time scales with film thickness for both copolymers and blends (e.g. for the 35:65 blend:  $t_{\text{tr}} \sim 8 \mu\text{s}$  for  $d = 2.8 \mu\text{m}$ , compared to  $\sim 18 \mu\text{s}$  for  $d = 5.7 \mu\text{m}$ ).

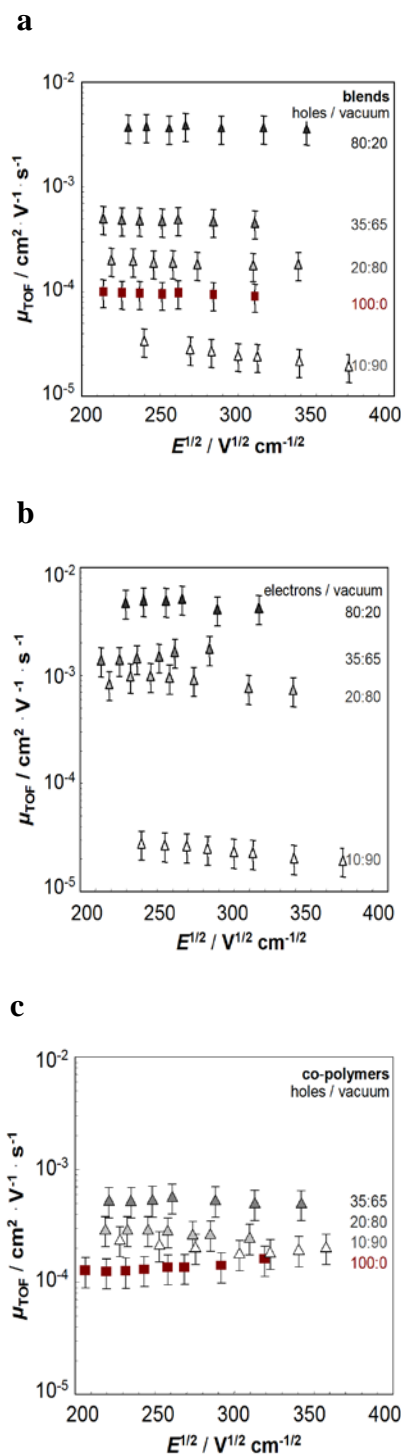
Charge transport is not affected even at a high HDPE content of 80 wt% or more (Figure 2a,d). In fact, for hole transport (Figure 2a), arrival times of less than a few tens of  $\mu\text{s}$  are observed for most P3HT:HDPE systems (highlighted with red shaded areas). Indeed, nearly field-independent charge-carrier mobilities,  $\mu_{\text{TOF}}$  are found for the P3HT:HDPE systems (Figure 3a,b)<sup>20, 24</sup> with hole mobilities



**Figure 2.** Photocurrent transients of various poly(3-hexylthiophene):high-density polyethylene P3HT:HDPE systems measured under vacuum, at an applied electric field of  $\sim 10^5 \text{ V cm}^{-1}$ . (a) Hole photocurrent transients in blends ( $d = 5 - 6 \mu\text{m}$ ) and (b) copolymers. Both of the P3HT:HDPE blends and copolymers show dispersive hole transport for systems with a P3HT content larger than 10 wt %, whereas for 5:95 P3HT:HDPE featureless photocurrent decays are observed. (c) Electron photocurrent transients in P3HT:HDPE blends and (d) copolymers. In contrast to neat P3HT and the P3HT-HDPE block copolymers, P3HT:HDPE blends display stable ambipolar transport down to a P3HT content of 10 wt %.

of  $\approx 5 \cdot 10^{-5}$  to  $5 \cdot 10^{-4} \text{ cm}^2 \text{ V}^{-1} \text{ s}^{-1}$  for both blends and block copolymers (Figure 3a,c); which is in the same order of magnitude to those  $\mu_{\text{TOF}}$  values reported in literature for neat P3HT.<sup>19, 20, 25</sup> Exceptions are the 5:95 and 10:90 blends, which display slower transport with an arrival time of  $t_{\text{tr}} \sim 180 \mu\text{s}$ , resulting in a drastic reduction in the hole mobility (in the case of the 10:90 system), if not in an entirely





**Figure 3.** (a) Field-dependence of bulk charge transport in poly(3-hexylthiophene):high-density polyethylene P3HT:HDPE blends and copolymers, illustrated by Poole-Frenkel plots of calculated carrier mobilities. Essentially field-independent hole mobilities of the order of  $10^{-4}$  to  $10^{-3} \text{ cm}^2 \text{ V}^{-1} \text{ s}^{-1}$  are observed in blends of compositions of  $>20$  wt% P3HT, whereas a negative field dependence is observed for the 10:90 blend. Interestingly, the hole mobilities ( $\sim 10^{-3} \text{ cm}^2 \text{ V}^{-1} \text{ s}^{-1}$ ) of 80:20 P3HT:HDPE blends are about one order of magnitude higher than those observed in neat P3HT (b) Field independent electron mobilities are observed, which are equal or higher to the corresponding hole mobilities. (c) Calculated hole mobilities for P3HT-HDPE copolymers.

featureless photoresponse (P3HT content <10 wt%), indicating that the charge carriers are being trapped, and thus do not reach the counter-electrode.

### **A2.2.2. Electron charge transport**

Interestingly, we find that addition of HDPE in the blends stabilizes electron transport. Indeed, ambipolar charge-transport is observed in P3HT:HDPE blends of compositions of >5 wt% HDPE (Figure 2c), in strong contrast to both our neat P3HT and the block copolymers, which display a featureless decay of the electron photocurrent (Figure 2d). In fact, the electron mobilities in blends are found to be equal to – if not higher than – the hole mobilities measured for the same P3HT:HDPE architecture (Figure 4a,b). This contrasts with previous work on neat P3HT, which reported lower electron mobilities when compared to holes.<sup>19</sup>

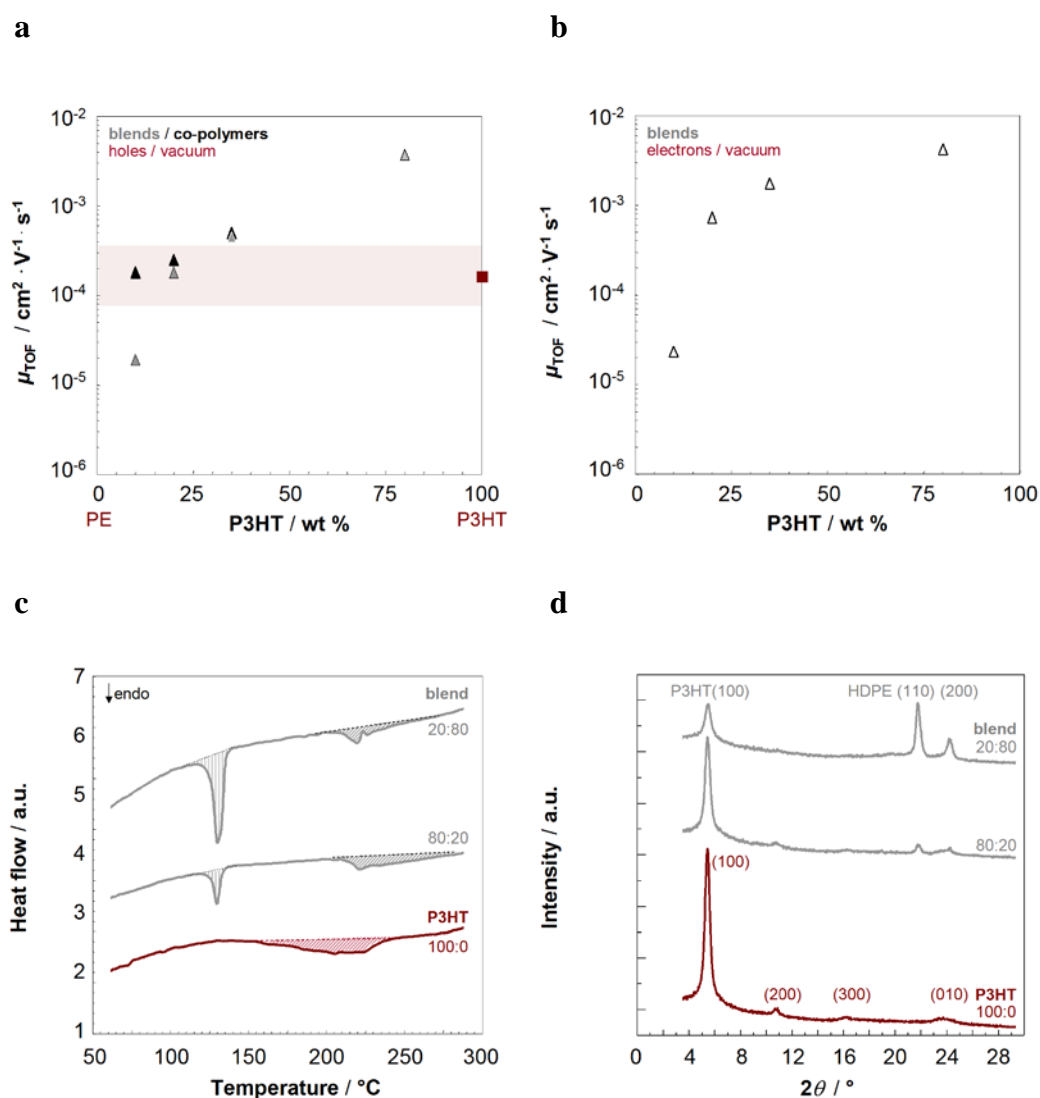
### **A2.2.3. Percolation behaviour**

Somewhat unexpectedly when considering the stratification behaviour observed in amorphous/semicrystalline insulator/semiconductor systems, the bulk behaviour of the P3HT-HDPE copolymers do not differ strongly from the observations made for such binaries when used as active layers in FETs. Clean photocurrents are observed for the copolymers comprising up to 90 wt% of the insulator, with charge carrier mobilities being comparable to those found for neat P3HT (Figure 4a). This corresponds well with the FET percolation behaviour of such copolymers, for which it was reported that field-effect transistor performance degraded at a similar content of the HDPE moiety (*i.e.*, 90 wt%).<sup>12</sup> Block copolymers seem, though, to allow for the addition of a higher content of the insulator moiety without affecting the bulk charge transport compared to the

blends. In fact, 10:90 P3HT:PE blends display distinctly lower electron and hole mobilities than those found for the copolymers – or neat P3HT for that matter – whereas in FETs more than 97 wt% of the insulator HDPE could be added without deteriorating FET device performance.<sup>1</sup>

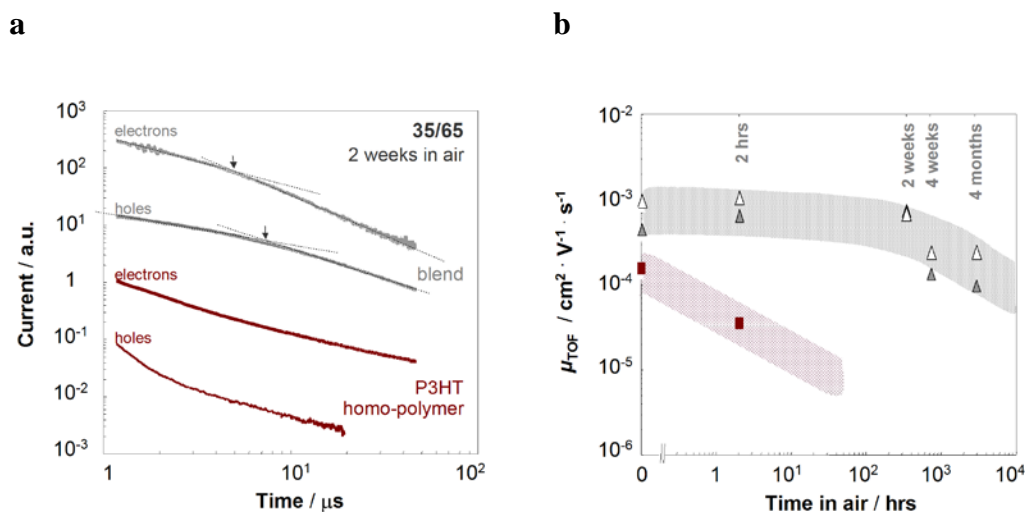
Our observations, thus, strongly indicate that the two phases (HDPE vs. P3HT) separate in a slightly different fashion in the blend and copolymer systems. The copolymers do not permit large-scale phase separation, thus, providing percolating charge-transport pathways in the bulk. In blends, the two components will separate on a much larger scale, which can result in enrichment of the semiconductor at the interfaces,<sup>2, 3, 13</sup> in agreement with the depth distribution of P3HT in thin P3HT:HDPE blends films as measured previously in Rutherford backscattering spectroscopy.<sup>1</sup> As a consequence, FET performance identical to neat P3HT devices may be found for blends of very high HDPE concentrations, but obviously at the expense of bulk charge transport. This possibly explains the excellent transistor characteristics of such blends even at contents of >95 wt% HDPE;<sup>1</sup> and gives guidelines for material selection depending on optoelectronic application (blends for FETs vs, copolymers in OPV structures).

Most intriguingly, certain blend compositions displayed significantly enhanced charge transport properties compared to neat P3HT, with  $\mu_{\text{TOF}}$  measured for 80:20 wt% P3HT:PE blends being up to one order of magnitude higher than those found in the single component P3HT system (Figure 4a,b). This is a rather surprising observation – not readily rationalized with general percolation considerations – possibly with interesting implications, e.g., for the photovoltaic



**Figure 4.** Time-of-flight charge-carrier mobility as a function of poly(3-hexylthiophene), P3HT, content in blends and copolymers, as deduced from the Poole-Frenkel field-dependant mobility at  $10^5 \text{ V cm}^{-1}$ . **(a)** Hole mobilities, measured under vacuum for blends (grey symbols), copolymers (black symbols), and neat P3HT (red square). **(b)** Electron mobilities (blends); no ambipolar charge transport was observed in poly(3-hexylthiophene)-high density polyethylene P3HT-HDPE copolymers. **(c)** Differential scanning calorimetry thermograms. Enthalpy of fusion,  $\Delta H_f$  (shaded areas in left panel). The respective enthalpies, as deduced from the shaded areas are:  $\Delta H_f(20:80 \approx 8 \text{ J g}^{-1}$ ;  $\Delta H_f(80:20) \approx 29 \text{ J g}^{-1}$ ,  $\Delta H_f(100:0) \approx 45 \text{ J g}^{-1}$ ). **(d)** Wide-angle X-ray diffraction patterns of as-cast 20:80, 80:20 P3HT:HDPE blends and neat P3HT films. The (100) P3HT diffraction intensity increased essentially in linear fashion with P3HT content suggesting that the P3HT component in these systems is of similar crystallinity.

applications, in which the enhancement in hole mobility is believed to be one of the most important tools for the overall improvement of solar cell efficiency.<sup>26, 27</sup>



**Figure 5.** (a) Air-stability of 35:65 poly(3-hexylthiophene):high-density polyethylene P3HT:HDPE blends and, for comparison, neat P3HT. Photocurrent transients of holes and electrons at 46 V for 2.8  $\mu\text{m}$ -thin neat P3HT (red symbols) and 35:65 P3TH:HDPE blend films (grey and white symbols), which had been exposed to air for 2 weeks. The arrows indicate the arrival time of the charge carriers. Only featureless decays are observed for the homopolymer P3HT (i.e. neat P3HT), in strong contrast to the blends, for which clean photocurrent transients are obtained. (b) Environmental stability is significantly enhanced by adding HDPE to P3HT as evidenced by the fact that charge carrier mobilities (both holes *and* electrons) for these blends were not significantly affected over a period of 4 months, whereas charge transport in neat P3HT deteriorated after 2 hours exposure to air.

Whereas the origin for this enhanced charge transport is so far unclear, it does *not* appear to result from an increased crystallinity in the specific case of 80:20 wt% blends. This is deduced from the fact that melting enthalpies and wide angle X-ray diffraction intensities (WAXD) increase with P3HT content, without exceptionally high values being found for the 80:20 P3HT:HDPE (Figure 4c,d). Obviously, small changes in molecular order and orientation, for instance, from an edge-on to face-on configuration of the polythiophene backbone, cannot not be excluded.<sup>28</sup>

#### **A2.2.4. Stability**

Finally, we like to also note that blending P3HT with HDPE appears to improve the environmental stability of the organic semiconductor, as is already evident by the fact that we observe clean electron charge transport in all blends, whilst no ambipolar behaviour was found for either the neat P3HT grades or the block copolymers. (Molecular oxygen impurities are frequently proposed as one possible electron traps<sup>19</sup>; HDPE furthermore may act as excellent encapsulating material, e.g., as barrier for water penetration). Interestingly, we find that both electron and hole charge transport are essentially not affected even after four months exposure of P3HT:HDPE blend films to light and air (Figure 5a,b).

#### **A2.3. Conclusions**

Clearly, the high apolarity and crystallinity of the added insulator may be the origin of the beneficial attributes we observe in our systems; yet further investigations are required to elucidate this in more detail. Without doubt, though, it is a highly desirable characteristic of these binaries, especially when considering technological exploitation of such systems.

#### **A2.4. Experimental**

##### **A2.4.1. Materials**

Regio-regular poly(3-hexylthiophene) ( $M_n = 14 \text{ kg mol}^{-1}$  and  $M_w = 22 \text{ kg mol}^{-1}$ ) was generously supplied by Merck Chemicals, and high-density polyethylene ( $M_n = 100 \text{ kg mol}^{-1}$  and  $M_w = 119 \text{ kg mol}^{-1}$ ) was purchased from the Sigma-Aldrich. The P3HT-HDPE block copolymers were received from Dr. Christopher P. Radano

**Table 1.** The molecular weight  $M_w$  and number average molecular weight  $M_n$  of the neat P3HT, PE and various copolymers.

<b>P3HT / PE</b>	$M_w$ kg mol <sup>-1</sup>	$M_n$ kg mol <sup>-1</sup>	$M_n$ (P3HT) kg mol <sup>-1</sup>	$M_n$ (HDPE) kg mol <sup>-1</sup>
<b>neat materials</b>				
100:0	22	14	-	-
0:100	119	100	-	-
<b>copolymers</b>				
35-65	94	74	19	55
20-80	71	61	14	47
10-90	140	93	13	80
5-95	197	121	13	108

and Prof. René Janssen, Technical University of Eindhoven, The Netherlands, synthesized according to Ref. 11 (see Table 1).

#### **A2.4.2. Sample preparation**

Homogeneous thin films for TOF photoconduction experiments were prepared by first dissolving blends and copolymers (total polymer content: 0.2 wt%) in xylene at 130 °C. The hot solutions were then cast onto gold-coated substrates (Au thickness = 50 nm) kept at 125 °C until the solvent had evaporated. This resulted in films of 5 – 6  $\mu\text{m}$  thickness (as measured with a Veeco Dektak<sup>3</sup> ST surface profile measuring system). 50 nm thin counter-electrodes were then thermally evaporated (aluminium: for hole-transport measurements; gold: for electron charge-transport). For wide-angle X-ray diffraction, thinner films of

approximately 0.5 to 2  $\mu\text{m}$  were prepared accordingly, using less concentrated solutions of 0.1 wt%.

#### **A2.4.3. Thermal analysis**

Differential scanning calorimetry (DSC) was conducted under nitrogen at a scan rate of 10  $^{\circ}\text{C min}^{-1}$  with a Mettler Toledo DSC822 instrument. The enthalpy of fusion ( $\Delta H_f$ ) of as-cast films was deduced from the first heating DSC thermograms (indicated with shaded areas in Figure 4c).

#### **A2.4.4. Wide-angle X-ray diffraction**

Standard transmission wide-angle X-ray diffraction was carried out with an X'Pert PRO PANalytical instrument using  $\text{CuK}\alpha$ -radiation ( $\lambda = 1.5418 \text{ \AA}$ ).

#### **A2.4.5. Time-of-flight photoconductivity**

All photoconduction experiments were performed in a vacuum chamber (typical pressure  $10^{-5}$  mbar, unless noted differently) at room temperature. The 6 ns, 337 nm-wavelength, pulsed output of an EG101 Lambda Physik gas laser provided the optical excitation to create electron-hole pairs within a penetration depth of  $\sim 100$  nm of the top electrode in the case of P3HT:HDPE blends and copolymers, where the HDPE absorbs strongly in the UV. For neat P3HT, the 6 ns, 532 nm wavelength output of a frequency doubled insert model Nd:YAG laser provided the optical excitation, as the P3HT displays an absorption peak close to this wavelength. All measurements were carried out under a reverse DC bias from a low noise power supply. The laser pulse intensity was kept sufficiently low. As a consequence, the photogenerated charge was less than 10 % of the charge stored



across the sample ( $C \cdot V$ , where  $C$  is the sample capacitance and  $V$  the applied potential), avoiding space charge effects that would result in a non-uniform electric field. The transient current was measured as a voltage drop across a range of load resistors (typically  $47 \Omega$  for fast signals and  $2.31 \text{ k}\Omega$  for slow signals) at the input of a gain 11 amplifier whose output was connected to an Agilent Infinium digitizing oscilloscope. Signal averaging (typically over 128 pulses) and background subtraction were performed in order to minimize both random and coherent radio frequency noise. Charge carrier mobilities  $\mu_{\text{TOF}}$  were calculated using the expression:

$$\mu_{\text{TOF}} = d^2/V \cdot t_{\text{tr}} \quad (\text{A2.1})$$

where  $d$  is the sample thickness and  $t_{\text{tr}}$  the inflection point arrival time obtained from a double logarithmic plot of the photocurrent transient, and  $V$  the applied voltage. The electronic response time of the circuit  $\tau$  was at all times kept well below the time base of the measurement.

## A2.5. References

1. S. Goffri, C. Muller, N. Stingelin-Stutzmann, D. W. Breiby, C. P. Radano, J. W. Andreasen, R. Thompson, R. A. J. Janssen, M. M. Nielsen, P. Smith, H. Sirringhaus, Multicomponent semiconducting polymer systems with low crystallization-induced percolation threshold, *Nat. Mater.* **2006**, *5*, 950.
2. A. C. Arias, Vertically segregated polymer blends: their use in organic electronics, *Polymer Reviews* **2006**, *46*, 103.

3. A. C. Arias, F. Endicott, R. A. Street, Surface-induced self-encapsulation of polymer thin-film transistors, *Adv. Mater.* **2006**, *18*, 2900.
4. A. Babel, S. A. Jenekhe, Morphology and field-effect mobility of charge carriers in binary blends of poly(3-hexylthiophene) with poly [2-methoxy-5-(2-ethylhexoxy)-1,4-phenylenevinylene] and polystyrene, *Macromolecules* **2004**, *37*, 9835.
5. B. A. Brown, D. Cupertino, J. Veres, J. D. Schofield, S. W. Leeming, S. G. Yeates, U.S. Patent US2004/0038459 A1, **2004**.
6. P. Wolfer, C. Muller, P. Smith, M. A. Baklar, N. Stingelin-Stutzmann,  $\alpha$ -Quaterthiophene-polyethylene blends: phase behaviour and electronic properties, *Synth. Met.* **2007**, *157*, 827.
7. N. Stingelin-Stutzmann, Organic electronics - complexity made simple, *Nat. Mater.* **2008**, *7*, 171.
8. J. S. Liu, E. Sheina, T. Kowalewski, R. D. McCullough, Tuning the electrical conductivity and self-assembly of regioregular polythiophene by block copolymerization: nanowire morphologies in new di- and triblock copolymers, *Angew. Chem. Int. Ed.* **2002**, *41*, 329.
9. G. Sauve, R. Zhang, S. J. Jia, T. Kowalewski, R. D. McCullough, Synthesis, mobility and conductivity of well-defined regioregular poly(3-hexylthiophene) and diblock copolymers of regioregular poly(3-hexylthiophene), *Proc. SPIE* **2006**, *6336*, U164.
10. G. Sauve, R. D. McCullough, High field-effect mobilities for diblock copolymers of poly(3-hexylthiophene) and poly(methyl acrylate), *Adv. Mater.* **2007**, *19*, 1822.

11. C. P. Radano, O. A. Scherman, N. Stingelin-Stutzmann, C. Muller, D. W. Breiby, P. Smith, R. A. J. Janssen, E. W. Meijer, Crystalline-crystalline block copolymers of regioregular poly(3-hexylthiophene) and polyethylene by ring-opening metathesis polymerization, *J. Am. Chem. Soc.* **2005**, *127*, 12502.
12. C. Muller, S. Goffri, D. W. Breiby, J. W. Andreasen, H. D. Chanzy, R. A. J. Janssen, M. M. Nielsen, C. P. Radano, H. Sirringhaus, P. Smith, N. Stingelin-Stutzmann, Tough, semiconducting polyethylene-poly(3-hexylthiophene) diblock copolymers, *Adv. Funct. Mater.* **2007**, *17*, 2674.
13. L. L. Chua, P. K. H. Ho, H. Sirringhaus, R. H. Friend, Observation of field-effect transistor behaviour at self-organized interfaces, *Adv. Mater.* **2004**, *16*, 1609.
14. J. S. Kim, P. K. H. Ho, C. E. Murphy, R. H. Friend, Phase separation in polyfluorene-based conjugated polymer blends: lateral and vertical analysis of blend spin-cast thin films, *Macromolecules* **2004**, *37*, 2861.
15. A. R. Brown, C. P. Jarrett, D. M. deLeeuw, M. Matters, Field-effect transistors made from solution-processed organic semiconductors, *Synth. Met.* **1997**, *88*, 37.
16. F. Dinelli, M. Murgia, P. Levy, M. Cavallini, F. Biscarini, D. M. de Leeuw, Spatially correlated charge transport in organic thin film transistors, *Phys. Rev. Lett.* **2004**, *92*, 116802.
17. M. C. Scharber, D. Wuhlbacher, M. Koppe, P. Denk, C. Waldauf, A. J. Heeger, C. L. Brabec, Design rules for donors in bulk-heterojunction solar cells - Towards 10 % energy-conversion efficiency, *Adv. Mater.* **2006**, *18*, 789.

18. A. Hadipour, B. de Boer, J. Wildeman, F. B. Kooistra, J. C. Hummelen, M. G. R. Turbiez, M. M. Wienk, R. A. J. Janssen, P. W. M. Blom, Solution-processed organic tandem solar cells, *Adv. Funct. Mater.* **2006**, *16*, 1897.
19. S. A. Choulis, Y. Kim, J. Nelson, D. D. C. Bradley, M. Giles, M. Shkunov, I. McCulloch, High ambipolar and balanced carrier mobility in regioregular poly(3-hexylthiophene), *Appl. Phys. Lett.* **2004**, *85*, 3890.
20. A. J. Mozer, N. S. Sariciftci, A. Pivrikas, R. Osterbacka, G. Juska, L. Brassat, H. Bassler, Charge carrier mobility in regioregular poly(3-hexylthiophene) probed by transient conductivity techniques: a comparative study, *Phys. Rev. B* **2005**, *71*, 035214.
21. R. U. A. Khan, D. Poplavskyy, T. Kreouzis, D. D. C. Bradley, Hole mobility within arylamine-containing polyfluorene copolymers: a time-of-flight transient-photocurrent study, *Phys. Rev. B* **2007**, *75*, 035215.
22. T. Kreouzis, D. Poplavskyy, S. M. Tuladhar, M. Campoy-Quiles, J. Nelson, A. J. Campbell, D. D. C. Bradley, Temperature and field dependence of hole mobility in poly(9,9-dioctylfluorene), *Phys. Rev. B* **2006**, *73*, 235201.
23. C. Muller, C. P. Radano, P. Smith, N. Stingelin-Stutzmann, Crystalline-crystalline poly(3-hexylthiophene)-polyethylene diblock copolymers: solidification from the melt, *Polymer* **2008**, *49*, 3973.
24. H. Bassler, Charge transport in disordered organic photoconductors - a monte-carlo simulation study, *Phys. Stat. Sol. B* **1993**, *175*, 15.

25. G. Juska, K. Genevicius, K. Arlauskas, R. Osterbacka, H. Stubb, Charge transport at low electric fields in pi-conjugated polymers, *Phys. Rev. B* **2002**, *65*, 233208.
26. Y. Kim, S. Cook, S. M. Tuladhar, S. A. Choulis, J. Nelson, J. R. Durrant, D. D. C. Bradley, M. Giles, I. McCulloch, C. S. Ha, M. Ree, A strong regioregularity effect in self-organizing conjugated polymer films and high-efficiency polythiophene: fullerene solar cells, *Nat. Mater.* **2006**, *5*, 197.
27. V. D. Mihailetschi, H. X. Xie, B. de Boer, L. J. A. Koster, P. W. M. Blom, Charge transport and photocurrent generation in poly (3-hexylthiophene): methanofullerene bulk-heterojunction solar cells, *Adv. Funct. Mater.* **2006**, *16*, 699.
28. K. J. Ihn, J. Moulton, P. Smith, Whiskers of poly(3-alkylthiophene)s, *J. Polym. Sci., Part B: Polym. Phys.* **1993**, *31*, 735.



## Acknowledgements

Studying for a PhD was an unforgettable experience in my life which will live with me forever. I have enjoyed and learned from this experience so much and it has influenced me not only on the intellectual but also on the personal level. There have been a multitude of people involved in the completion of this thesis; whom have been exceptionally helpful and supportive.

First and foremost, I like to start with infinite thanks and appreciations to my supervisor Natalie Stingelin for her patience, guidance, support and advice through out this thesis, thus this work would not have been possible without her. She helped me to develop and progress not only scientifically but also in terms of personality, my gratitude to her is beyond words. In addition, I like to thank Prof. Paul Smith for agreeing to be my external examiner. I am already in advance very grateful for all his input to this thesis. Similar thanks go to Dr. Martin Heeney and Prof. Iain McCulloch.

I am very grateful to the following people whom have been very helpful and were always supportive, David Sparrowe (Merck Chemicals Ltd, UK), Avinesh Kumar (QMUL, UK), Christian Muller (Linköping, Sweden), Marc Simonet (TUE, Holland), Pascal Wolfer and Felix Koch (ETH, Switzerland).

In addition I would like to thank the following people for there fruitful scientific discussion and experimental assistance, from Imperial College London, Thomas Anthopoulos, Paul Wöbkenberg, Ester Buchaca, Liyang Yu, George Hicks, Gianluca Latini, Manuela Russo, Paul Westacott, Mohammed Al-Hashimi and last but not least Salahud Din. Moreover, from Merck Chemicals Ltd, UK, Steven Tierney, Warren Duffy, Philip May, Mark James, Katherine Patterson, Magda Gonçalves, Maxim Shkunov, Michael Cölle and Miguel Carrasco. I am very much indebted to those people at Queen Mary UoL, whom were supportive in every aspect of my PhD, Rory Wilson, Monisha Philips, Theo Kreouzis, Seema Barard, Nima Roohpour and Ken Scott.

Furthermore, I am extremely gratified to the ETH (Zurich) polymer technology group for making me feel like at home, whenever I visited there labs, Walter Steurer, Walter Caseri, Kiril Feldman, Markus Trummer, Jan Giesbrecht and Karin Bernland.

I would like to thank my friends whom have always been encouraging during the PhD period, Walid Ahmed, Alfahad Al-Fadhl, Fahad Al-Safar, Hicham Khodr, Jamal Al-Tarkait, Hanadi Suleiman and not to forget Khalid Al-Mezaini.

Finally, I would like to end with a sincere thank to everyone mentioned above for their continuous support, guidance and patience. They often say in **Arabic**, a dear and caring friend is one who always stands beside you, not only in good-happy moments, but also during tough- depressing- and sad- periods.



## (Acknowledgements) شكر و عرفان

في البداية أود أن أعترف ان دراسة الدكتور ه هي مرحلة و خبره لن أنساه طوال حياتي، حيث أنني أستمتعت كثير في الدراسة و كان لها أثر كبير ليس فقط على مستواي العلمي و لكن أيضاً على مستواي الشخصي.

لذلك أود أن أبدأ بالشكر و التقدير لمشرفة البحث *ناتالي ستجلين* و المساعد *شيف بول سميث* لدعمهم و إشرافهم اللامحدود للإطروحة، و لولا هذا الدعم لما تمكنت من إتمام الإطروحة. بالإضافة لذلك و خلال أيام الدراسة لم أشعر قط أنني اعلم لوحدي و لكن كانوا بمثابة العائلة بالنسبة لي. لقد ساعدوني في تنمية مهاراتي العلمية و كذلك مهاراتي على المستوى الشخصي.

كما أود أيضاً أن اقدم الشكر الخاص لكل هؤلاء الذين عملت معهم و كانوا معي في الأوقات التي احتجت لهم و ساعدوني في الأطروحة: *ديفيد سباروي* من معمل ميرك الكيميائي (Merck بريطاني)، *أفيناش كومار* (QMUL، بريطانيا)، *كريس مولير* (Linköping، السويد)، *مارتين هييني* (IC، بريطانيا)، *باسكال وليفرز* (ETH، سويسرا)، *مارك سيمونت* (TUE، هولندا) و *فيكس كوخ* (ETH، سويسرا).

بالإضافة الي ذلك أود ان اشكر هؤلاء الذين كانت نقاشاتهم معي مثمرة علمياً و دعمهم التجريبي في المعامل: من كلية امبيريل لندن (Imperial College)، *ايان مكولج*، *توماس انثوبولوس*، *بول وبكينبيرج*، *ايستر بوشاكا*، *ليانج يو*، *جورج هيكس*، *جيانلوكا لاتيني*، *مانويلا روسو* و أخيراً و ليس آخرأ *صلاح الدين و محمد الهاشيمي*.

أيضاً أود ان اقدم الشكر لستيف تيرني من معامل ميرك الكيميائي (ساوث هامبتون Merck)، *ورين دوف*، *فل ماي*، *مارك جميس*، *كاتي باتيرسون*، *ماجدا كونكالفيس*، *ماكسيم شكونفو*، *مايكل كورول* و *ميجل كاراسكو*. كما اقدم شكر خاص لفريق جامعة لندن – *كوين ماري* و التي كان دعمهم في كل ما يتعلق بداراستي: *روري ويلسن*، *مونشا فيليبس*، *ثيو كريوزيس*، *سيما بارارد* و *كين سكوت*.

و اود ان اقدم جزيل الشكر لETH (زيورخ) و مجموعة بوليمر للتكنولوجيا لمعاملي كفرد من عائلتهم في كل زيارتي لمعاملهم: *بروفيسر وولتر ستيورير*، *ولتر كاسيري*، *كيريل فيلدمان*، *ماركوس ترومير*، *جان جيسبرخت* و *كرين بيرلند*

و في النهاية شكرا جزيل لأعز أصدقائي لدعمهم المعنوي في كل الأوقات الصعبة و الجيدة، *وليد احمد*، *الفهد الفضل*، *فهد السافار*، و لا أنسى أيضاً *هشام خضر* و *خالد المزيني*.



## Curriculum Vitae

*Moe* Baklar was born in Kuwait (January 24<sup>th</sup> 1980), where he lived until the first Gulf war (1990-1991). After completing his secondary education at Newham College (Stratford campus), he studied for a Bachelor degree in Natural Sciences at Queen Mary UoL and then worked at King College London (Department of Pharmacy) for few years as a junior scientist, before joining Natalie Stingelin's group at Queen Mary UoL (department of Materials), where he completed the work described in this thesis.



